

3-23-2018

# United States Air Force Applications of Unmanned Aerial Systems: Modernizing Airfield Damage Assessment

Samuel M. Clark

Follow this and additional works at: <https://scholar.afit.edu/etd>

Part of the [Management and Operations Commons](#), and the [Other Engineering Commons](#)

---

## Recommended Citation

Clark, Samuel M., "United States Air Force Applications of Unmanned Aerial Systems: Modernizing Airfield Damage Assessment" (2018). *Theses and Dissertations*. 1882.  
<https://scholar.afit.edu/etd/1882>

This Thesis is brought to you for free and open access by the Student Graduate Works at AFIT Scholar. It has been accepted for inclusion in Theses and Dissertations by an authorized administrator of AFIT Scholar. For more information, please contact [richard.mansfield@afit.edu](mailto:richard.mansfield@afit.edu).



**LEVERAGING UNMANNED AERIAL SYSTEMS TO MODERNIZE AIRFIELD  
DAMAGE ASSESSMENT**

THESIS

Samuel M. Clark, Captain, USAF

AFIT-ENV-MS-18-M-188

**DEPARTMENT OF THE AIR FORCE  
AIR UNIVERSITY**

**AIR FORCE INSTITUTE OF TECHNOLOGY**

---

---

**Wright-Patterson Air Force Base, Ohio**

**DISTRIBUTION STATEMENT A.**  
APPROVED FOR PUBLIC RELEASE; DISTRIBUTION UNLIMITED.

The views expressed in this thesis are those of the author and do not reflect the official policy or position of the United States Air Force, Department of Defense, or the United States Government. This material is declared a work of the U.S. Government and is not subject to copyright protection in the United States.

AFIT-ENV-MS-18-M-188

LEVERAGING UNMANNED AERIAL SYSTEMS TO MODERNIZE AIRFIELD  
DAMAGE ASSESSMENT

THESIS

Presented to the Faculty

Department of Systems and Engineering Management

Graduate School of Engineering and Management

Air Force Institute of Technology

Air University

Air Education and Training Command

In Partial Fulfillment of the Requirements for the  
Degree of Master of Science in Engineering and Environmental management

Samuel M. Clark, M.B.A., BS

Captain, USAF

March 2018

**DISTRIBUTION STATEMENT A.**  
APPROVED FOR PUBLIC RELEASE; DISTRIBUTION UNLIMITED.

AFIT-ENV-MS-18-M-188

LEVERAGING UNMANNED AERIAL SYSTEMS TO MODERNIZE AIRFIELD  
DAMAGE ASSESSMENT

Samuel M. Clark, M.B.A, BS

Captain, USAF

Committee Membership:

David R. Jacques, PhD  
Chair

Lieutenant Colonel Amy M. Cox, PhD  
Member

Alfred E. Thal, Jr., PhD  
Member

### **Abstract**

Modernizing airfield damage assessment has long been a priority mission at the Air Force Civil Engineer Center (AFCEC). Previously, AFCEC has made advances to expedite unexploded ordnance (UXO) neutralization and pavement repair. Missing from these initiatives is the initial assessment component. This thesis expands the idea of using Small Unmanned Aerial Systems (SUAS), applies it to the Air Force mission, and provides SUAS vehicle configuration and sensor recommendations.

In this study, 25 civil engineer officers reviewed airfield imagery gathered using two small air vehicles. For the first review, participants attempted to identify UXOs and foreign object debris (FOD) in a computer interface that leverages images collected by a fixed-wing air vehicle. The second review uses a two-dimensional map created using a hex-rotor. The results of both systems were then compared to the status quo. Resulting statistics indicate that, irrespective of image resolution, additional analysis time does not result in greater object detection or correct identification.

Overall, this thesis concludes that SUAS use for airfield damage assessment shows promise. Moreover, they can provide the Air Force improved precision for locating UXOs and FOD, as well as estimate dimensions of damage. Dedicating resources to developing this technology will also assist with improving object detection and manpower efficiency. Further research is required for optimal image characterization requisite for reducing and/or eliminating the occurrence of false negative events.

## Acknowledgments

This thesis was made possible by the generosity and support of the Air Force Institute of Technology faculty and staff, the Air Force Civil Engineer Center, the Civil Engineer School House, the 823rd RED HORSE Squadron, Sinclair Community College, the Ohio Department of Transportation, and the 436th Civil Engineer Squadron. I would like to specially thank Dr. David Jacques for creating an environment that allowed civil engineers to explore unmanned aerial systems and learn about aerospace engineering. Without his help, I would not have had the knowledge nor access to all of the expertise required herein. I am also grateful to Rick Patton, David Thacker, Jeremy Gray, and John Haugan for assisting with vehicle design, fabrication, and tuning.

I would also like to thank my committee for their guidance and keeping me focused on the big picture. I am grateful for all of the excellent instructors I have had the opportunity to learn from during my stay at AFIT. I would also like to thank the Graduate Engineering Management Classes of 2017, 2018, and 2019 as well as the 2017 Systems Engineering 550-650-651 sequence team – Gregory Roth, Kijun Lee, Timothy Allen, Mike Kaniut, Robert McGaha, and Taylor Bodin – for their helpful advice, knowledge, and camaraderie throughout this process.

Finally, words cannot express my gratitude for the support of my family; in the past and all that is yet to come. This thesis is the culmination of ten years of rigorous study; know that your personal sacrifices have not gone without notice. In conclusion, I would like to thank my wife for her optimism and doing her absolute best. I love you very much, you make me a better man than I could have imagined, and I certainly could not have accomplished all that I have without you.

## Table of Contents

	Page
Abstract.....	iv
Table of Contents.....	vi
List of Figures.....	viii
List of Tables.....	ix
I. Introduction.....	1
General Issue.....	2
Background.....	3
Problem Statement.....	5
Research Objective.....	6
Overview.....	8
II. Literature Review.....	9
Traditional airfield damage assessment methodology.....	9
Variations of performing pavement damage assessment.....	16
Manpower requirements.....	26
Market analysis.....	31
Summary.....	32
III. Methodology.....	34
Acquiring baseline airfield damage assessment metrics.....	34
Civil engineer officer testing and evaluation procedures.....	41
Air vehicle configuration.....	49
IV. Analysis and Results.....	58
Baseline metrics.....	59
Civil engineer officer metrics.....	63
V. Conclusions and Recommendations.....	71
First investigative question.....	71
Second investigative question.....	73
Third investigative question.....	74
Summary.....	77
Recommendations.....	79
Further Research.....	80
Appendix A. R-1, R-2, and R-3 Vehicle and Equipment Sets.....	86



Appendix B. Airfield Damage Reconnaissance Organization Concept .....	88
Appendix C. Emergency Operations Center Team Organization.....	89
Appendix D. Types of Pavement Damage.....	90
Appendix E. UXO Classifications .....	91
Appendix F. MOS Selection Checklist, Desirable- & Undesirable Considerations.....	94
Appendix G. Enlisted Civil Engineer Evaluation Protocol .....	96
Appendix H. Civil Engineer Officer Evaluation Protocol .....	101
Appendix I. Small Unmanned Aerial Systems Components .....	110
Equipment.....	110
Software.....	118
Appendix K. Baseline Metrics and Civil Engineer Officer Statistics.....	124
Appendix L. MAIN.m MATLAB™ Script .....	131
Appendix M. AnalyzeFrames.m MATLAB™ Script.....	134
Appendix N. Air Force Institute of Technology, SENG 651 Capstone Presentation.....	136
Bibliography .....	159
Vita .....	168

## List of Figures

	Page
Figure 1. Airfield Recovery Cycle.....	5
Figure 2. Installation Recovery Sequence .....	10
Figure 3. Altavian F7200 Nova (www.altavian.com).....	21
Figure 4. Altavian R8700 Galazy (www.altavian.com) .....	22
Figure 5. Crack detection on three representative images (Meeks, 2016).....	24
Figure 6. Subsurface Damage .....	38
Figure 7. Skywalker X-8, "Flying Wing" .....	51
Figure 8. Skywalker X-8 Camera Mount.....	52
Figure 9. Skywalker Catapult Launch Apparatus .....	52
Figure 10. Tarot Hex-rotor, Storm Pro-3 Gimbal, & Sony α6000 Camera .....	55

## List of Tables

	Page
Table 1. MOS Launch or Recovery Capability .....	14
Table 2. Airfield Assessment Alternative Cost/Benefit Summary .....	26
Table 3. Airfield Assessment Alternatives Summary .....	30
Table 4. Airfield Assessment Criteria Summary .....	33
Table 5. Position Accuracy Summary Table .....	62
Table 6. Baseline Positioning Deviation.....	62
Table 7. Image Analysis vs. Status Quo Assessment Time Summary Table .....	64
Table 8. MATLAB vs. 2D Ortho-mosaic Statistics.....	69

# LEVERAGING UNMANNED AERIAL SYSTEMS TO MODERNIZE AIRFIELD DAMAGE ASSESSMENT

## I. Introduction

*“It is only through labor and painful effort; by grim energy and resolute courage; that we move on to better things” – Theodore Roosevelt*

Airfields are the predominant medium through which personnel, equipment, and supplies are transported to and from United States military installations worldwide. In the pre-attack status, airfields serve as a conveyor of personnel and supplies to various theaters of operation as well as provide the medium for aviators to refine their skills. In the post-attack condition, airfields must be able to launch and recover aircraft to respond to mission requirements and continue facilitating global operations. In today’s United States Air Force, active duty personnel number 200,000 less than the start of the Gulf War (Losey, 2016). This reduction in airmen reduces targeted installations’ or neighboring mission partners’ ability to respond and execute recovery measures. Thus, compared to the air force of 30 years ago, an incapacitated airfield represents a significantly greater degradation in the ability to respond to threats and continue sustainment, humanitarian, and contingency operations, both at home and abroad.

“If an enemy attacks an airbase [whether that be through kinetic or nonconventional means], the [installation] commander’s immediate problem is to launch and recover mission aircraft as soon as possible” (Air Force Civil Engineer Center, 2015b).” As such,

the Base Civil Engineer (BCE) is responsible for responding to these events and are charged with the mission to expediently identify airfield infrastructure damage and recommend the most efficient repair solution.

## **General Issue**

In its current expression, the conventional methods employed to assess and repair airfield damage has – for the most part – relied upon the same procedures as when military aviation was newly minted. Recent improvements have been realized in the means by which debris and live munitions are cleared. Further, the filling and repair of craters has become more time and resource efficient. However, the method by which airfields are assessed for Foreign Object Debris (FOD), Unexploded Ordnance (UXOs), and damage has largely remained unchanged over the course of the past century.

What this undertaking entails is a dangerous and potentially inaccurate manual effort that consumes time and manpower resources proportional to the size of the airfield and servicing installation. Since the first grassy field in Dearborn, Michigan, was fortified with concrete in 1928 (“First Concrete Runway - Ford Field - Dearborn, MI,” 2016), FOD walks and damage assessments have been carried out manually, requiring personnel to physically examine the length of each and every runway, taxiway, and parking apron to characterize the operating surface’s readiness to launch and recover aircraft. In the post-attack condition, this process places troops in harm’s way, whether it be secondary bombardment, detonating UXOs, or venturing into a Chemical, Biological, Radiological, or Nuclear (CBRN) environment. In the year 2017, this approach to appraising airfields remains the same; there must be a better, safer, more efficient way.

## Background

Upon completion of a successful airfield damage assessment, a series of Minimum Operating Strip (MOS) solutions will be identified as well as which taxiways and parking aprons require repair. A MOS is “the smallest amount of area that must be repaired to launch and recover aircraft” (Department of Defense, 2002). When the MOS is combined with the adjoining access taxiways and relevant parking aprons, the collective area is referred to as the Minimum Airfield Operating Surface (MAOS) (Air Force Civil Engineer Center, 2015a). Prior to the determination of the placement of a MOS and/or MAOS, an assessment of airfield infrastructure must be undertaken to identify the presence and location of physical damage and debris, as well as to identify UXOs that are present on the airfield surfaces.

The Installation Control Center (ICC) provides operational and environmental requirements as well as expected operating conditions following the attack. Armed with this information, the MOS selection team locates potential operating strips to be repaired and recommends MOS candidates, as well as an overall MAOS to the ICC commander. Once approved, the Emergency Operations Center (EOC) director orchestrates the Explosive Ordnance Disposal (EOD) teams as they neutralize and clear areas identified as containing UXOs and other kinetic hazards. Finally, the Airfield Damage Repair (ADR) teams begin their crater and spall clearing and repair activities.

In general, from the instance that the attack condition expires and the ICC commander issues the “all-clear,” the BCE’s objective is to resume flying operations within 4 hours by “providing an accessible and functional MOS/MAOS that will sustain 100 passes of the particular aircraft identified by the ICC at its projected mission weight, or the

number of passes required to support the initial surge mission aircraft” (Air Force Civil Engineer Center, 2015a; Department of Defense, 2002). Depending on the aircraft type and operational requirements, repairs may require more time due to greater MOS width and length requirements in relation to the number of UXOs and craters identified.

Through their efforts to modernize and expedite ADR, the Air Force Civil Engineer Center (AFCEC) has improved the Air Force’s capability to expediently repair airfield damage. For instance, the R-1 Vehicle and Equipment Set enables three ADR teams to repair three (one each) 50-foot bomb craters with an AM-2 or Folded Fiberglass Mat (FFM) within 4 hours. Additional kits include the R-2 and R-3 Vehicle and Equipment Set Additives. The R-2 provides additional tools, equipment, and supplies, whereas the R-3 is an abbreviated version of the R-2. Refer to Appendix A. R-1, R-2, and R-3 Vehicle and Equipment Sets for information regarding the R-1, R-2, and R-3 vehicle and equipment sets. When used in combination, the R-1, R-2, and R-3 kits allow six ADR teams – three on the MOS and three on the taxiways – to repair two 50-foot craters each, for a total of twelve 50-foot bomb craters within 4 hours. By comparison, traditional methods require excavation, concrete cutting, backfilling, compacting, and flowing fresh concrete, all of which are present in the R-kits. However, due to concrete strength requirements, legacy repair times lasted weeks. Moreover, with the inclusion of freezing temperatures and precipitation, large area repairs could take months to fully cure (Duncan, 2007).

AFCEC’s efforts to expedite airfield recovery operations have improved turnaround time to restore an airfield. However, these improvements only address the reconstitution and repair functions. The damage assessment component poses an open opportunity to even further improve this process (Figure 1). Areas in which the assessment

phase may be improved include 1) reduction in the amount of time required to examine the airfield surfaces, 2) the precision and accuracy experienced in quantifying and characterizing damage and UXOs, 3) reduction in manpower and equipment resources employed throughout the damage assessment phase, and 4) mitigation of the threat posed to human life.

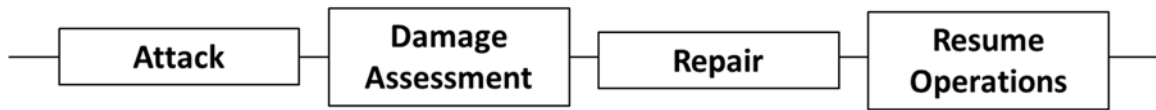


**Figure 1. Airfield Recovery Cycle**

With the recent advances in commercial off-the-shelf (COTS) Small Unmanned Aircraft Systems (SUAS) technologies, new capabilities have emerged that may render the post-attack inspection safer – from a manpower perspective – more accurate, and more time and resources efficient. Ultimately, an investigation of this technology is necessary to support the use of SUAS technologies during the assessment of runways and associated spaces to facilitate the mobilization of Civil Engineer resources.

### **Problem Statement**

The inspection and assessment of a runway, and associated spaces, following conventional and nonconventional attacks is a time-consuming and manpower-intensive undertaking. The efficiency of the airfield damage assessment process ultimately impacts the ability of civil engineer repair teams to meet repair criteria established in Air Force Pamphlet (AFPAM) 10-219, Volume 4 (Air Force Civil Engineer Center, 2015a). The



initial reconnaissance and assessment are the first steps in recovering the installation and enabling the generation and recovery of aircraft sorties. As such, it is essential that techniques that facilitate expediting the post-attack assessment process are investigated. Improvements to the post-attack assessment process can yield direct benefits to mission readiness restoration.

From the installation commander's issuance of limited release of recovery personnel to the mobilization of repair resources, 90 minutes have been allocated as a threshold for this task. This is based on the 4-hour repair criteria established in AFPAM 10-219, Volume 4, and the time necessary to complete repairs. This phase must produce precise assessment data that supports the immediate deployment of civil engineer repair teams. In addition, the assessment data must provide actionable information for clearing UXOs and debris, repairing damage, and establishing the MOS and/or MAOS.

### **Research Objective**

The outcome of this thesis is to analyze and demonstrate that an SUAS approach – at a relatively low price point – is capable of meeting Air Force Civil Engineer requirements for the survey and assessment of airfield pavements in the post-attack condition. Moreover, it also demonstrates that the employment of SUAS can successfully identify, geo-locate, and classify airfield damage and UXOs, as well as serve to reduce manpower requirements for conducting damage and hazard reconnaissance following an attack.

### ***Investigative Questions.***

Each of the following investigative questions address one of the three major focus areas of SUAS design and employment which include: 1) SUAS employment efficacy, 2) resource requirements, and 3) sensor packages, vehicle characteristics, and airfield damage assessment specific optimization.

1. Are civil engineer personnel capable of reliably leveraging data collected via Small Unmanned Aerial Systems (SUAS) to meet or exceed traditional damage assessment methods?
2. What are the resource requirements – e.g. manpower, purchase costs, consumables, etc. – for an SUAS concept to accomplish an airfield damage assessment?
3. Given the target criteria specified in the problem statement, what sensor packages, aerial vehicle characteristics, and environmental optimization considerations are appropriate for conducting airfield damage assessments?

### ***Scope, Assumptions, and Limitations.***

This thesis focuses on pre-existing airfield images that were collected from two different air vehicles with distinct imaging platforms. Refer to Chapter III and Appendix I. Small Unmanned Aerial Systems Components for full air vehicle configuration information. Therefore, the data used in this thesis is limited to the environmental conditions present on the day the data was collected. This includes 1) fair weather, absent precipitation or extreme heat/cold and low-wind periods, and 2) daylight operations. In addition, configuration limitations excluded sensor packages beyond image capturing techniques, such as LIDAR, Infrared, Sonar, etc., as well as data processing algorithms or

artificial intelligence. Lastly, data supporting improvements to personnel safety through the employment of SUAS technologies was not collected in this thesis. Any threat mitigation conclusions are purely speculative in nature.

## **Overview**

In the following chapter, a literature search is provided to demonstrate the body of knowledge – as of this writing – pertaining the state-of-the-art in terms of SUAS and what it has to offer Air Force airfield damage assessment. In addition, multiple applications of SUAS employment in related fields are described. In Chapter III, the approach to test the existing dataset by using 1) baseline metrics established from enlisted civil engineer airmen whose profession it is to conduct airfield damage assessments and 2) civil engineer officers to analyze the pre-existing dataset and compare performance levels across the baseline metrics. Chapter IV will provide quantitative statistics to compare the civil engineer results with the baseline metrics. Lastly, Chapter V will provide evidence supporting whether or not SUAS can meet Civil Engineer requirements through the measures of time and quality. This thesis acknowledges that, as weather limitations are relaxed, mission capabilities degrade. However, the intent of the study is not to develop an all-weather SUAS; instead, the objective is to demonstrate that SUAS may be employed to modernize CE airfield damage assessment requirements.

## II. Literature Review

The current state of airfield damage assessment is a time-consuming and manpower-intensive mission that requires many parts and pieces to operate in unison to ensure the highest quality and actionable information is collected in a timely manner. In the literature review that follows, the current state-of-the-art for United States Air Force airfield damage assessment and Minimum Operating Strip (MOS) plotting will be presented to serve as a baseline for the alternative methods that follow.

Succeeding sections examine three technology-based alternatives: 1) in-situ wireless sensors, 2) Small Unmanned Aerial Systems (SUAS), and 3) Unmanned Ground Vehicles (UGV) that serve as the catalysts for modernizing how airfield damage assessment is accomplished. Harnessing technologies such as these promises a reduced labor burden for installations and reduces the hazard exposure of base recovery personnel. Beyond the baseline comparison, novel capabilities can be enabled by introducing these technologies. Lastly, by delivering on-scene images to the Emergency Operations Center (EOC), the higher quality damage repair estimates may be realized. This may be achieved through reductions in miscommunication of Unexploded Ordnance (UXO) and damage, as well as significantly reduced error via a greater number of personnel reviewing the post-attack images.

### **Traditional airfield damage assessment methodology**

For this initial section, the current practice for airfield damage assessment will be detailed through the following six categories: 1) why damage assessment is important, 2)

airfield damage assessment and MOS plotting team composition, 3) damage assessment methodology, 4) MOS characteristics, 5) MOS dimensions, and 6) damage plotting and candidate MOS selection.

### *Why damage assessment?*

In the post-attack condition, damage assessment is one of the earliest base recovery functions to be performed. **Error! Reference source not found.** depicts the installation recovery sequence following an attack. Personnel occupying observation posts and flight line cameras begin reporting the presence of infrastructure damage, fires, and UXO sightings to the EOC and/or the Damage Control Center (DCC). Reporting procedures are specific by local guidance as provided in local Installation Emergency Management Plan (IEMP) 10-2 (Air Force Civil Engineer Center, 2015a). Appendix B. Airfield Damage Reconnaissance Organization Concept depicts the Airfield Damage Reconnaissance (ADR) organization concept that is being employed in current practice.

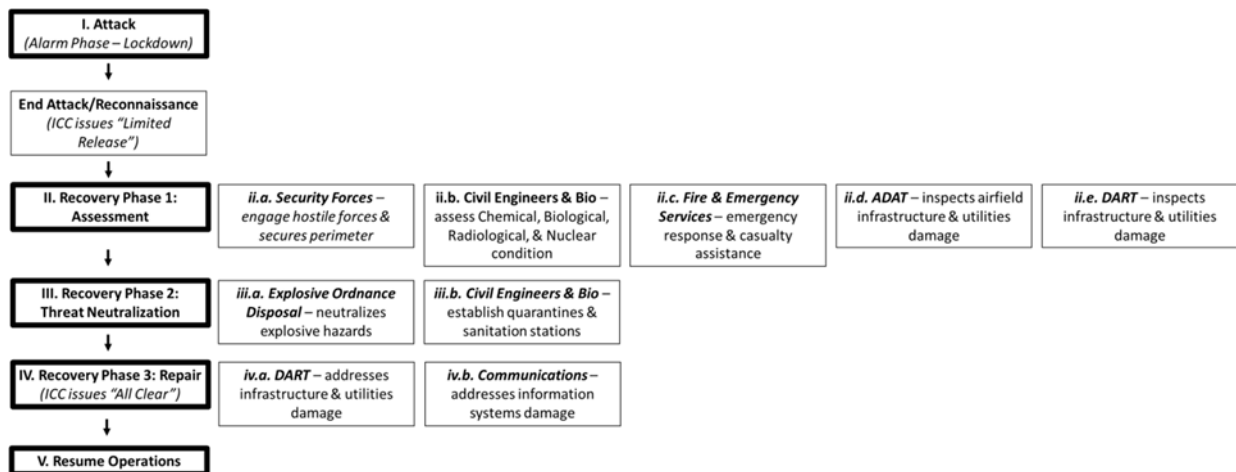


**Figure 2. Installation Recovery Sequence**

The sooner that damage and UXOs are identified, the sooner installation recovery operations may begin. The weapons system platform for many installations is their airfield(s); without the ability to launch or recover aerial assets, many installations' missions – such as strategic airlift, aerial combat, and Intelligence, Surveillance, and Reconnaissance (ISR) – become impossible. Therefore, a rapid, highly detailed, and accurate depiction of the existing infrastructure damage as well as explosive hazards must be identified to start recovery activities necessary to restore a base to its operational mission.

***Team composition.***

Once the installation commander(s) have ordered the release of recovery personnel following an attack, installation Civil Engineer Squadrons (CES) deploy their Damage Assessment Response Teams (DART) as well as Airfield Damage Assessment Teams (ADAT). Depending on manning levels, ADATs typically consist of four – but no less than three – members: one engineering technician (commonly referred to as an “EA”), one Explosive Ordnance Disposal (EOD) technician, and two augmentees. Appendix C. Emergency Operations Center Team Organization depicts the current standard for airfield damage assessment team organization within the EOC. The EA catalogues airfield damage, such as craters, spall fields, and other surface/subsurface damage. The EOD Tech identifies UXOs and other kinetic hazards; and the augmentees serve as vehicle and radio operators, as well as additional observers, to assist with recording damage and identifying UXO/kinetic threats. Appendix D. Types of Pavement Damage and Appendix E. UXO

Classifications provide information concerning the specific types of pavement damage and UXO classifications, respectively.

Separate from the DART and ADAT teams, the MOS selection team is located in the EOC, where damage information and recovery planning is centralized. At a minimum, the MOS selection team is comprised of two personnel, one of which should be an EA, who is responsible for plotting damage and UXO data, whereas the second team member may be from any civil engineer functional area who serves as a radio operator and data recorder.

For installations of sufficient size, the EOCs will be stood up and operated independently, thus providing multiple MOS selection teams who work towards producing three candidate MOS locations (each). In situations in which there are multiple runways, as well as a large number of UXOs and craters, the MOS plotting team may require augmentation to ensure that data fidelity is maintained and the plotter does not become overwhelmed. In some locations, staging multiple EAs in addition to multiple radio operators in the EOC is a standard practice.

***Damage assessment methodology.***

The number of ADATs dispatched to survey an airfield depends on the size of the installation; however, there are typically three to four ADATs that survey damage. Airfield damage assessment is conducted in two phases: 1) initial reconnaissance and 2) detailed damage assessment. Phase I provides a gross assessment from prepositioned locations around the airfield. These locations can either be manned observation points, previously installed camera systems, or other approaches that provide a quick assessment. This information is reported to the EOC (or DCC) such that Phase II assessments may begin.

When the MOS selection team positioned within the EOC has analyzed the Phase I data, they assume positive control over the ADATs and direct them through Phase II.

In Phase II, the ADATs conduct a detailed assessment of areas specified by the EOC, such that the MOS may be generated with accuracy and precision. The teams navigate coordinated routes through areas where damages are the least severe such that ADATs “avoid areas which are too heavily damaged to warrant consideration in MOS selection” (Air Force Civil Engineer Center, 2015a). These routes utilize a grid-reference system (in conjunction with visual reference markers (such as runway distance markers, the centerline, runway edge lighting, taxiway markers, etc.) to survey the 1) runways, 2) taxiways, and 3) major aircraft parking aprons and staging areas (Air Force Civil Engineer Center, 2015a).

#### ***MOS characteristics.***

The overarching objective in MOS candidate determination is to plot all reported damages and UXO locations on runway surfaces to determine a MOS that will minimize the repair time required. This is driven by the lengthy process of crater repair and the desire to – initially – repair no more damage than is necessary (Air Force Civil Engineer Center, 2015a). This is achieved by integrating aircraft and operational requirements with the areas containing the least amount of damage, FOD, or UXOs.

An essential aspect of MOS selection is the capability to launch and recover aircraft; as such, it is essential that a MOS be considered such that adjoining taxiways allow for aircraft to transition to and from the airfield from staging and maintenance areas (Air Force Civil Engineer Center, 2015a). This is referred to as the Launch or Recovery (LOR) status. LOR status indicates the airfield’s ability to generate sorties, independent of other



variables (such as mission time, aircraft attrition, and origin of the aircraft). LOR capabilities are shown in **Error! Reference source not found.**

**Table 1. MOS Launch or Recovery Capability**

Two Access Taxiways	One Access Taxiway	Taxi Backtrack > 1,000 Ft.	Taxi Backtrack > 2,000 Ft.	Arresting System Engagement w/Each Aircraft	Air Traffic Control Eqpmt Not Functional	Relative LOR Capability
X						100%
X				X		34%
X				X	X	25%
X		X				60%
X			X			50%
	X					40%
	X			X		27%
	X			X	X	19%

“The Relative LOR Capability of a MOS represents the total number of launches and recoveries the surface can handle per unit time compared to the number that could be handled by the same, undamaged airfield” (Air Force Civil Engineer Center, 2015a). A 100% Relative LOR status indicates that the MOS and its access points do not restrict aircraft launch and recovery operations, whereas a 50% LOR status represents a 50% reduction in sortie generation and recovery capability. As a minimum, at least two access routes are desired, preferably one at each end of the MOS. Appendix F. MOS Selection Checklist, Desirable- & Undesirable Considerations describes a standard MOS selection

checklist. In addition, eight desirable and six undesirable MOS selection considerations have also been provided.

***MOS dimensions.***

The Installation Control Center (ICC) provides MOS dimensions to the MOS plotting team based upon the known requirements of aircraft to be recovered and/or launched and mission objectives, aircraft performance and payload, weather, and environmental conditions. The MOS plotter then constructs a physical template of the MOS dimensions in the scale of the airfield map. This enables the plotter to rapidly identify candidate MOSs by superimposing the MOS template on the airfield damage plot (Air Force Civil Engineer Center, 2015a).

***Damage plotting and candidate MOS selection.***

MOS selection confirms “the amount of munitions that need to be neutralized and the amount of damage that will need to be repaired” (Duncan, 2007) to reestablish flying operations. As such, the three candidate MOSs “must satisfy mission requirements for sustained operation and must be suitable for the type of aircraft specified by the ICC” (Air Force Civil Engineer Center, 2015a). MOS selection is completed through the following four phases: 1) alert status preparation, 2) plotting and candidate MOS generation, 3) evaluation of candidate MOSs (includes identification of access routes), and 4) briefing the MOS candidates to the ICC commander for final approval (Air Force Civil Engineer Center, 2015a; Duncan, 2007).

Upon completion, three [candidate] MOSs are recommended to the ICC commander, of which the best of the three is typically chosen. It is a good idea to have a couple of alternate MOS possibilities available in case previously unknown

operational requirements surface which impact the suitability of the originally recommended MOS. At bases where there are two (or more) runways/primary takeoff and landing surfaces, MOS selection should consider both surfaces. (Air Force Civil Engineer Center, 2015a)

### **Variations of performing pavement damage assessment**

In the previous subsections, the current state of Air Force airfield damage assessment has been summarized. The AFPAM 10-219, Volume 4 captures the operating procedures for United States Air Force Civil Engineers, which closely mirrors that of allied European nations where United States Air Forces and assets are present, such as the Royal Air Forces of the United Kingdom, the Italian Air Force (Regia Aeronautica), and the German Air Force (Luftwaffe). In the sections that follow, alternative methods for conducting airfield damage assessment will be discussed. While they are not a primary focus of this research, wireless remote sensors will be mentioned with respect to their recent contribution to reducing the manpower and resources requirements through remotely monitoring infrastructure conditions. The majority of the remaining research will focus on examining image-based infrastructure condition assessment through the use of small unmanned aircraft systems and unmanned ground vehicles.

#### ***Remote sensors.***

Over the course of the past decade, greater attention has been placed on harnessing sensing technologies for monitoring infrastructure and structural systems health. For example, "...wireless sensor networks (WSNs) are increasingly utilized as alternatives to traditional structural engineering monitoring systems" (Alavi, Hasni, Lajnef, Chatti, &

Faridazar, 2015). Through the use of gene expression programming (GEP), probabilistic neural network (PNN), and three-dimensional finite element (FE) analysis, Alavi et al. (2016) have been able to demonstrate that sensors imbedded in pavements are “efficiently capable of detecting different damage states in spite of high-level [electric disturbance] contamination...[by identifying and] interpreting cumulative time distributions at preselected discrete strain levels... [thereby facilitating the identification of] crack propagation as well as possibly localizing the damage and quantifying its severity” (Alavi et al., 2015).

This breakthrough is not without its limitations, however; “...a major concern for the application of wireless sensors is related to the difficulties of powering them” (Alavi et al., 2015). Their methodology requires a substantial quantity of sensors to be imbedded in throughout paved assets. As such, the requirement to power and maintain each individual sensor through traditional means (i.e., the power distribution grid) would become a utility infrastructure project of its own. However, to address this issue, the authors demonstrated that energy may be harvested from the mechanical loading experienced by the pavement surface using piezoelectric transducers, thereby enabling the sensors to be self-powered (Alavi et al., 2015).

The mechanical signal that the piezoelectric transducers detect serve more than a singular purpose; the traffic loading can be used both for feeding the self-powered sensors as well as facilitating damage diagnosis (Alavi et al., 2016, 2015). Despite this advantage, a major area of concern entails “managing the huge amount of data generated by the dense array of sensors... [data processing is] challenging and costly” (Alavi et al., 2016, 2015). Conversely, due to noise and distortion in wireless, as well as wired, transmitted

information, the potential for loss of sensed information further increases the complexity of remote infrastructure damage assessment and condition monitoring (Alavi et al., 2015). In addition, for situations in which USAF assets operate out of pre-existing pavements, such as the occupied Iraqi airfields during Operation Inherent Resolve (2014), civil engineers would not have access to this infrastructure or data to inform their repair requirements.

Similarly, the Air Force Civil Engineer Center (AFCEC) investigated the use of insitu-sensors for airfield damage assessment during the infancy of their Rapid Airfield Damage Assessment System (RADAS) project. In 2013, AFCEC consulted the Stratech Group's iFerret™ tower system and Super Bullseye II™ damage and object scoring software. This pair performed change detection and analysis to indicate the presence of damage of foreign objects (Stratech Group, 2013). This approach allows for occupied airfields to be retrofitted and allow for automated damage detection. However, due to infrastructure requirements and operational considerations, this approach has been discontinued.

### ***Unmanned aerial vehicles.***

This category consists of both large unmanned aerial vehicles, such as the Northrop-Grumman surveillance drone, RQ-4 “Global Hawk,” as well as Small Unmanned Aircraft Systems (SUAS), and commercial off-the-shelf (COTS) and vendor builds using customer specifications. Similar to remote sensors, UAVs have been shown to be a viable solution to meeting infrastructure assessment requirements. As a proof of concept, numerous research teams have developed physical models and computer based algorithms for the assessment of pavements, as well as structural infrastructure via photographic

imagery obtained using UAVs (Ellenberg, Kotsos, Moon, & Bartoli, 2011; Eschmann, Kuo, Kuo, & Boller, 2013; Grandsaert, 2015; Henrickson, Rogers, Lu, & Valasek, 2016; Na & Baek, 2016; Sankarasrinivasan, Balasubramanian, Karthik, Chandrasekar, & Gupta, 2015; Shepherd & Storm, 2017c, 2017a, 2017b; Siebert & Teizer, 2014; S. Zhang, Bogus, & Lippitt, 2015; S. Zhang, Lippitt, Bogus, & Neville, 2016).

In 2015, an unmanned, fixed-wing aircraft system was able to capture road pavement imagery suitable for semi-automated Pavement Condition Index (PCI) processing. Despite incompleteness in his algorithm, Grandsaert's (2015) research was able to demonstrate that using SUAS to collect infrastructure data is a viable alternative to current Air Force Civil Engineer pavement evaluation methods. In similar studies, the degradation of natural infrastructure, such as soil erosion (Casella et al., 2016; Colomina & Molina, 2014; D'Oleire-Oltmanns, Marzloff, Peter, & Ries, 2012; Lindner, Schraml, Mansberger, & Hübl, 2016; Sinclair Community College, 2017), deforestation and natural resource management (Getzin, Nuske, & Wiegand, 2014; Getzin, Wiegand, & Schöning, 2012; Johnson, Smith, & Wescott, 2015; Messinger, Asner, & Silman, 2016; Sinclair Community College, 2017; C. Zhang & Kovacs, 2012), and natural disaster reconnaissance (Hu, Wu, & Tan, 2012; Iqbal et al., 2015; Xu et al., 2014; Yuan, Zhang, & Liu, 2015) have been demonstrated through the application of SUAS and computer algorithms. In addition, some State agencies – such as the Ohio Indiana Unmanned Aerial Systems Center – have also invested in drone technologies for precision agriculture, infrastructure assessments, and construction surveys, as well as search and rescue operations (Gallagher, 2017).

The United States Department of Defense has also been developing SUAS for military uses. Some of the earliest drones were collapsible systems that could be carried

in a backpack, such as the AeroVironment RQ-11 “Raven,” which was developed and fielded by the United States Army in 1999 (AeroVironment, 2018). In the mid-2000s, AFCEC began work on an aerial reconnaissance version of the RADAS project. This platform was designed to rapidly survey damaged airfields (within 90 minutes), thereby replacing the four-person teams required to manually conduct damage assessments. However, under the current approach, AFCEC has acknowledged that their proposed employment of SUAS usage does not conserve time and consistently requires additional time to survey, process data, and identify objects of interest (Filler & Diltz, 2016). The objective of the research was to provide the United States Air Force manpower, time, and resource savings, as well as improve object detection and quantification (Earth Imaging Journal, 2015; Echerri, 2015; Idaho National Laboratory, 2009).

Early prototypes of the RADAS incorporated catapult launched, hand launched, and rolling takeoff fixed-wing air vehicles. These SUAS were outfitted with video cameras, high-resolution cameras, Sonar, LIDAR, and Infrared sensors, as well as flood lights to enable night time operations. Over the course of the RADAS project’s evolution, the fixed-wing approach was abandoned in favor of a multi-rotor. In current use, AFCEC’s approach includes a fleet of octo-rotors, each equipped with a cooled, mid-wave infrared sensor. One of the biggest hurdles is leveraging the data such that desired outcomes may be achieved. A data analysis algorithm has long been in the works; in current practice, data must be analyzed manually (Filler & Diltz, 2016).

Due to the scope of the RADAS project, AFCEC asked the Air Force Institute of Technology (AFIT) to investigate alternatives as well as develop their own prototype. Beginning in the winter of 2017, seven graduate students began rapid prototyping of a

system that could survey an airfield, identify pavement damage as well as explosive hazards, and produce a minimum operating strip solution in under 90 minutes. Initial designs resembled that of the approach fielded by Shephard and Storm (2017), who utilized the Altavian F7200 “Nova”, fixed-wing air vehicle (**Error! Reference source not found.**), the “Fusion” MP22 modular sensor package, and “Flare” mobile ground control station to conduct a series of infrastructure assessments. Shephard and Storm’s research team surveyed two airfields and one highway overpass. Combining the individual flight times and processing time, the research team generated reports for a 290-acre airfield in 120 minutes and a 30-acre airfield in 15.5 minutes (Shepherd & Storm, 2017a, 2017b) using the Pix4D™ software. In addition, using the Altavian R8700 “Galaxy” octo-rotor (**Error! Reference source not found.**) to survey a seven-acre highway overpass and generate a report in 82.5 minutes (Shepherd & Storm, 2017c). Ultimately, the AFIT research team decided upon an approach similar to the RADAS current concept; however, they also incorporated elements from previous iterations. Their air vehicles and methodology are described in Chapter III and Appendix I. Small Unmanned Aerial Systems Components



**Figure 3. Altavian F7200 Nova (www.altavian.com)**





**Figure 4. Altavian R8700 Galazy ([www.altavian.com](http://www.altavian.com))**

***Unmanned ground vehicles.***

Akin to unmanned aircraft systems, unmanned ground vehicles (UGVs) are purely that, a vehicle operated on the ground without a human operator onboard. This category applies to both programmed robots as well as those controlled remotely via a ground station. Aside from their current military employment for munitions and explosive ordnance disposal, Carroll, Mikell, and Denewiler (2004) have demonstrated that UGVs may be used for force protection via perimeter monitoring and surveillance, as well as for providing security for exterior environments (materiel storage yards, arsenals, petroleum storage areas, airfields, rail yards, port facilities, etc.). Ultimately, the employment of UGVs enables the military, law enforcement, and other organizations requiring depot

security to reduce their manpower requirements, as well as provide security with the reduced threat to human life.

Similarly, Meeks (2016) demonstrated that UGVs may provide manpower savings in terms of time and human resources when used for storm sewer pipe condition assessment. Figure 5 depicts three representative images of Meeks' (2016) crack detection. Her research drew upon the work of Grandsaert's (2015) algorithm, through varied threshold intensity shifts, to identify storm sewer pipe cracking and distresses. Her research demonstrated that it is possible to complete infrastructure inspections using commercial off-the-shelf (COTS) UGVs and that the "photographic imagery collected was of sufficient quality and quantity such that [pipe cracking] could be detected" (Meeks, 2016).

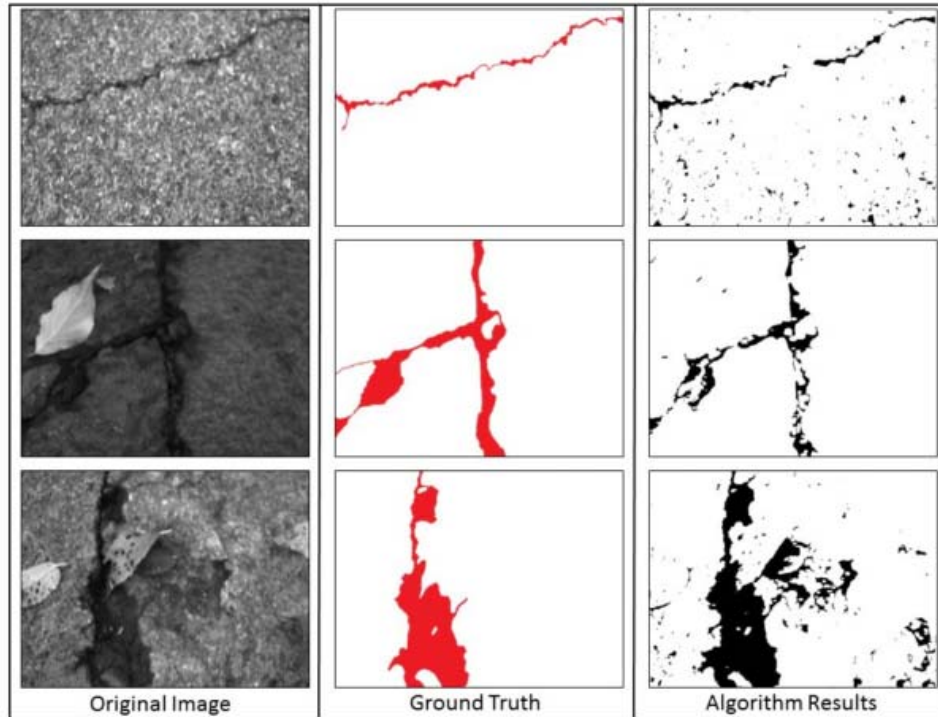


**Figure 5. Crack detection on three representative images (Meeks, 2016)**

Despite Meeks' (2016) work focusing on photographic imagery collected from a ground vehicle, her thesis contributes to constructing the foundation for this thesis. Akin to Grandsaert (2015), her research as well as this research employ drone technologies for the assessment and management of Department of Defense infrastructure and assets with the additional benefit of reduced manpower demands and improved security of civil engineer personnel.

While not autonomous or remotely piloted, for the previous two decades, the Ohio Department of Transportation (ODOT) has been fielding technologies to assist with their biennial paved infrastructure survey. As of March 2017, ODOT has added four pavement inspection vehicles to their inventory. One of the vehicles collects a series of still images

from forward, left, right, and rear facing high resolution cameras. Images are collected at a rate of 200 images per mile (per camera), or one image every 26.4 feet. These images are tied to Global Positioning Satellite (GPS) coordinates and are supplemented with an inertial measurement unit (IMU) which fills in gaps where satellite connection is unavailable (i.e., tunnels or dense city sections). This data is compiled and published in Environmental Systems Research Institute (ESRI) format, which is a geographic information systems (GIS) compatible software.

In addition to the high-resolution camera approach, two light-duty vehicles have been equipped with a 90-degree, sweeping spot laser. This sensor utilizes a technology similar to a miniature Light Detection and Ranging (LIDAR) device to obtain measurements of the pavement surface and is accurate to within 0.25 millimeters or less (Schleppi, 2018). Finally, within the previous three years, ODOT has commissioned a heavy-duty cargo van equipped with a higher-powered version of the light-duty vehicle's sweeping spot laser system. These latter three vehicles measure the surface profile of 28,000 to 30,000 of the state's 48,371 lane miles (Federal Highway Administration, 2000) of paved infrastructure per cycle. Compared to the high-resolution photo-van and other detection mediums, the data collected with this technology is substantial. For every assessment, 30 terabytes of storage space is required to house the profile data. In addition, ODOT has built a dedicated high-performance computer to handle processing profile data. Lastly, to process this data, ODOT's computer harnesses a 32-core processor and requires 3-to-6 days to compile the data. While a supercomputer may not be available at all USAF installations, it would make quick work of processing an airfield survey. For example, Edwards Air Force Base's primary runway is among the largest in the USAF inventory and

consists of 9.8 miles of pavement. This amounts to 0.0203% of the State of Ohio’s paved infrastructure. Thus, for the ODOT equipment to profile the Edwards AFB runway, it would require less than two minutes to process the data. Unfortunately, the presence of damage, UXOs, and bomblet fields exclude this approach as the vehicle would not be able to profile across upheaval, craters, or cross over explosive hazards.

**Table 2. Airfield Assessment Alternative Cost/Benefit Summary**

<b>Pro</b>	
Conventional Airfield Damage Assessment	Human presence
Wireless Sensor Array	Reduces manpower requirements, ensures CE personnel safety, instantaneous
Unmanned Aerial Vehicles	Reduces manpower requirements, ensures CE personnel safety, Geolocation accuracy
Unmanned Ground Vehicles	Reduces manpower requirements, ensures CE personnel safety, Geolocation accuracy
Manned Ground Vehicles (ODOT)	Reduces manpower requirements, highly precise data
<b>Con</b>	
Conventional Airfield Damage Assessment	Time consuming, hazardous to ADATs, potentially inaccurate
Wireless Sensor Array	Susceptible to distortion, transmission medium vulnerable to damage, expensive to install
Unmanned Aerial Vehicles	Susceptible to climatological conditions, data transfer may degrade data quality
Unmanned Ground Vehicles	Requires numerous passes to survey runway, incompatible with craters and explosives
Manned Ground Vehicles (ODOT)	Incompatible with craters and explosives, Sophisticated data processing requirements

### **Manpower requirements**

In terms of identifying alternative methods for airfield pavement evaluation, this literature review would not be complete without considering the manpower ramifications of each proposed system. Serving as a baseline with which to measure efficiencies, the first method to be assessed is the current state of Air Force airfield damage assessment.

#### ***USAF status quo.***

Following an attack, the EOC (or DCC) will need to have been activated. The average installation requires that the following civil engineer specialties are represented:

one EOC Manager (Civil Engineer Officer or Civilian Equivalent), one Fire Emergency Services representative or civilian equivalent, one Engineering Technician or civilian equivalent, and one radio/phone operator (any civil engineer). At a minimum, the EOC requires four CE personnel (refer to Figure 12 in Appendix C. Emergency Operations Center Team Organization). For installations requiring that the alternate EOC be activated simultaneously, this number increases to eight. In addition to the EOC, the Civil Engineer Squadron's (or Group) Unit Control Center (UCC) will also be activated. The CE UCC is the main hub for dispatching ADAT and DART teams, as well as mobilizing installation recovery assets and resources. At a minimum, the CE UCC requires the following personnel: one UCC Manager (Civil Engineer officer or civilian equivalent), one Operations Engineer or civilian equivalent, and one to two radio/phone operators (any civil engineer). Thus, the CE UCC manpower staffing requires – at minimum – four personnel. Irrespective of the alternative approaches described in subsequent sections, these manpower requirements remain fixed; eight personnel will always be required as a collective summation of the EOC and CE UCC manning requirements. As such, in the alternative approaches that follow, only the ADAT manpower requirements will be described.

For the majority of installations, personnel assigned to ADAT and DART teams fulfill both roles. This arrangement is driven largely by manpower, equipment, and asset availability. In general, three to four, four-member teams are standing by for the Installation Commander's order to begin recovery actions. Thus, the combined manpower requirements from the Civil Engineer Squadron (or Group) ranges between 17 and 28 personnel. Of note, this only accounts for one shift of civil engineers manning either the

EOC, UCC, or ADAT/DART duties. Therefore, in order to support 24-hour operations, these numbers will need to be doubled (at least). However, as it pertains to conducting the damage assessments following an attack, only one shift of engineers should be required if the 4-hour recovery of airfield damage standard is to be upheld (Air Force Civil Engineer Center, 2015a).

***Wireless sensor array.***

For the scenario in which the airfield has been constructed with Alavi et al.'s (2015) piezoelectric transducer powered in-situ sensors, the manpower requirements change significantly. The manpower demands of the EOC and UCC remain unchanged; either four personnel each or two EOCs, thus requiring 12 personnel. The difference lies within the airfield assessment; due to the sensors performing the job of the ADATs, the aforementioned three to four teams of three to four personnel will not be required to leave the CE compound. Instead, damage location and information will be wirelessly transmitted to either the EOC or UCC (or both) throughout the bombardment. Therefore, the damage information is available immediately; other units will not be required to call in phase one airfield damage, thus enabling them to direct their efforts to other endeavors.

A few significant roadblocks emerge from this approach: UXOs, sensor system status, and unintelligible data (electronic disturbance). The one factor that this approach does not consider is the identification or classification of UXOs. Therefore, to enable CE repair crews to mobilize, a visual inspection will still be required such that UXOs may be identified and cleared. Finally, this approach relies on the sensor array to be operational following the attack and that the data transmitted is clear enough such that candidate MOSs may be identified. Of note, Alavi et al.'s (2016) research focused on sensors that were

positioned within asphalt pavements that were self-powered by the mechanical loading of vehicle traffic. Within the context of airfield pavements, mechanical loading may occur too infrequently to be feasible for airfield pavement health monitoring. Due to these shortcomings, it may be said that the wireless sensor array does not save manpower demands. However, it may serve as a means to expedite the candidate MOS selection process via the instant data feedback immediately following an attack.

***Unmanned aircraft systems and ground vehicles.***

Similar to the manpower composition using the wireless sensor array, the employment of unmanned air and ground vehicles require the same EOC and UCC staffing. In addition, an SUAS approach to airfield damage assessment would require significantly less manpower to accomplish versus the traditional ADAT method. In the methodology that follows, the method described herein requires only four personnel to operate the fixed-wing SUAS: one Ground Control Station (GCS) operator, one Safety Pilot (SP), and two technicians, whereas the hex-rotor requires three personnel (one GCS Operator, one SP, and one tech) (refer to Table 27. AFIT SUAS 217m Airfield Assessment Times & 3000m in Appendix K. Baseline Metrics and Civil Engineer Officer Statistics). This effectively cuts ADAT team requirements by 67-75%. Furthermore, by only requiring a GCS operator and an SP, the employment of UGVs further reduces the boots-on-the-ground presence by 83-88%. Comparatively, the Sinclair research team only required three personnel to operate their SUAS: one GCS operator, one safety pilot, and one observer/technician. This approach reduces ADAT requirements by 75-81.3%.

Conversely, the current concept of the RADAS project may increase ADAT presence by 200-400%. This is driven by the quantity of air vehicles being fielded



simultaneously (16 octo-rotors). To effectively pilot an SUAS, it is highly recommended that a dedicated ground control station, operator, and safety pilot must monitor each air vehicle individually. However, given adequate ground control station configuration and team coordination, a dual ground control station, with dedicated operators, may control all 16 of the octo-rotors simultaneously. This provides similar manpower savings of 67-75% compared to this thesis.

Lastly, with respect to the manned ground vehicles fielded by ODOT, at least two operators are required per vehicle. In addition, at least one dedicated technician will be required for data processing and support functions. Thus, if only one vehicle is fielded, a total of four personnel will be required. However, if the ODOT method is to be applied with traditional airfield damage assessment methods, two vehicles will be required, thereby requiring an additional vehicle operation pair and data analyst, which amounts to seven personnel. Strictly comparing the number of personnel in the field, this method saves 42-56% of manpower requirements.

**Table 3. Airfield Assessment Alternatives Summary**

	Manpower*	Time Requirement (3km Rwy**)	Data Processing (3km Rwy**)	Data Analysis (3km Rwy**)
Conventional Airfield Damage Assessment	12-16	20-30 min	N/A	5-10 minutes
Wireless Sensor Array	0	Instantaneous	Instantaneous	45-minutes**
Unmanned Aerial Vehicles	3	90-105 min	3.2-hours	45-minutes**
Unmanned Ground Vehicles	3	No Data	No Data	No Data
Manned Ground Vehicles (ODOT)	2	20-30 min	15-seconds	45-minutes**

\*Excludes EOC and UCC personnel

\*\*Baseline and experimental data in this thesis (see Chapter IV)

## **Market analysis**

A market analysis was performed on the commercial SUAS market to identify potential candidates to meet Air Force airfield damage assessment requirements. For a complete breakdown of unit costs (including subsystem components, software, and labor fees), refer to Table 16 (Appendix I).

### ***Fixed-wing air vehicles.***

The complete system used in this thesis required a fixed-wing air vehicle (Skywalker X8), a catapult launcher, a Sony HD Block Camera, communications equipment, and a ground station. Excluding assembly, tuning, and configuration labor costs, this thesis's fixed-wing air vehicle amounted to \$7,034.10. Excluding batteries, an imaging device, and shipping and handling fees, a ready-made Skywalker X8 costs \$7,455.97 ("UAV Systems International: Skywalker Ready-to-fly Drone," 2018). The Altavian air vehicle used by Shepherd and Storm (2017) (the F7200 "Nova") ranged from \$15,180 to \$19,260 (price includes Altavian's ground station, software, and sensor package) (Altavian, 2018).

### ***Vertical Takeoff and Landing air vehicles.***

The Vertical Takeoff and Landing (VTOL) air vehicle used in this thesis (Tarot hex-rotor) cost \$6,105.86. A comparable, ready-to-fly multi-rotor using either a DJI S800, S900, S1000 or the CineStar 8 frame (including the same ground station, software, gimbal, and imaging device used in this thesis) ranges between \$6,965.21 and \$7,975.21 (www.RC-Drones.com, 2018). The Altavian multi-rotor (the R8700 "Galaxy") used by Shepherd & Storm (2017) cost \$15,100 (price excludes assembly, tuning, and shipping

fees) (Altavian, 2018).

## **Summary**

This literature review has identified a few useful themes with respect to measuring the efficacy of employing remote sensing technologies for airfield damage assessment. Included in the body of knowledge was evidence supporting infrastructure condition monitoring through self-powered sensor arrays. In addition, numerous research teams demonstrated the ability of aerial as well as ground-based unmanned vehicles with respect to condition assessment and data collection. Moreover, each of the aforementioned mediums examined in this review provide solutions for organizations to conserve their manpower while remaining true to their mission requirements and directives.

Unfortunately, based upon the body of knowledge, the area that requires additional investigation is remote airfield damage assessment in the post-attack environment. Numerous studies surveyed the aftermath of natural disasters, identified the presence of deforestation and landmass topography changes due to erosion, and detected the presence of cracking and distresses in infrastructure. However, the area that requires further examination is the ability of remote sensing technologies to provide actionable information pertaining to the location, quantity, and scope of recent airfield damage, as well as the presence of explosive hazards for the generation of a minimum airfield operating surface. Furthermore, while these technologies have proven successful in identifying objects of interest, they have not been used to survey a large area and identify UXO and other kinetic threats under considerable time constraints. Moreover, each of these technologies

presented were tested irrespective of the time required to unpack, assemble, launch, conduct the mission, recover, and process their data.

In the methodology that follows, this thesis will establish the baseline performance level of conventional airfield assessment methods and survey a runway using SUAS to identify and geo-locate the presence of UXOs. Table 4 summarizes conventional airfield assessment measures identified in AFPAM 10-219, Volume 4. In addition, the measures this thesis will investigate are provided.

**Table 4. Airfield Assessment Criteria Summary**

<b>Conventional Airfield Damage Assessment Measures</b>	<b>Baseline &amp; SUAS Airfield Damage Assessment Measures</b>
Airfield Assessment Time	Equipment Assembly & Airfield Assessment Time
MOS Plotting Time	Data Processing & Analysis Time
Quantity Craters	Crater, Spall Field, UXO, & Bomblet Field False Positives
Quantity Spall Fields	Crater, Spall Field, UXO, & Bomblet Field False Negatives
Quantity UXOs	Crater, Spall Field, UXO, & Bomblet Field Mis-Identification
Quantity Bomblet Fields	Crater, Spall Field, UXO, & Bomblet Field Sizing
Crater, Spall Field, & Bomblet Field Sizing	Crater, Spall Field, UXO, & Bomblet Field Locating
Crater, Spall Field, UXO, & Bomblet Field Locating	Manpower Requirements

### III. Methodology

This chapter discusses the four aspects of the research method. First, the establishment of baseline metrics for conventional airfield damage assessment – including the sizing and locating of craters, spall fields, and Unexploded Ordnance (UXO) – is discussed. This section includes a description of the test subjects who were evaluated to produce the baseline metrics, an overview of what the subjects were evaluated on as well as how they were evaluated, and establishes the status quo. Second, Civil Engineer damage assessment performance is measured using a pre-existing set of aerial imagery and two distinct analysis platforms. This section includes a description of what levels of performance are measured, a description of how they are evaluated, presents summary statistics for each of the separate damage assessment methods, and single-tail hypothesis testing to compare their performance against the baseline metrics. Third, evaluation methods for using SUAS imagery will describe object identification accuracy – for false positives as well as false negatives – and define time requirements to complete a damage assessment. Finally, assessment of manpower requirements, costs, and savings related to SUAS use will be described. In addition, a cost breakout of required equipment and consumables, as well as comparable COTS systems, will be provided.

#### **Acquiring baseline airfield damage assessment metrics**

To produce a relevant model for implementing positive change in the current airfield damage assessment techniques, an understanding of the status quo is required. To achieve this, anonymous test subjects from the enlisted Engineering and Explosive

Ordnance Disposal career fields were sampled at the Silver Flag Contingency Training site, located at Tyndall Air Force Base, Panama City, Florida. The EOD technicians and Engineers – alternatively referred to as “engineering assistants” or “EAs”– were evaluated while participating in a field exercise during their triennial Silver Flag encampment. Every three years, all enlisted and commissioned Civil Engineer specialties travel to a Silver Flag training site to sharpen their contingency skills and rehearse base recovery procedures in the post-attack condition. For this study, three encampments – composing nine, four-person teams – were observed on 10 August 2017, 28 September 2017, and 12 December 2017. Teams were evaluated by subject matter experts (SMEs) from their respective specialty, monitored for proficiency, and instructed in the pursuit of further contingency response skill development.

*Evaluation focus areas.*

The EAs were evaluated using three attributes. The first attribute was the time required to respond, assess, record, plot damage and UXOs on an airfield map, and determine the optimal MOS solution(s). An assumption was made that the EAs had already received the aircraft operational requirements from the Crisis Action Team (CAT) prior to mobilization of ADAT assets. The second attribute was the accuracy of identifying craters, spalls, and UXOs. This also included the incidence of false positives (i.e., the misclassification of debris as a UXO or the incorrect sizing of a crater or spall field) and false negatives (missing airfield damage or explosive hazards). Lastly, the third attribute described the accuracy with which findings were identified in relation to their position on the airfield map. Location errors have the potential to produce an incorrect operating picture of the scale and quantity of damage, debris, and UXOs, as well as their positions

relative to one another on the airfield. Incorrectly locating objects may render MOS plots, and eventual recovery procedures as well as material quantities and time estimates, insufficient or vastly suboptimal. Similarly, the EOD technicians were evaluated on their ability to 1) identify the presence of explosive hazards, 2) correctly classify the hazard identified, and 3) accurately identify the location and/or scale/quantity of the hazard present.

To establish baseline metrics, the study of enlisted civil engineers produced five quantitative metrics and one qualitative metric. From the first attribute – time – the baseline metric will be the summation of the average ADAT run and MOS plotting components. This metric accounts for the range of time required to conduct an airfield damage assessment using the conventional approach. A limitation of the baseline data set lies within the omission of exact ADAT airfield assessments. The test administrators annotated that, on average, ADATs took no less than 20 minutes and no longer than 30 minutes to complete the 3,000-meter route (Abrego & Moore, 2017). In addition, the time required to produce a MOS solution was not provided. However, within the context of the conventional airfield damage assessment methodology, damage and explosive hazards are communicated to the EOC/UCC during the assessment. Therefore, all identified damage and objects are known to the MOS plotting team upon completion of the ADAT run. Thus, identifying candidate MOS solutions adds no more than five minutes to the total time.

The second attribute – identification accuracy – produces three metrics: correct identification of damage and/or objects and debris, quantity of false positive identifications, and quantity of false negative identifications. The correct identification metric is comprised of each of the nine ADAT exercises' objects. A binary value was recorded for

this measure, either if the team correctly identifies the object in question, it is marked correct, whereas if they identify the object as anything other than what the Silver Flag test cards specified, it is marked as an incorrect identification. For the second and third metrics from the identification accuracy attribute, false positives occur when 1) pavement damage (i.e., a crater or spall field) is misidentified as an explosive hazard or 2) a UXO is identified that was not provided by the test administrators' test cards. Similarly, the false negative metric describes the ADATs' failure to identify explosive hazards (UXOs and bomblet fields). The occurrence of pavement damage false positives – the identification of damage that does not exist or multiple counting of the same damage feature – is eliminated via the use of either a single ADAT team or ADAT teams assessing predefined sectors. As such, this thesis does not acknowledge pavement damage false positives. Similarly, with the exception of subsurface damage (Figure 6), pavement damage false negatives do not occur. Data in Chapter IV as well as Appendix G supports this claim. Due to limitations in the airfield dataset used in this thesis, subsurface damage is not addressed.





**Figure 6. Subsurface Damage**

The third attribute – location accuracy – produces two metrics: conformance with assessment solution and conformance with GPS accuracy. At the test administrator’s admission, during the first five evaluations, explosive hazard coordinates were not recorded (Abrego & Moore, 2017). Therefore, for these metrics, damage features and explosive hazards will be measured separately. In the latter four evaluations, coordinates were provided for all objects included in the assessment, thus explosive hazard locations may be measured over 16 of the 36 total explosive hazards.

Finally, position accuracy versus GPS will be measured individually for centerline positioning of craters and spall fields, centerline positioning of explosive hazards, left-to-right (of the runway centerline) positioning of craters and spall fields, and left-to-right positioning of explosive hazards. Enlisted civil engineers use a combination of the pavement reference marking system (PRMS) and approximation to derive their coordinates. In addition to edge markers, typical airfields are paved in 20-foot square

sections. The pavement seams, therefore, allow for fairly accurate approximation to occur. By contrast, civilian GPS systems have a horizontal accuracy of 4.0 meters and may be as precise as 3.0 meters in some locations without the addition of corrective devices (Department of Defense & NAVSTAR, 2008). Therefore, the occurrence of conventional damage and explosive hazard positioning will be compared with standard GPS accuracy.

Due to the nature of the MATLAB™ GUI and the 2D ortho-mosaic (to be described in subsequent sections), all airfield images used in this thesis are timestamped and positioned within space via the telemetry logs recorded by each air vehicle's autopilot. Previous AFIT experimentation has determined that an air vehicle using the Pixhawk autopilot and GPS unit may be located to within 3.0 meters at any given time. However, the spatial information of images is subject to instantaneous body angle distortion and time delays that further decrease the confidence level of the precise location of an object. Thus, for each pixel represented on screen using the MATLAB™ GUI and the Pix4D™ software, objects and damage indicated using onscreen commands elicits an xy-positioning accuracy within 10 meters. However, with the inclusion of surveyed Ground Control Points (GCP), Pix4D™ is capable of locating features within the degree of accuracy of the GCPs.

#### ***Evaluation procedure.***

Due to the need to keep airfield damage assessment testing strict, the ADAT runs are conducted separately from the other civil engineer exercise scenarios. Thus, the EAs and EOD Techs being evaluated do not experience any interference or distraction from other activities that may lead to incorrect measurements or reports. Once the ADAT has been staged – as would occur under real-world conditions – the test administrators call into the mock EOC to begin the exercise. Once the “All Clear” message has been provided, the

ADAT(s) disembarks from their staging location in a six-passenger, light-duty pickup to begin the airfield assessment. Upon arrival, the front passenger manages navigation and communications for the driver, whereas the rear passengers (one EA and one EOD Tech) begin identifying objects and damage along the runway. All objects and damage are annotated in a log book and radioed back to EAs manning the EOC such that MOS plotting may begin as soon as the ADAT(s) complete their route.

Upon completion of the ADAT run, the EAs inside the EOC begin plotting the damage on a scaled airfield map, identifying areas in which the EOD Techs need to neutralize explosive hazards, and determining if an aircraft arresting system may need to be installed (based upon aircraft operational requirements). In addition, this plot identifies areas in which the pavement repair team should focus to make the fewest number of repairs such that the runway can return to operational status in the least amount of time. Throughout the initial response and mobilization, airfield assessment, and MOS plotting, the EA and EOD evaluators annotate each team's strengths and weaknesses. At no time during the evaluation are teams permitted to ask for additional information regarding the quantity, scale, or placement of objects and damage along the runway surface.

***Evaluation parameters.***

During the baseline study, test facilitators placed a total of eight objects on a 3,000-foot section of runway. Typical assessment configurations include four damage locations and four explosive hazards. An example scenario includes two craters, two spall fields, three UXOs, and one bomblet field. The average time to assess the runway surface ranges between 20 and 30 minutes. Any surveys shorter than this range tend to elicit high false negative rates, whereas surveys in excess of the 30-minute mark, while detailed, tend not

to provide any additional benefit. The relationship between these parameters will be described in Chapter IV. Each of the nine teams evaluated during the three encampments were comprised of two EOD Techs and two EAs – each ranging in skill levels three (novice) through seven (relative expert). The six-baseline metrics will be essential in evaluating the efficacy of aerial images for airfield damage assessments, which will be discussed in the following section.

### **Civil engineer officer testing and evaluation procedures**

Using data gathered during the AFIT, Small UAS Test and Evaluation (SENG 651), summer 2017 capstone experiment (refer to **Error! Reference source not found.**), civil engineer officers were evaluated on their ability to identify and locate a series of craters and UXOs on a digital airfield map using two disparate versions of the same data set. Compared to the enlisted performance evaluated in the previous section, Civil Engineer officers are not subject matter experts on airfield damage assessment. Instead, they possess a generalized knowledge of each specialty within the career field. However, for the two methods that follow, specialized training on airfield damage assessment is not required; instead, general knowledge of airfield pavements and explosive ordnance is. In addition, where the enlisted civil engineers were evaluated for assessment speed and precision, the officer assessments did not include time constraints. As such, assessment times were normally distributed.

The first expression leveraged a series of still images collected by a 1080p Sony Block Camera mounted to the underside of a Skywalker X8 (Fpvmodel, 2017) SUAS flying at an altitude of 40 meters. Test subjects reviewed a sequence of images within a custom MATLAB™ script written by Allen (2017). The Graphical User Interface (GUI) provided test subjects with the ability to advance through images, identify UXOs, and create polygons outlining craters and/or spall fields. The net result produced Mission Planner™ waypoints for a Tarot T960 hex-rotor (Helipal, 2017b) SUAS to fly as well as produce a MOS superimposed on a satellite image of the Wright-Patterson Air Force Base Area B. The MATLAB waypoint file enables the generation of a detailed inspection of UXOs. One limitation of this approach is the final image resolution viewed by the user. Through the inclusion of the Epiphan™ Av.io 4K capture card, images were transmitted from the air vehicle at full resolution. However, due to the size of the ground control station monitor, images were scaled down from 1080p (1920x1080) by 20% within the GUI. Resulting image resolution was approximately 864p (1536x864). This allows users to view images alongside on-screen commands.

The second dataset was built upon the former, based upon the waypoints generated by the MATLAB™ GUI during the original airfield assessment. Thus, the second data set's images were dependent upon the image analysis of the first data set. This approach leveraged a two-dimensional (2D) ortho-mosaic of the runway constructed through a series of still images collected using a Sony α6000 camera, which was mounted to the underside of a Tarot hex-rotor flying at an altitude of 80 meters. Unlike the fixed-wing image resolution, airfield data was transferred via micro-USB on the ground. This allowed the 24.3-megapixel image resolution to be maintained, resulting in a 21.4-megapixel image

(37,014 x 5,801) with a horizontal resolution of 96 Dots Per Inch (DPI), and a vertical resolution of 96 DPI.

Air vehicle configurations for both the Skywalker X8 and the Tarot hex-rotor will be discussed later in this chapter as well as in Appendix I. Small Unmanned Aerial Systems Components. Test subjects were provided with the ortho-mosaic (produced using the Pix4D™ software). Using the output image file, subjects indicated the presence of damage and UXOs as they appeared. Due to licensing restrictions, civil engineer officer evaluations were limited to the 2D ortho-mosaic sans the Pix4D™ software. As such, the 2D map was viewed as an image file and manipulated manually with a pointing device. When assessed using the Pix4D™ software, objects identified on screen would have the same level of GPS accuracy as those identified using the MATLAB™ GUI. This is enabled by the software's integration of telemetry logs collected during the hex-rotor's flight and aerial imaging.

Finally, between both CE officer analysis procedures, test subjects did not perform practice trials or repeat trials. Prior to evaluation, subjects were provided 5 to 10 minutes of instruction on how to use each interface as well as provided with the desired outcomes. For this analysis, the research sought to exclude the effects of learning-curve and assess the performance of each analysis medium. Moreover, subjects were not placed under any time constraints; instead, once participants felt satisfied with their analysis of the airfield imagery, they self-terminated the evaluation. It is the researcher's opinion that additional trials would not improve object detection or identification. Furthermore, it is hypothesized that time constraints would decrease object detection performance. Lastly, the author hypothesizes that, due to the generalized skillset of civil engineer officers (as well as their

lack of familiarity with the airfield prior to imaging), their UXO and damage detection proficiency will be less than the EAs and EOD Technicians.

***MATLAB™ GUI analysis procedure.***

For the first look at the airfield data, after a 5-minute introduction to the interface, subjects operated two MATLAB scripts, “Main.m” and “analyzeFrames.m” (Appendix L. MAIN.m MATLAB™ Script and Appendix M. AnalyzeFrames.m MATLAB™ Script, respectively). The former served as the bedrock for the GUI; it built the register for onscreen commands and ingested the telemetry and image pairs. The latter script used the visual display and a mouse click to identify features associated with telemetry information. In addition, this script reached externally to Google Earth™ to produce an airfield map with pins and polygons indicating the presence of damage or explosive hazards.

When images and telemetry logs were loaded, subjects advanced through the dataset using the following onscreen commands: “Previous Frame”, “Next Frame”, “UXO”, “Crater”, “Generate Waypoints”, and “Locate MOS.” The first two options advanced or reversed the frame-telemetry log pair. These commands were used at will until the subject was comfortable with their assessment. The “UXO” button produced a popup window – mirroring the current image – with a new menu of options: “Delete Placement”, “Confirm Placement”, and “Go Back.” On this screen, the analyst hovers their cursor over the object, single-left clicks, and then chooses the class of ordnance from a dropdown menu. When complete, the subject deletes the placement, confirms placement, or – should they have selected the UXO button in error – returns to the main GUI. This process is repeated for each object identified. One of the limitations of the MATLAB GUI is that the UXO screen can only record one input at a time.

Similarly, when subjects encountered a damaged section of pavement, they selected the “Crater” button. This menu operates in much the same fashion as the UXO screen; however, it has its differences. The menu options now include: “Confirm Placement”, “Cancel Last P[oin]t”, and “Go Back.” Similar to the UXO screen, subjects hover their cursor over an aspect of the damage and single-left click to place a pin. However, in the Crater screen, subjects may continue to add pins until they have created a polygon surrounding the damage. When subjects are satisfied with their placement, they may click “Confirm Placement” or – if they have made an error – they may remove a point or return to the main screen. This process is also repeated for each damage location until the subject is confident in their airfield assessment.

When subjects have completed their UXO and crater detection and geo-location, they single-left click the “Generate Way Points” button. This produces a field requesting an altitude for the hex-rotor to fly. Finally, subjects single-left click the “Locate MOS” button. The GUI then automatically produces an image of the airfield and overlays the indicated damage and UXOs and produces a rectangle indicating the placement of a MOS. This rectangle is based upon MOS dimensions that have been hardcoded into the script and is optimized via particle swarm optimization. The evaluation is over when the subject has produced a MOS plot. At this point, the total time to analyze the frames and produce a MOS is recorded. Additionally, the test proctor annotates correct UXO and crater/spall field placements, false positives, and false negatives on a test card. For the purpose of this thesis, the only metrics that were considered were the time to analyze, correct identification of objects, and number of UXO false negatives. Due to test subject unfamiliarity with airfield conditions prior to placement of objects, false positive rates would be artificially



high. In numerous instances, airfield image analysts – both for the MATLAB GUI and the 2D ortho-mosaic – identified rust spots and discolored pavement as damage or FOD. It is the researcher’s opinion that, under real-world conditions, analysts will be keenly aware of the state of their runway surfaces prior to attack. As such, the occurrence of false positives would be significantly lower than identified in this thesis. For further details regarding the MATLAB GUI procedures, refer to

Appendix H. Civil Engineer Officer Evaluation Protocol.

***Ortho-mosaic analysis procedure.***

For the second dataset analysis, the approach is far more user friendly than the MATLAB GUI. Due to licensing limitations, subjects were not provided with a copy of the Pix4D™ software with which to analyze images and identify objects. Instead, the images collected from the hex-rotor were stitched together using telemetry logs, point clouds, and common features to produce a 2D ortho-mosaic in .jpeg format. Compared to the ODOT data processing system, the computer that produced this image was equipped with an Intel® i7-6700, 2.60GHz processor, with 32 gigabytes of random access memory, and an Intel® HD 530 graphics processing unit. This device required 14 minutes to stitch 46 images into a 2D ortho-mosaic.

This approach allows virtually any computer to access the file – as opposed to the MATLAB GUI that requires a license of MATLAB 2016b (in addition to various graphics and analysis add-ons) – thereby making the 2D ortho-mosaic a more versatile tool. In analyzing the ortho-mosaic, subjects zoomed in on the image – either using the scroll wheel on their pointing device or using onscreen commands – to an average zoom level of 250% and hovered their cursor over objects of interest. The maximum zoom level used was 350%

magnification; beyond this level of zoom (up to 500%), image resolution did not improve any further and resulted in users losing their frame of reference within the ortho-mosaic. In the same fashion that the test administrator annotated progress during the MATLAB trials, subject object detection was similarly annotated on a test card. The assumption with this approach is that, had Pix4D™ been used, objects could be pinned the same as the MATLAB GUI and a Python™ script could be run concurrently such that a similar MOS plot could be drawn using Google Earth™. However, for this thesis, the only factors considered were: time to analyze, correct identification of objects, and false negatives. For the same reason provided in the MATLAB approach, false positives were not analyzed; despite the higher image resolution provided by the 2D ortho-mosaic, subjects lacked the familiarity with the runway surface to distinguish damage or UXOs from existing oil and rust stains or known pavement distresses.

#### ***Civil engineer officer hypothesis testing.***

Upon completion of CE officer performance measurement using the MATLAB GUI and the 2D ortho-mosaic, hypothesis testing is conducted to measure relative performance. The three CE officer metrics are measured against 1) the corresponding baseline metric and 2) the corresponding metric of the opposing analysis method (i.e., MATLAB versus the 2D ortho-mosaic). The first series of hypothesis tests use single-tail t-tests to compare performance of the experimental approaches to the control (baseline metrics). The second set of hypothesis tests use single-tail t-tests to compare performance of the experimental approaches against one another (i.e., MATLAB versus the 2D ortho-mosaic).

#### ***Summary and metrics.***

This comparison sought to identify the ideal amount of processing time and quantity of images commensurate with a fast, accurate, and reliable airfield damage assessment and eventual MOS plotting. In addition, the difference between the Sony Block Camera (MATLAB GUI) and the Sony  $\alpha$ 6000 (2D ortho-mosaic) indicate whether greater pixel density and/or camera resolution results in greater object detection.

These tests produce the following three metrics: 1) the average time required to conduct an airfield assessment, 2) correct identification of damage, explosive hazards, and debris, and 3) quantity of explosive hazard false negatives. Due to limitations previously described, civil engineer officer subjects did not have familiarity with the runway surface at the time the airfield images were collected. As such, false positive detection would be artificially inflated; therefore, the false positive metric was not observed. In future examinations, there are two alternatives to allow for the inclusion of this metric: 1) scan the airfield prior to object placement and allow analysts to review the pavement's preexisting conditions, or 2) utilize test subjects familiar with pavement conditions prior to object placement. In addition, civil engineer officer subjects are limited to the geo-location accuracy of the airfield images. Therefore, location accuracy metrics were not measured against their performances.

The first metric evaluates the sum of the average time required to complete the digital assessment and the SUAS operation component times that were obtained during the SENG 651 capstone experiment (Appendix K. Baseline Metrics and Civil Engineer Officer Statistics). The second metric measures accuracy of the civil engineer officers' findings (i.e., correct identification of a crater versus a UXO versus FOD). Lastly, the third metric measures the rate at which false negatives present themselves in relation to the amount of

time spent analyzing airfield imagery.

### **Air vehicle configuration**

In the section that follows, descriptions, specifications, and the applications for each of the components of the SUAS used to collect data in support of the thesis have been provided. The rationale for including each piece of equipment is discussed as well as how each component contributes to completing the research objective. Refer to Appendix I. Small Unmanned Aerial Systems Components for complete descriptions of the SUAS components and Table 16. SUAS Equipment Cost Summary for a cost summary sheet.

#### ***Air vehicles.***

As previously indicated, two distinct SUAS platforms were used: a fixed-wing airframe and a multi-rotor airframe. The total system, which is referred to as the “Pave Scout System,” incorporates both air vehicles as well as their respective ground stations. The fixed-wing air vehicle is a custom Skywalker X-8 build (Fpvmodel, 2017), whereas the multi-rotor is a custom hexa-copter (six, non-coaxial propellers) built on a Tarot T960 frame (Helipal, 2017b). The Pave Scout mission is broken down into two phases: survey and inspection. The Skywalker fulfills the survey mission by rapidly flying the length of the runway(s), relevant taxiway(s), and parking apron(s). Data collected by the Skywalker is then used to develop a constellation of waypoints for the Tarot hex-rotor to inspect. Phase two is a detailed assessment of areas identified during the previous phase. The following are configuration and mission parameters for each of the airframes.

The Skywalker X-8, “Flying Wing” (Figure 7) is a commercial off-the-shelf

(COTS) ‘delta-wing’ shaped lifting body that is readily available through a multitude of online vendors. With a wingspan of 2.12 meters, the Skywalker employed in this thesis has been modified for greater control and in-flight stability. Structural modifications of note include stiffened wing spars, elevators, and winglets. The propulsion system consists of a Turnigy G46 brushless, outrigger electronic 670 kV motor and 13x7 foldable, pusher propeller. The sensor package is a Sony HD Block Camera that has been mounted forward facing at a 60-degree downward pointing angle (**Error! Reference source not found.**) The interior has been customized for mounting Lithium-Polymer (Li-Po) batteries, communications components, and optimizing the air vehicle’s center of gravity. Lastly, this application of the Skywalker X8 does not call for a landing gear. The research team determined that, in the post-attack condition, the airfield surface may not be conducive to rolling takeoffs or landings. Therefore, a catapult assisted takeoff (Figure 9) and “belly landing” approach was implemented. Further fixed-wing air vehicle configuration information can be found in Appendix I.



**Figure 7. Skywalker X-8, "Flying Wing"**



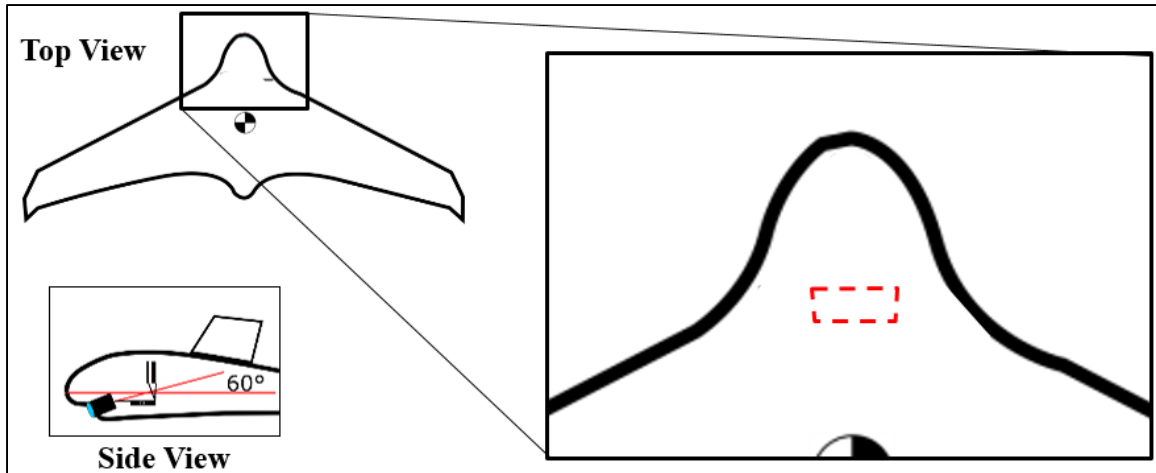


**Figure 8. Skywalker X-8 Camera Mount**



**Figure 9. Skywalker Catapult Launch Apparatus**

The objective of the fixed-wing airframe is to rapidly launch a stable platform for

aerial imaging. It must be power efficient for sufficient endurance and be durable for multiple launches and recoveries. In addition, data collected must provide an image resolution that allows accurate object detection. For this thesis, the minimum image resolution requirement is 720p (1,280x720). Lastly, individual component times (assembly, system checkout, launch, mission, and data collection), should amount to a cumulative time less than the status quo for an airfield surface of 3,000x50 meters. The Skywalker X8 fits this description perfectly; it is light, stable in-flight, and enables GCS operators to gather the preliminary HD video footage necessary to produce the waypoints required for phase two inspections. This air vehicle is flown at an airspeed of 17 meters per second and is operated at an altitude of 40 meters above the airfield surface.

If the airframe and catapult launcher are assembled and systems checked independently – using a crew size of four (one GCS operator, two technicians, and one safety pilot) – assembly and systems checkout requires 12 minutes to complete (refer to Appendix N). Launching the vehicle requires a safety pilot (SP) and a GCS operator. From the time of launch to achieving stable flight at an altitude of 40 meters, this step in the survey phase takes 30-45 seconds. Once stable flight has been achieved, the SP switches the air vehicle over to “Auto Mode” and the pre-planned flight pattern will be executed in accordance with the GCS Operator and Mission Planner’s™ instructions.

As the Skywalker navigates the pattern, the Sony Block Camera transmits a live preview of the airfield surfaces to the secondary GCS operator using the Connex HD transmitter and receiver (Amimon Ltd., 2016), as well as to the AV.io 4K video capture card. As objects appear within the field of view, the secondary GCS operator clicks – anywhere in the frame – to begin capturing still images of that position and moment in



time. The Sony camera continues to capture images at a rate of 0.14 seconds/image, producing an overlap of 40%. This procedure continues throughout the duration of the flight until all affected areas have been surveyed and/or the Skywalker no longer has sufficient battery voltage (3.3 volts/cell) and must be recovered. Following recovery, the secondary GCS operator reviews the still images gathered to identify craters, spall fields, and provide initial detection of UXOs. Utilizing MATLAB™, Python™, Google Earth™, and the Skywalker's telemetry logs, the secondary GCS operator is able to discriminate between damage and UXOs as well as precisely geo-locate the objects appearing on the airfield surfaces.

Phase one – “survey” – is complete when the Skywalker air vehicle has been recovered and the secondary GCS operator has completed his/her post-processing of the still images. The deliverables of this first phase are a digital MOS and plot of UXOs and craters on a satellite image of the runway, as well as a set of waypoints that may then be ingested back into Mission Planner™ for the second phase – “inspection” – to complete the airfield damage assessment. In addition to the data collected for this thesis, fixed-wing air vehicle component times and manpower requirements have been provided in Appendix K.

The second air vehicle employed in this thesis is a hex-framed, VTOL, multi-rotor built on the Tarot™ 960-millimeter, carbon-fiber frame (Figure 10). The structural components used in this custom build include a Tarot T96013 foldable landing gear; a Storm Pro-3, three-axis, universal camera gimbal; and carbon-fiber battery mounting rails. The propulsion system includes six 465-kV brushless motors (KDE Direct, 2015) individually linked to 95 Amp electronic speed controllers (KDE Direct, 2015) and driven by 15-inch carbon-fiber, two-blade propellers (with a pitch of 5.5). This air vehicle is

serviced by the Pixhawk™ 2.0 autopilot, a GPS receiver, two 6S 10,000 milliamp hour Li-Po batteries wired in parallel (primary flight power source), and one 3S Li-Po battery (autopilot backup and gimbal power sources). Additional features include stiffened landing gear, directional light-emitting diodes, and a Sony α6000 camera. Further hex-rotor air vehicle configuration information can be found in Appendix I.



**Figure 10. Tarot Hex-rotor, Storm Pro-3 Gimbal, & Sony α6000 Camera**

The objective of the Tarot T960 build was to utilize the waypoints generated by the Survey Phase to thoroughly inspect the airfield surfaces, thereby providing recovery teams with high resolution images of the objects present on the airfield operating surfaces. This

phase required an air vehicle to loiter about a waypoint long enough to collect sufficient imagery, without distortion, and at a low enough altitude such that an acceptable ground sampling distance (GSD) accommodates accurate UXO identification. These requirements prohibited a fixed-wing air vehicle from fulfilling this aspect of the mission; therefore, the hex-rotor was the ideal candidate.

A “hex” frame was chosen over a traditional “quad” – four arms – to achieve a more stable imaging platform during windy or otherwise adverse environmental conditions. Within the context of hobbyist drones, as the quantity of limbs supporting the payload is reduced, fewer motors can be attached to the vehicle, thereby requiring a higher thrust output per motor. This in turn develops a tendency to produce oscillation along members supporting motors and propellers. Given that the Tarot T960’s carbon fiber limbs are 405 millimeters long (with a tube diameter of 25 millimeters), oscillatory effects are magnified as thrust requirements increase. As such, the hex-frame provided a satisfactory degree of rigidity and allowed for required thrust to be dispersed over additional members. In addition, the hex-configuration provided redundancies in the event of partial propulsion system failure. For this same reason, the hex was chosen over a co-axial quad-rotor due to efficiency, thrust characterization, and mission endurance requirements. Specifically, in terms of structural configuration, the quad-frame with co-axial motors tends to weight the ends of each member to a greater extent than a single motor and propeller alone. This in turn develops oscillation throughout propeller/motor supporting members and adversely impacts air vehicle positioning consistency and forces image stabilizing devices (i.e., gimbals) to consume additional power to stabilize payloads during imaging operations.

Upon completion of the Survey Phase, a GCS operator, a technician, and an SP prepare the hex-rotor for launch. This entails a systems checkout of communications equipment, the gimbal, imaging device, structural and propulsion components, and the attachment of the required power supplies. System checkout and assembly required 5.15 minutes to complete. The SP then initiated a manual takeoff and achieved stable flight – amounting to an additional 42 seconds – where he/she then turned the hex-rotor over to “Auto Mode.” The hex-rotor then flew to the first waypoint (established in Mission Planner™), hovered at 80 meters for five seconds, and collected three images. Once complete, the hex-rotor resumed its course to the next waypoint – until all waypoints and imaging commands had been fulfilled. When complete, the hex-rotor returned to the launch point where it was recovered manually by the SP, whereupon the images were manually recovered from the Sony α6000’s on-board Secure Digital (SD) card. In addition to the data collected for this thesis, hex-rotor air vehicle component times and manpower requirements have been provided in Appendix K.

The primary and secondary GCS operators reviewed the inspection phase imagery and updated the survey phase damage plot. In accordance with AFPAM 10-219, Volume 4, the GCS operators identified which taxiways and parking areas best accommodated the needs of the flying mission, thereby producing an acceptable MOS. This repair solution is then delivered to Civil Engineer recovery teams such that assets, personnel, and equipment may be mobilized to begin the airfield recovery process.

#### IV. Analysis and Results

In this chapter, the baseline metrics will be compared to civil engineer officer performance using the MATLAB™ GUI and the 2D ortho-mosaic. Recall that the baseline test group consists of nine, four-person teams, dispersed over three separate evaluation periods. From these trials, six metrics have been identified: 1) the average time required to conduct an airfield assessment, 2) correct identification of damage, explosive hazards, and debris, 3) quantity of explosive hazard false positives, 4) quantity of explosive hazard false negatives, 5) object location conformance to Silver Flag test cards, and 6) object location conformance with GPS. The civil engineer officer data set consists of 25 independently observed analyses of aerial imagery using 1080p video captured images presented within the MATLAB™ GUI interface (previously described) and a 2D ortho-mosaic composed of 46, 24-megapixel still images (previously described). CE officer performance will be evaluated across the following metrics: 1) the average time required to analyze airfield images, 2) correct identification of damage, explosive hazards, and debris, and 3) quantity of explosive hazard false negatives. For this thesis approach, civil engineer officer subjects were limited to the geo-location accuracy of the airfield images. Therefore, location accuracy metrics were not measured against their performances. Instead, a description will be provided outlining reasonable expectations for location accuracy among the airfield images. In addition, airfield images did not contain craters or spill fields; therefore, damage identification and position could not be measured.

## **Baseline metrics**

The following six metrics have been summarized in Appendix K.

### ***Metric #1: assessment time and MOS plotting.***

During the baseline evaluations, test subjects were not evaluated on damage assessment duration. According to Abrego and Moore (2017), airfield assessments took no less than 20 minutes and no longer than 30 minutes to complete. In addition, ADAT's remain in constant communication with the EOC throughout the airfield assessment; thus, the MOS plotting team is able to annotate ADAT findings on a scaled airfield map as damage and UXOs are identified. Therefore, damage and UXO plotting is completed when the ADAT(s) finish their sweep of the airfield, thereby requiring no additional time. Lastly, it is the author's experience that, depending on the proficiency of the MOS plotting team, identification of all potential MOS solutions and labeling of the three best candidates can range between 5 to 15 minutes to complete. From this we arrive at a range of 25 to 45 minutes to complete an airfield damage assessment and MOS plotting via conventional methods.

### ***Metric #2: correct identification.***

For the first five teams (evaluated August – October 2017), their exercises consisted of eight objects per exercise, resulting in a total of 40 objects. For the latter four teams (evaluated in December 2017), their exercises consisted of seven objects per exercise, resulting in a total of 28 objects.

Across all nine evaluations, 68 objects (craters, spall fields, UXOs, and bomblet fields) were present. 50 of the 68 total objects were correctly identified, thus producing a 73.5% correct identification rating. Within the first five assessments, however, the test

administrator indicated that, due to the repeated use of the Silver Flag site, there was confusion among teams regarding which objects were considered “in play” as opposed to previous repairs (Abrego & Moore, 2017). Therefore, 13 of the misidentified objects could have been seen, yet were not recorded. The results of the first five exercises produced a 67.5% correct identification rate (27 of 40 objects were correctly identified). To navigate this, the third series of evaluations (the final four conducted in December of 2017), were adequately briefed on existing conditions and what areas were testable. Familiarizing the teams with the preexisting pavement conditions yielded an 89.3% identification rate (25 of 28 objects were identified). Of the object identified, 23 of 25 objects were correctly identified, thereby producing a 92% correct identification rating (refer Appendix K). Based on the difference between the first five teams’ performance and the latter four, the former correct identification rating has been discarded.

***Metric #3: quantity of explosive hazard false positives.***

Across all nine evaluations, there were 36 objects classified as explosive hazards (32 UXOs and four bomblet fields) and 32 objects classified as damage (18 craters and 14 spall fields). Across the nine teams, only two false positives occurred; two of the teams misidentified a spall field as a bomblet field. Of the 68 total objects, this false positive detection rating amounts to 3% of all objects identified (refer to Appendix K). For the same reasons provided in the previous metric, due to test subject confusion regarding damage in the first five evaluations, only the latter four exercises were considered in this metric. Both false positive events occurred during these last four exercises, thus, two explosive hazard false positives out of 28 objects demonstrates that, 7.1% of the time, objects were misidentified as explosive hazards.



***Metric #4: quantity of explosive hazard false negatives.***

Recall that, across all nine exercises, there were 36 explosive hazards placed upon the runway (exercises one through five: 15 UXOs and five bomblet fields, exercises six through nine: 16 UXOs). Only one of the 36 explosive hazards were overlooked; therefore, a 2.78% false negative rating may be assigned to the explosive hazards category (refer to Table 18 in Appendix K).

***Metric #5: object location.***

Damage located along the centerline of the runway ranged between 1.5 and 175 meters from the test administrators' test cards. However, 25% of the time, centerline positioning was within 10 meters of the test card. Positioning to-the-left or right of the centerline ranged between zero and 7.6 meters, and 44% of the time, left-to-right positioning was within 10 meters of the test cards. For explosive hazards, within the latter four evaluations, there were four UXOs and four teams, amounting to sixteen objects. UXOs located along the centerline of the runway ranged between zero and 15.2 meters of the test cards, where 81% of the time, positioning was within 10 meters of the test cards. UXOs located to-the-left or right of the centerline ranged between zero and 16.8 meters from the test cards, where left-to-right position accuracy was within 10 meters 94% of the time.

***Metric #6: manual object locating versus GPS.***

**Error! Reference source not found.** summarizes the centerline and left-to-right position accuracy of the nine enlisted civil engineer teams. Compared to GPS positioning accuracy, conventional methods produce results within 10 meters: 25% of the time for damage along the centerline, 44% of the time for damage to-the-left or right of the



centerline, 81% of the time for explosive hazards along the centerline, and 94% of the time for explosive hazards to-the-left or right of the centerline. As per Table 6, however, the conventional approach ranged up to 6.4 and 28.3 meters away from the true location along the centerline for UXOs and damage, respectively.

**Table 5. Position Accuracy Summary Table**

	<10m	>10m	Min (m)	Max (m)	Avg (m)
Damage CL	25%	75%	1.5	175	19.4
UXO CL	81%	19%	0	15.2	6.4
GPS CL	100%	0%	<< within 3-4 meters		
Damage L/R	44%	56%	0	7.6	1
UXO L/R	94%	6%	0	16.8	1
GPS L/R	100%	0%	<< within 3-4 meters		

**Table 6. Baseline Positioning Deviation**

	GPS (w/o correction)		GPS (w/ correction)		GPS (w/ correction)	
	feet	meters	feet	meters	feet	meters
Damage CL Accuracy	93.0	28.3	13.1	4.0	4.9	1.5
UXO CL Accuracy	21.1	6.4	13.1	4.0	4.9	1.5
Damage L/R Accuracy	7.7	2.3	13.1	4.0	4.9	1.5
UXO L/R Accuracy	11.9	3.6	13.1	4.0	4.9	1.5

*Baseline Data (Status Quo)*

As can be seen in Table 2, centerline positioning within 10 meters is achieved to a

greater degree for UXOs when compared to damage features. This may be due to the method through which UXOs are located. Engineer Assistants (EAs) identify, categorize, and locate pavement damage, whereas EOD Techs focus on explosive hazards. The EAs use PRMS whereas the EOD Techs use the Military Grid Reference System (MGRS). Comparing the two systems was not a planned outcome of this thesis; however, the observed outcome suggests that the MGRS may be a more accurate tool to use. Furthermore, when comparing the three approaches – PRMS, MGRS, and GPS – it is clear that objects identified with a GPS unit (assuming a non-GPS denied environment and without the inclusion of corrective devices) will produce a higher degree of location accuracy. The improvement in location accuracy via GPS merits further investigation by the civil engineering community. These metrics are summarized in Appendix G and Appendix J.

### **Civil engineer officer metrics**

The following three metrics have been summarized in Appendix K.

#### ***Metric #1: airfield assessment time.***

The minimum assessment times for the MATLAB GUI and 2D ortho-mosaic were 95 seconds and 61 seconds, respectively. The maximum assessment times were 370 seconds and 354 seconds, respectively. Within the 2D ortho-mosaic dataset, a 600 second outlier was eliminated. The mean assessment times were 217 seconds and 203.4 seconds, respectively. In the following metric, evidence suggesting that time plays an insignificant role will be supported via their respective  $R^2$  values and Pearson Correlation coefficients. In Table 7, a summary of assessment times has been provided. In addition, linear

extrapolations for a 3,000-meter runway have also been included.

**Table 7. Image Analysis vs. Status Quo Assessment Time Summary Table**

	217m Sample (WPAFB, Ohio)			3,000m (Silver Flag, TAFB, Florida)		
	Minimum (min)	Average (min)	Maximum (min)	Minimum (min)	Average (min)	Maximum (min)
Baseline	--	--	--	20	25	30
MATLAB GUI	1.58	3.62	6.17	21.89	50.00	85.25
2D Ortho-mosaic	1.02	3.65	10.00	14.06	50.46	138.25
<i>*Linearly Extrapolated</i>						

Based upon the average amount of time spent processing images for each of the approaches, collective assessment times have been detailed in Appendix J. Composite times amounted to 93.8 minutes to assemble, launch, survey, and analyze images using the MATLAB approach, and 102 minutes to do the same using the hex-rotor. The researcher hypothesizes that data analysis time can be reduced with the inclusion of outsourcing and sectoring fields of regard. A greater number of personnel reviewing small sets of images promises to both 1) increase correct object detection performance/decrease false negative performance and 2) reduce data analysis time.

***Metric #2: correct identification of objects.***

For both the MATLAB GUI and 2D Ortho-mosaic, each of the 25 subjects had eight objects to identify. Thus, across all evaluations, there were 200 total objects. The number of objects correctly identified ranged 1-6 out of eight for the MATLAB GUI; 83 of the 200 objects were correctly identified (41.5%). In relation to analysis time versus correct object identification, the MATLAB  $R^2$  value was 0.0289. For the 2D ortho-mosaic, correct identification ranged 3-7 out of eight objects; 151 of the 200 objects were correctly

identified (75.5%). Similarly, analysis times versus correct identification produced an  $R^2$  value of 0.0169.

The MATLAB GUI's  $R^2$  value unequivocally demonstrates that time and correct identification performance do not interact. The Pearson coefficient confirms this (amounting to 0.17), indicating that time has a weak, positive linear correlation with correct identification performance. This suggests that, although time makes a microscopic contribution to object identification in the MATLAB GUI, other factors are more likely candidates for effecting correct identification performance. Similarly, the 2D ortho-mosaic  $R^2$  value demonstrates a less significant interaction between image analysis time and correct identification performance. The Pearson coefficient amounts to 0.1699, which also approximates zero (no correlation).

***Metric #3: false negative UXO detection.***

For the MATLAB GUI, UXO false negative detection ranged from 1-7, whereas the 2D Ortho-mosaic ranged from 1-5 of the eight objects placed on the runway. The average false negative rates were 4.4 (117 of 200, or 58.5%) and 2.0 (49 of 200, or 24.5%) respectively (refer to Appendix J for the civil engineer officer responses). In the MATLAB GUI, the  $R^2$  value is 0.0089, demonstrating that time has an insignificant effect on UXO false negative performance. Moreover, the Pearson coefficient amounts to -0.0943 (approximately zero), which indicates that time and false negative performance do not show a significant correlation.

Similarly, in the 2D ortho-mosaic, the  $R^2$  value is 0.1937, which demonstrates a modest correlation between time and false negative performance. However, the Pearson coefficient in this second approach amounts to -0.4402, which shows a weak-moderate,

negative linear (or inverse) correlation; as assessment time increases, false negative performance improves (the occurrence of false negatives decreases) to a moderate degree. Between the MATLAB GUI and the 2D ortho-mosaic and their nearly identical assessment times, these relationships indicate that factors other than assessment time (such as the higher image resolution provided by the 2D ortho-mosaic) are more likely to affect false negative performance.

For the MATLAB GUI, 56 pavement features were incorrectly identified as a UXO and 58.5% of the time, analysts failed to identify the presence of a UXO. For the 2D ortho-mosaic, despite spending a comparable amount of time analyzing imagery, analysts identified 30 more pavement features as UXOs than in the MATLAB GUI. Finally, 24.5% of the time, subjects analyzing the 2D ortho-mosaic failed to identify the presence of a UXO.

*Status quo hypothesis tests.*

The performance of the MATLAB GUI and the 2D ortho-mosaic methods were evaluated against the baseline using single-tail t-tests. Due to differences in populations performing the CE officer assessments and the baseline assessments, independent means testing must be conducted. The performance of each test is as follows (and are summarized in Appendix K):

*MATLAB GUI vs. Status Quo: Pure Object False Negative Detection.* The mean false negative of the status quo is 0.2059, whereas the MATLAB GUI mean is 4.68. With significance level of 0.05, the test-statistic is 9.869, whereas the critical value is -1.711; therefore, in accordance with the critical value approach, the null hypothesis is rejected in favor of the alternative: the average false negatives for MATLAB were greater than the

status quo.

*2D Ortho-mosaic vs. Status Quo: Pure Object False Negative Detection.* The mean false negative of the 2D ortho-mosaic is 1.96. With significance level of 0.05, the test-statistic is 4.610, whereas the critical value is -1.711; therefore, in accordance with the critical value approach, the null hypothesis is rejected in favor of the alternative: the average false negatives for the 2D ortho-mosaic were greater than the status quo.

*MATLAB GUI vs. Status Quo: Explosive Hazard False Positive Detection Rate.* The mean false positive of the status quo is 0.0299, whereas the MATLAB GUI mean is 2.24. With significance level of 0.05, the test-statistic is -0.558, whereas the critical value is -1.976; therefore, in accordance with the critical value approach, the null hypothesis is rejected in favor of the alternative: the average false positives for MATLAB were greater than the status quo.

*2D Ortho-mosaic vs. Status Quo: Explosive Hazard False Positive Detection Rate.* The mean false positive of the 2D ortho-mosaic is 3.44. With significance level of 0.05, the test-statistic is 0.679, whereas the critical value is -1.976; therefore, in accordance with the critical value approach, the null hypothesis is rejected in favor of the alternative: the average false positives for the 2D ortho-mosaic were greater than the status quo.

*MATLAB GUI vs. Status Quo: Incorrect Object Identification Rate.* The mean incorrect identification rate of the status quo is 0.0556, whereas the MATLAB GUI mean is 4.68. With significance level of 0.05, the test-statistic is 9.869, whereas the critical value is -1.654; therefore, in accordance with the critical value approach, the null hypothesis is rejected in favor of the alternative: the average number of incorrectly identified objects for MATLAB were greater than the status quo.

*2D Ortho-mosaic vs. Status Quo: Incorrect Object Identification Rate.* The mean incorrect identification rate of the 2D ortho-mosaic is 1.96. With significance level of 0.05, the test-statistic is 4.610, whereas the critical value is -1.654; therefore, in accordance with the critical value approach, the null hypothesis is rejected in favor of the alternative: the average number of incorrectly identified objects for the 2D ortho-mosaic were greater than the status quo.

***Civil engineer officer hypothesis tests.***

The performance of the MATLAB GUI and the 2D ortho-mosaic methods were evaluated against each other using single tail t-tests. Dependent means testing could be performed due to the shared use of test subject populations.

*MATLAB vs. 2D Ortho-mosaic: Pure Object Detection False Negatives.* In Table 8, the resulting performance between the MATLAB GUI and the 2D ortho-mosaic for pure object false detection and incorrect identification have been summarized. With a significance level of 0.05, the mean false negative detection rate for the 2D ortho-mosaic was 1.96, whereas the MATLAB GUI exhibited an average of 4.68 false negatives. The test-statistic is 9.869, whereas the critical value is -1.654; therefore, in accordance with the critical value approach, the null hypothesis is rejected in favor of the alternative: the average number of false negatives for the MATLAB GUI were greater than the 2D ortho-mosaic.

*MATLAB vs. 2D Ortho-mosaic: Incorrect Object Identification Rate.* With a significance level of 0.05, the mean false negative detection rate for the 2D ortho-mosaic was 1.96, whereas the MATLAB GUI exhibited an average of 4.68 objects incorrectly identified. The test-statistic is 9.869, whereas the critical value is -1.654; therefore, in

accordance with the critical value approach, the null hypothesis is rejected in favor of the alternative: the average number of incorrectly identified objects for the MATLAB GUI were greater than the 2D ortho-mosaic.

**Table 8. MATLAB vs. 2D Ortho-mosaic Statistics**

<i>MATLAB vs. 2D Ortho: Pure Object False Negative Detection Rate</i>		<i>MATLAB vs. 2D Ortho: Object Incorrect Identification Rate</i>	
Mean	4.68	Mean	4.68
Standard Error	0.314749	Standard Error	0.314749
Median	5	Median	3
Mode	6	Mode	2
Standard Deviation	1.573743	Standard Deviation	1.573743
Alpha	0.05	Alpha	0.05
Ho: MATLAB <=	1.9600	Ho: MATLAB <=	1.9600
Ha: MATLAB >	1.9600	Ha: MATLAB >	1.9600
Range	5	Range	1
Minimum	2	Minimum	6
Maximum	7	Maximum	83
Sum	117	Sum	25
Count (n)	25	Count (n)	24
Degrees of Freedom	24.00	Degrees of Freedom	23.00
t-Statistic	9.869	t-Statistic	9.869
p-Value	1.000	p-Value	1.000
Critical Value	-1.711	Critical Value	-1.714
<b>Goal:</b> find evidence suggesting that the avg qty of false neg detection for MATLAB is <= the 2D		<b>Goal:</b> find evidence suggesting that the avg qty of incorrect identifications for 2D are <= MATLAB	
MATLAB vs. 2D Ortho: T-Stat (9.869) > Critical Value (-1.711); therefore, Reject Ho		MATLAB vs. 2D Ortho: T-Stat (9.869) > Critical Value (-1.711); therefore, Reject Ho	

***Positioning accuracy.***

Throughout the civil engineer officer evaluations, positioning accuracy along the centerline or to-the-left or right of the centerline was not measured. However, the differences between baseline positioning accuracy and GPS accuracy was discussed in the



baseline metrics. Recall that, centerline positioning ranged from 6.4 to 28.3 meters away from the true location, whereas left-to-right positioning ranged from 2.3-3.6 meters away from true. Furthermore, that objects were located along the centerline to less than 10 meters away from true 25-81% of the time, whereas objects were located to the left or right of the centerline less than 10 meters away 44-94% of the time. Contrast these performances with that of GPS location accuracy. According to NAVSTAR (2008), GPS is accurate to within 3-5 meters of a known location without the inclusion of corrections such as Real Time Kinematics (RTK) and surveyed reference points. Compared to baseline results, GPS offers the ability to improve object positioning up to 550%.

## V. Conclusions and Recommendations

In culmination of this thesis, the preceding sections provide evidence for the investigative questions, which provide support for the following conclusions: that Small Unmanned Aerial Systems (SUAS) may provide engineers with a promising alternative to conventional airfield damage and repair methods. In addition, recommendations in support of fielding SUAS for airfield damage assessment are provided. Lastly, topics for further research into air vehicle and sensor package optimization are discussed.

### First investigative question

Are civil engineer personnel capable of reliably leveraging data collected via SUAS to meet or exceed traditional damage assessment methods?

Given the resulting performance of the MATLAB™ GUI and the 2D ortho-mosaic map detailed in Chapter IV, Air Force civil engineers cannot fully replace traditional airfield damage assessment methods with this thesis' configuration; however, it comes close. Recall that, for the baseline metrics (status quo), correct object detection was 92% and false negative events occurred 2.8% of the time. The correct object identification for MATLAB GUI and 2D ortho-mosaic were 41.5% and 75.5%, respectively, whereas their false negative occurrences were 58.5% and 24.5%, respectively. In this thesis, the MATLAB GUI was used to provide an overview of the damaged features, foreign objects, and explosive hazards present on a section of a runway. The researcher hypothesizes that the lesser image resolution, coupled with the inability to magnify images resulted in a greater occurrence of false negatives. The second interface (2D ortho-mosaic) provided a

higher resolution snapshot of the waypoints produced by the former. Thus, with a 41.5% correct identification level, engineers were at least provided with an area to further evaluate. This in turn, resulted in a 34% increase in identification and a 30% decrease in the occurrence of false negative events.

Between the identification level of the status quo and the 2D ortho-mosaic, the difference of 6.5% amounts to missing 6.6 objects per 100, whereas the MATLAB GUI amounts to missing 41 objects per 100. Suffice it to say, a 6.5% decrease in object identification as well as a 55.7 and 21.7% increase in the occurrence of false negatives for MATLAB and the 2D ortho-mosaic, respectively are considerable hurdles. Despite the object detection limitations experienced with this thesis' configuration, the 1.0-5.56 times greater location accuracy along the centerline provided by SUAS demonstrates that this approach has value and merits further investigation. Finally, the total time required to conduct a 217-meter airfield damage assessment using a fixed-wing SUAS approach resulted in 18.7 minutes to complete, whereas a hex-rotor, 2D ortho-mosaic approach resulted in 26.1 minutes to complete. Using linear extrapolation to scale the 217-meter test sample to match the 3,000-meter sample used in the enlisted civil engineer baseline metrics, the airfield assessment times are estimated to be 93.8 minutes and 102 minutes, respectively (refer to Table 19 in Appendix K). Compared to the status quo, the average assessment time ranges between 20-30 minutes to complete with MOS plotting and deliberating requiring an addition 5-15 minutes. By contrast, the fixed-wing approach doubles this time whereas the hex-rotor scales it by a factor of 2.25.

## **Second investigative question**

What are the resource requirements – e.g. manpower, purchase costs, consumables, etc. – for an SUAS concept to accomplish an airfield damage assessment?

Numerous AFIT trials and experimentation with SUAS has demonstrated that each aerial vehicle has its specific supporting requirements. However, in general, the use of SUAS is supported by the following manpower, equipment and consumable requirements.

### ***Manpower.***

Each aerial vehicle requires, at a minimum, three personnel to operate: one ground control station (GCS) operator, one safety pilot (SP), and one observer/technician (paired with the SP to assist with visual confirmation and verbal communications back to the GCS operator). This process could be repeated for subsequent air vehicle launches up to the limit capabilities of the GCS(s), GCS operators, and safety pilot confidence, thereby enabling swarm operations. In addition, for aerial assets of substantial size, additional personnel may be required to perform maintenance operations on active and inactive air vehicles including: exchanging and charging batteries, hand or catapult launching non-rolling takeoff vehicles, and assembling/disassembling support apparatus (such as a catapult launcher).

### ***Equipment.***

Each aerial vehicle is serviced by a launching device, GCS, and remote controller. Depending on the vehicle type, a launching device may not be required. However, as has been used by this thesis, the fixed-wing surveyor was designed as a catapult launch vehicle. This was to account for the potential non-availability of a suitable surface for a rolling takeoff, as well as improve stability in the air and mission endurance time without the

added drag and weight of landing gear. The accompanying GCS runs mission planning software that collects telemetry logs (time, GPS location, body positioning/angles, acceleration, velocity, etc.) and plans – as well as executes – predefined missions. In this thesis, the GCS operated using Mission Planner™ software. Further details of the fixed-wing air vehicle’s video subsystem configuration are provided in Appendix I. Finally, the remote controller used in this thesis was an FrSky Electronics Co., Taranis, with a 2.4GHz Digital Telemetry Radio System. This device allowed the safety pilot to take manual control over the air vehicle through the launch and recovery stages as well as override the mission plan should the vehicle begin to perform erratically or uncharacteristically. Lastly, this device provides full control of pitch, yaw, roll, air speed, and tuning presets.

### ***Consumables.***

The expendable materials used to support SUAS operations include fasteners, adhesives, and power supply sources. Due to air vehicle design, the vibration applied to the vehicle frame and subcomponents requires periodic adjustment to ensure proper fit and air worthiness. As such, consumables included zip-ties, Lock-Tite™, rapid setting adhesives (i.e., Super Glue™), and replacement fastening screws. In addition, the power supply units were a combination of Lithium-Polymer (“Li-Po”) and Nickel-Cadmium (“Ni-Cad”) rechargeable battery packs. Depending on the mission duration, to ensure optimum performance, battery packs were replaced between each takeoff and landing.

### **Third investigative question**

Given the target criteria specified in the problem statement, what sensor packages, aerial vehicle characteristics, and environmental optimization considerations that are

appropriate to assessing airfield damage assessments?

In this thesis, two sensor packages were investigated within the area of image-based sensors. In the fixed-wing, MATLAB™ approach, a 1080p video stream (scaled down by 20%) was used to capture still images – with a 40% overlap – while the air vehicle was in motion (approximately 15 meters per second) at an altitude of 40 meters (+/-1 meter). The second air vehicle utilized a two-axis (pitch and yaw) gimbal stabilized, 24-megapixel camera (yielding a 21.3-megapixel image), affixed to a hex-rotor hovering at an airspeed of zero meters-per-second and an altitude of 80 meters (+/- 1 meter). As per the findings discussed in Chapter IV, both sensor packages were successful in identifying a percentage of objects placed upon the airfield surface. However, the 24-megapixel camera demonstrated a significantly greater degree of detection accuracy.

As discussed in the previous chapter, visual sensor packages – while useful for conducting minimum threat/low operational tempo missions – are insufficient when used alone for the purpose of airfield damage assessment. This thesis did not start with an image resolution goal in mind. Based on the findings, future tests should strive for greater resolution than the 2D ortho-mosaic. It is recommended that either a higher resolution camera or a secondary (multi-spectral) sensor be incorporated in future trials. A relevant sensor package that can assist in the detection rate of objects placed upon the airfield surface is an Infrared (IR) sensor.

The fixed-wing air vehicle used in this thesis required an imaging device that could be synchronized to the airspeed of the vehicle. Common approaches to this form of imaging are either the use of an intervalometer affixed to a camera or – as was implemented in this thesis – a Python™ script that took screen captures from the live video stream and

coupled them with telemetry information. The amount of lift produced by the Skywalker X8 frame and light weight ensured ample mission endurance and in-flight stability. For the hex-rotor, the 2D ortho-mosaic required the air vehicle to remain motionless – in pitch, yaw, and roll, as well as in the north, east, and downward directions. This is a requirement that cannot be met by typical fixed-wing air vehicles; therefore, the multi-rotor – whether that be a tri-, quad-, hex-, or octo-rotor – was the only choice. Image stabilization and clarity is the primary factor in deciding the final configuration of the multi-rotor. As such, a hex-rotor (six arms, one motor per arm) was the best of both worlds in terms of the quad-copter’s endurance and the octo-copter’s stability in hover.

The airfield damage assessment mission required full coverage of all aircraft operating surfaces. This includes parking aprons, taxiways, and runways. As such, launch, mission execution, and recovery must account for the total endurance required to cover the combined airfield features (previously identified). Optimization would require an efficient flight pattern such that wasted flight time is kept to a minimum. In addition, with lower kV motors, larger propellers, and higher capacity batteries, inflight endurance may be increased. Lastly, to ensure optimum performance, the connection from the GCS to the air vehicle must remain intact. As such, signal boosting infrastructure or, at the very least, rapidly deployable signal boosting systems, must be in place to allow for full coverage of the airfield operating surfaces. The system used in this thesis had an advertised range of 1,000 meters (radially). This signal range was untested; however, video dropout began to occur roughly two-thirds of the way down the remaining length of runway, which was approximately 1,500 meters.

For austere environments, final configuration of an SUAS will vary by the region

of concern. For hotter climates – such as the Middle East –the presence of fine particulate dust will be a maintenance consideration for operating in desert environments. In arctic climates – such as Thule, Greenland – operations may experience degraded pitot sensor performance for fixed-wing air vehicles. Lastly, for high-wind climates, motor kV ratings and propeller configurations may require optimization. In addition, moisture barriers may be required for frequently precipitous environments. Each of these additions will ultimately lead to greater vehicle mass and maintenance considerations. With greater mass, a more powerful motor and/or propeller configuration, a higher capacity power source to sustain its operation, or the inclusion of additional air vehicles will be required.

## **Summary**

The use of remote sensing technologies (to include SUAS) provides Air Force civil engineers with a multitude of benefits. While SUAS approaches investigated in this thesis may not meet or exceed the status quo, their manpower conservation is a considerable factor favoring their adoption. The Sinclair approach (Shepherd & Storm, 2017d), as well as the method leveraged by this thesis, reduces the ADAT team requirements by 75%. In addition, these modern approaches to solving airfield damage assessment and UXO identification promise to improve civil engineer safety by mitigating and nearly eliminating boots on ground presence. From this perspective, post kinetic- and/or Chemical, Biological, Radiological, Nuclear, and Explosive (CBRNE) attack events become much safer for civil engineers to begin the base recovery process.

With respect to the ability of SUAS to accomplish airfield damage assessment as well as UXO identification and classification missions, AFCEC (RADAS) data as well as



AFIT preliminary experimentation has shown the 2D ortho-mosaic approach to be a promising solution. This technique could be further improved through reductions in Ground Sampling Distance (GSD), inclusion of surveyed Ground Control Points, 3D Digital Elevation Mapping, or the implementation of other sensors. Using overhead imagery with geolocation, the size, quantity, and depth of both large and small craters, as well as spall fields, UXOs, and bomblet fields, can be reliably identified using post image processing. Unfortunately, an algorithm to automate this process and identify features of interest continues to demonstrate inconsistent results (Filler & Diltz, 2016). This thesis has provided an interface utilizing MATLAB to digest the fixed-wing video feed, which, in conjunction with Installation Commander (ICC) defined aircraft parameters, can produce a single, optimal solution for the location of the MOS. However, this does not account for the AFPAM 10-219, Volume 4 stipulation that MOS selection teams must produce three candidate MOSs for ICC consideration and final approval. Marginally, UXO identification and classification is dependent upon the color and size of the UXO in relation to the image resolution of images collected. Objects painted in neutral colors that blend into native vegetation remain just as challenging – if not more so – to identify via SUAS using still images as they are for personnel conducting damage assessments manually. With these two facets combined (damage detection, location, and quantification, as well as UXO detection, classification, and location), while the minimum operating strip may be easier to identify via remote sensing or SUAS techniques, the identification and classification of UXOs remains a daunting challenge.

## Recommendations

With respect to the findings of this thesis, a case for the employment of SUAS during airfield damage assessment can effectively be made. First, the Air Force should invest in strategies to remotely detect UXOs without the use of visual identification. This leverages the advantages in manpower efficiency and safety that SUAS use provides. In addition, it underscores the fact that a visual sensor package alone leaves room for improvement (as is often the case in manual methods). Second, SUAS should be applied to the airfield damage assessment mission as it has demonstrated the capacity to save time, improve sizing and location accuracy, and significantly reduce the risk to base recovery personnel. In addition, visual outputs from SUAS can be a great asset to personnel producing MOS solutions remotely (i.e., Emergency Operations Centers and/or Damage Control Centers). Moreover, the usefulness of SUAS does not only apply to airfield damage assessment. The versatility of SUAS suggests that they should also be applied to infrastructure assessments, including vehicle pavement surveys (Grandsaert, 2015; Schleppe, 2018) and exterior facility assessments following storms (Meeks, 2016), as well as a host of other applications currently being investigated in the private sector.

Lastly, due to the inclusion of AFCEC's RADAS project in Air Force Tactics, Techniques, and Procedures (AFTTP) 3-32.11, SUAS use in future civil engineer operations will be an eventuality. At the present time, the expected delivery and associated training dates for the RADAS system are unknown. As an interim improvement, it is recommended that the damage plotting algorithm used in this thesis be applied to current Air Force procedures to enhance and expedite MOS and MAOS identification and selection.

## **Further Research**

### ***Baseline study and airfield imaging.***

A retrial of the baseline experiment is in order. Given the learning curve that occurred between the first five baseline evaluations and the latter four, better methods should be implemented to improve assessment data quality. An area that needs to be addressed are the individual ADAT airfield assessment times. In the data provided by the Silver Flag exercises, each team's time to conduct the airfield assessment was omitted. In addition, the time it took for the team to respond, process the airfield information, and generate MOS plots was missing. Future studies should incorporate these component times to provide greater context for airfield assessment accuracy and time resource requirements. In addition, the original intent of this thesis was to assess an airfield using the status quo concurrently with the SUAS approach. Further experimentation should strive to merge the evaluation schedule with the SUAS team such that baseline metrics will be collected on the same configuration of pavement damage and explosive hazards and under the same climatological conditions as the SUAS team.

### ***MATLAB and 2D ortho-mosaic testing.***

For future trials, test subjects should be made familiar with the conditions of the airfield prior to placement of UXOs and damage and the use of CE officers should be avoided. In a real-world scenario, the personnel performing airfield damage assessments will have a general concept of various pavement and infrastructure features that were present prior to an attack. In addition, EAs and EOD Techs should be used to determine performance of each airfield data analysis method. Civil Engineer officers are provided with a general knowledge of how airfield damage assessments are performed; however,

their knowledge and proficiency are not maintained throughout their careers. The greatest exposure they receive is a general overview during their triennial Silver Flag encampment, which is merely informative in nature. Future assessments would benefit from utilizing the personnel who conduct airfield damage assessments regularly.

***Air vehicle modifications.***

An available candidate for further research is modifying the air vehicles used in this thesis' data collection (Appendix I), followed by a reimaging of the Wright Patterson, Area B airfield. The author theorizes that, if the 24-megapixel Sony camera were to be fixed to the underside of the fixed-wing air vehicle, and airspeed and altitude were optimized to conform to the Sony  $\alpha 6000$ 's shutter speed, reduced mission times and higher image resolution would surely result. Alternatively, the hex-rotor air vehicle would benefit from a lower kV rated motor and larger propeller combination (assuming that electronic speed controllers suit motor voltage requirements). This modification would enable greater payloads to be carried (i.e., larger sensors) or greater distances to be flown, thus enabling a complete imaging of an airfield section. This thesis' performance was obtained solely by leveraging still imagery that was collected from a single pointing angle at 80 meters above the pavement surface. Had multiple perspectives been gathered, the mission been flown at a lower altitude, and access to photogrammetric software (i.e., Pix4D™), civil engineer officers would have a greater degree of image resolution at their disposal as well as a 3D digital elevation map with which their efforts would be vastly improved. These changes promise improved hazard detection as well as enhanced object location and sizing accuracy.

Finally, a combination of approaches could be applied; utilize the hex-rotor at a

lower altitude, operated in the same manner as the fixed-wing air vehicle. The author hypothesizes that, given a moderate air speed, the hex-rotor could be used to collect a series of images covering two lengths of the runway (one in either direction) in less than 20 minutes, thereby producing a higher resolution 2D ortho-mosaic or a 3D digital elevation map.

### *Communications systems and equipment.*

The methods used by the SUAS team that supplied airfield data to this thesis used a line-of-sight, short range SUAS configuration. In an operational scenario, the SUAS would need to traverse the entire airfield. Some airbases have runways two miles long. Others have multiple runway surfaces and extensive taxiways to munitions storage locations. The live video subsystem used on the fixed-wing air vehicle for this thesis had an estimated range of 1,000 meters (radially). Towards the upper limits of that range, video feed suffered considerable lag. Moreover, outside of that range, video feed became unavailable for the ground station operator. Additionally, although data is collected at 1080p, it is not guaranteed to meet that resolution once it has been transmitted to image analysis terminals. Therefore, if the thesis approach is to be applied in an operational capacity, signal boosting infrastructure or equipment is an essential field that needs to be studied. Subsequent to these limits, an investigation of data management must also be undertaken.

Due to the high storage capacity requirements of a 1080p live video feed (estimated three to five gigabytes per minute), the SUAS team made the decision to omit recording the video feed. Instead, they designed an input method to trigger the camera to collect a series of still images when they were passing a particular section of the runway. If images

are to be coupled with telemetry logs over a full-sized runway (including adjacent spaces), a greater emphasis must be placed on data management and post-processing techniques.

Finally, efforts to optimize image analysis tools and techniques must be investigated. For the dataset leveraged by this thesis, image analysis occurred on the flight line, in an open environment, under a cloth cover. Deleterious effects of glare, an unclean monitor, and peripheral distractions contribute to higher false negatives and poor object identification. Latter trials placed analysts in a dark room, however, ambient light, dirty computer screens, and other non-sterile experimental conditions (i.e., noise) contributed to erroneous data points and experiment inconsistency. Therefore, all image analysis must occur in a darkened room, removed from outside noise and visual disturbance. In addition, images must be presented on a clean monitor that is in good working condition (devoid of any horizontal or vertical defects), is of sufficient size – monitors with a greater diagonal measurement (17 inches or greater) tend to produce better results, and complete with full-spectrum back lighting, such as a Light Emitting Diode (LED) backlit, Liquid-Crystal Display (LCD). The LED-LCD monitor allow for higher contrast between the brightest and darkest aspects of imagery. In addition, LED backlit monitors provide a greater degree of control of the backlight (Morrison, 2013) thereby allowing for improved user-system integration.

### ***Positioning systems.***

The SUAS employed in this thesis used the Pixhawk 2.0 and standard GPS unit. Previous AFIT experimentation determined that air vehicle body angle and location accuracy was known to be within 1-2 degrees and three meters of the true location, respectively. For a visual sensor package, these two factors combined reduce positional

confidence to 10 meters (at best). To combat this, the combination of differential GPS, such as RTK, and previously surveyed ground features may deliver a greater level of location accuracy for individual pixels displayed on aerial images. Instead of a positional confidence of within 10 meters, the inclusion of these methods have the potential to increase positional confidence to within one meter. These improvements would contribute to producing more accurate depictions of airfield surface conditions and lead to optimization of MOS solutions, repair priorities, and precise locations of explosive hazards.

### ***Sensor packages.***

Further research into the optimum sensor packages will be required. This thesis' approach leveraged a 1080p live video stream and a 24 megapixel still camera. Each could benefit from variation in their implementation (i.e., orientation, altitude, shutter speed, data transfer, etc.). In addition, other sensors are prime candidates for airfield damage assessment, such as Infra-Red/Multi-spectral (Filler & Diltz, 2016), Sonar, piezoelectric transducers (Alavi et al., 2015), magnetometers, or combinations. Moreover, with the inclusion of multi-spectral sensing (e.g., Infra-Red, Sonar, etc.), data collected would benefit from additional filters for analysts to refine their assessments.

### ***UXO detection in vegetated areas.***

This thesis focused on objects placed upon paved surfaces to the exclusion of surrounding areas. As such, continuation efforts must consider adjacent spaces, to include grass, sand, gravel, unrefined earth, and other ground coverings accompanying airfield paved surfaces. The author hypothesizes that objects located in vegetated areas may be more easily identified using IR and magnetometers.

### ***Surface and subsurface damage.***

This thesis focused on explosive hazard detection and optimal MOS plotting. The identification of surface and subsurface damage (i.e., camouflages and concealed cavities) was not included in the dataset used for this thesis. Future experimentation should combine efforts with the Silver Flag to image craters, spall fields, and subsurface damage indicators. Due to their application in locating submarines during the Second World War as well as continuing use for locating mineral and petroleum deposits, the author hypothesizes that magnetometers would be an effective solution for identifying subsurface UXOs.

### ***Environmental conditions.***

Finally, design accommodation for climatological considerations (i.e., extreme heat/cold and inclement weather) will require investigation prior to fielding SUAS in austere locations. Specifically, for a desert climate, the ability to withstand fine particulate matter (dust) is required. For precipitous environments, weather sealants will need to include water proofing and/or vapor barriers. Overall, as a general consideration, air vehicle designs must consider sensor stabilization performance improvements to account for sporadic wind gusts and turbulent air as well as communications systems optimization.



## Appendix A. R-1, R-2, and R-3 Vehicle and Equipment Sets

(AFPAM 10-219, Volume 4)

**Table 9. R-1 Equipment and Vehicle Set**

VEHICLES	QTY
Excavator 3	
Grader	3
Dozer (T-7)	3
Front-End Loader (4-cy)	6
Front-End Loader (2.5-cy)	3
Vibratory Roller	3
Dump Truck (8-cy)	8
Dump Truck (5-ton)	4
Tractor (7.5-ton)	3
Tractor (10-ton)	3
Trailer (22-ton)	3
Trailer (60-ton)	3
Vacuum Sweeper	2
Tractor Mounted Sweeper (ADR)	2
Paint Machine (Part of MAOSMS)	2
HMMWV	2
ADR Trailer	3
1,500-Gallon Water Truck	3
Dolly Converter (8-ton)	3
Basic ADR Equipment Support Kit	1
Basic ADR Airfield Lighting Kit	1
AM-2 ADR FOD Cover Kit	*3/6/9
AM-2 Support Kit	*1/2
Folded Fiberglass Mat FOD Cover Kit (Kit-A)	1
Folded Fiberglass Mat FOD Cover Kit (Kit-B)—Anchoring Systems	2
Spall Repair Kit	4
Minimum Airfield Operating Strip Marking System (MAOSMS)	1
*The specific quantities needed at a given MOB will depend upon the perceived threat.	

**Table 10. R-2 Equipment and Vehicle Set Additives**

VEHICLES	QTY
Excavator 3	
Front-End Loader (4-cy)	3
Front-End Loader (2.5-cy)	3
Vibratory Roller	3
Dump Truck (8-cy)	7
HMMWV	4
ADR Trailer	3
Floodlight/Generator Set	6
Generator Set (Diesel)	1

**Table 11. R-3 Equipment and Vehicle Set Additives**

VEHICLES	QTY
Front-End Loader (4-cy)	4
Dump Truck (8-cy)	7
Vacuum Sweeper	2
Dirt Sweeper (ADR)	5
Floodlight/Generator Set	6

## Appendix B. Airfield Damage Reconnaissance Organization Concept

(AFPAM 10-219, Volume 4)

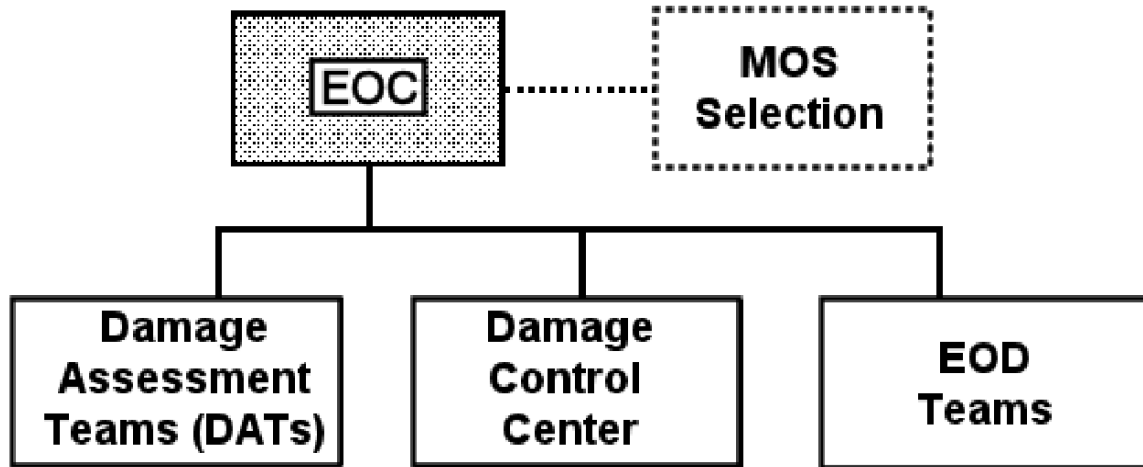


Figure 11. Airfield Damage Reconnaissance Organizational Concept

## Appendix C. Emergency Operations Center Team Organization

(AFPAM 10-219, Volume 4)

Position	Number of Personnel	Air Force Specialty	Required Skills	Responsibilities
BCE	1	32E3		Oversee engineer activities
Team Chief	1	32E3 or 3E5X1	Know MOS candidate selection criteria & RQC procedures.	
Plotter 1		3E5X1	Understand damage coordinates and plotting techniques	Plot data, select candidate MOSs, & calculate RQC
CE Radio Operator	2	3E5X1 or 3E6X1	Radio ops & data recorder	Receive/record data; assist with MOS selection
<b>Support Personnel</b>				
EOD Tech	1	3E8X1	Radio operations, data recorder, & technical EOD expertise	Receive/record data; provide technical advice
ADAT (per team)	1	3E5X1	Know airfield marking system, crater & spall damage assessment procedures. Also, be able to perform utility, facility, & NAVAID damage evaluations.	Assess pavement & supporting airfield systems damage & provide such data to the EOC.
	1	3E8X1	UXO identification	Provide EOD input to EOC.
	2	Augmentee	Vehicle operation/damage & UXO recording procedures	Operate ADAT vehicle & develop a "hard copy" re-port of information provided to EOC.

**Figure 12. Emergency Operations Center Team Organization**

## Appendix D. Types of Pavement Damage

(AFPAM 10-219, Volume 4)

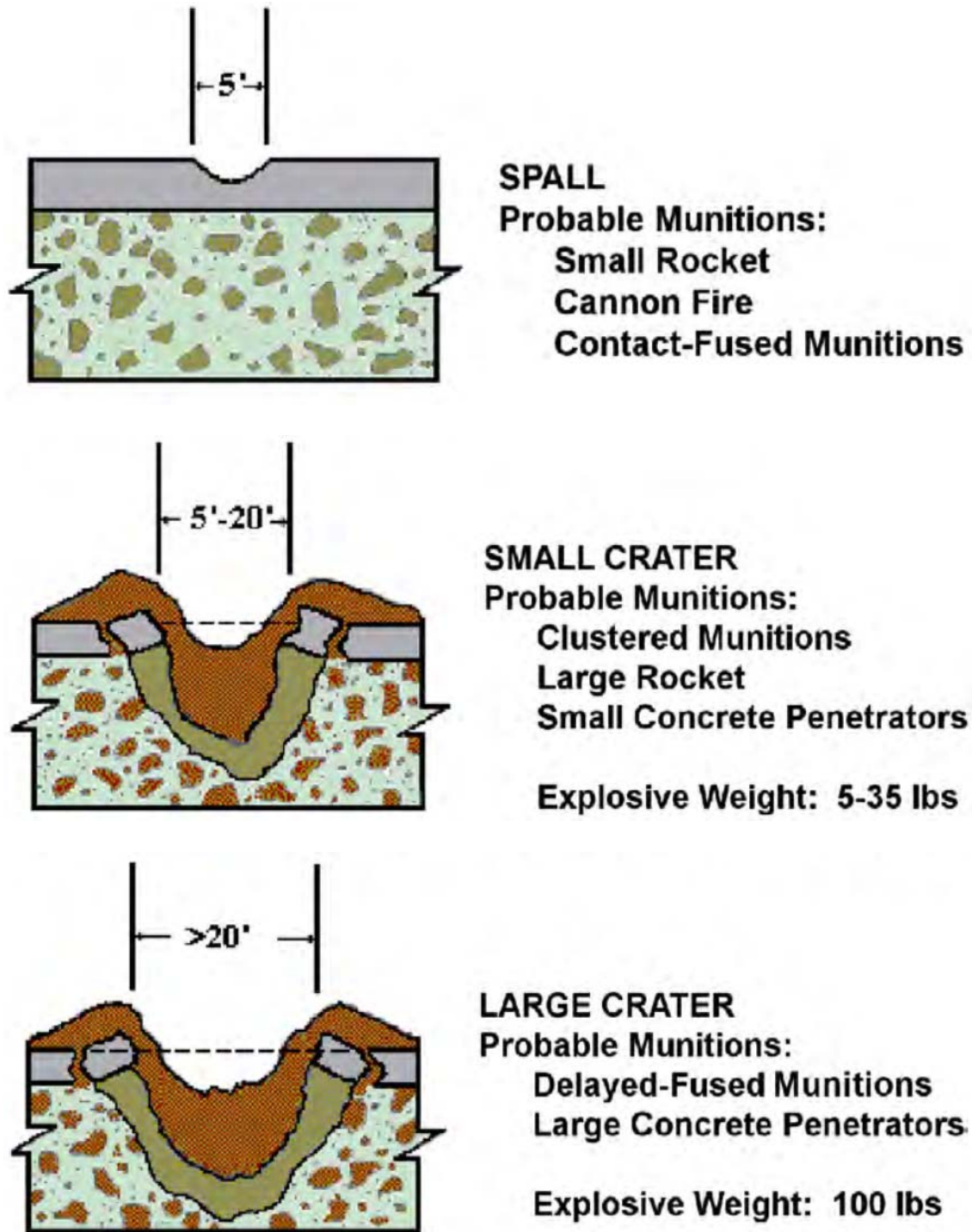


Figure 13. Airfield Damage Classifications

## Appendix E. UXO Classifications

(AFPAM 10-219, Volume 3)

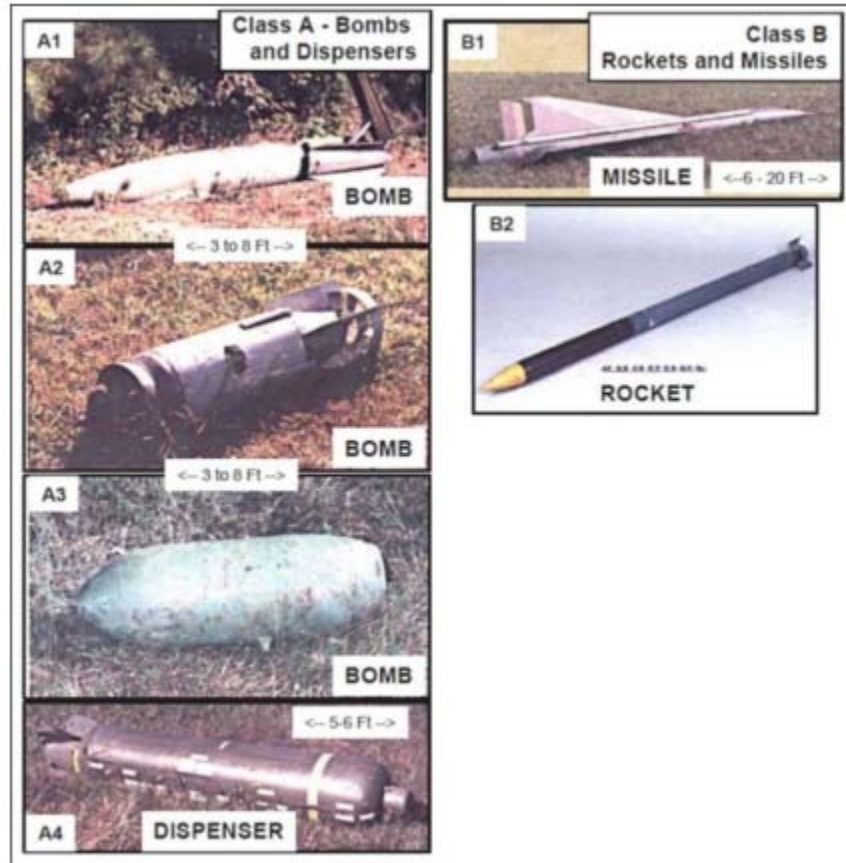


Figure 14. Class A (Bombs & Dispensers) & Class B (Rockets & Missiles) UXOs

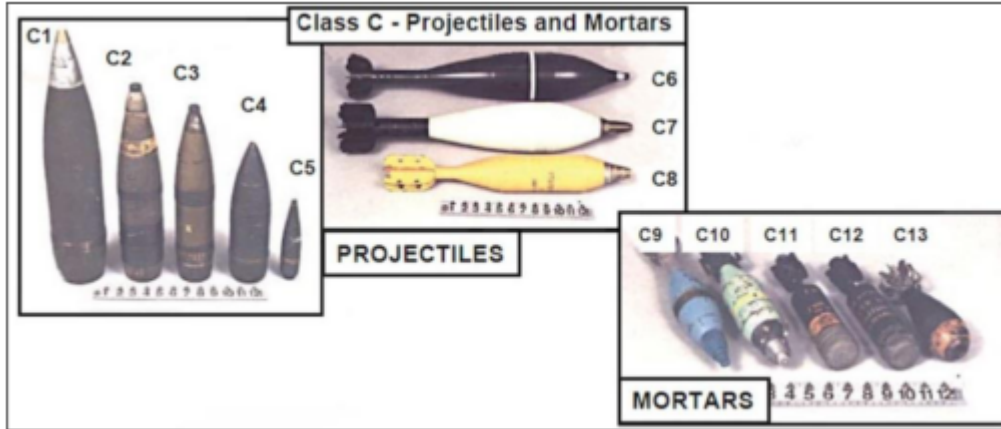


Figure 15. Class C UXOs (Projectiles & Mortars)

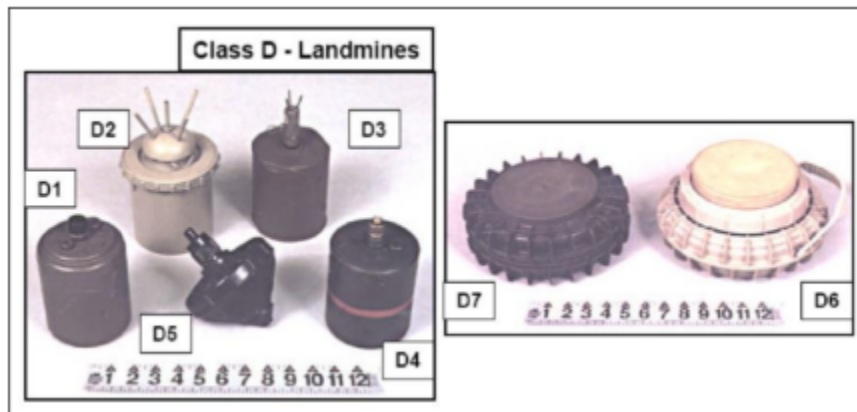


Figure 16. Class D UXOs (Land Mines)



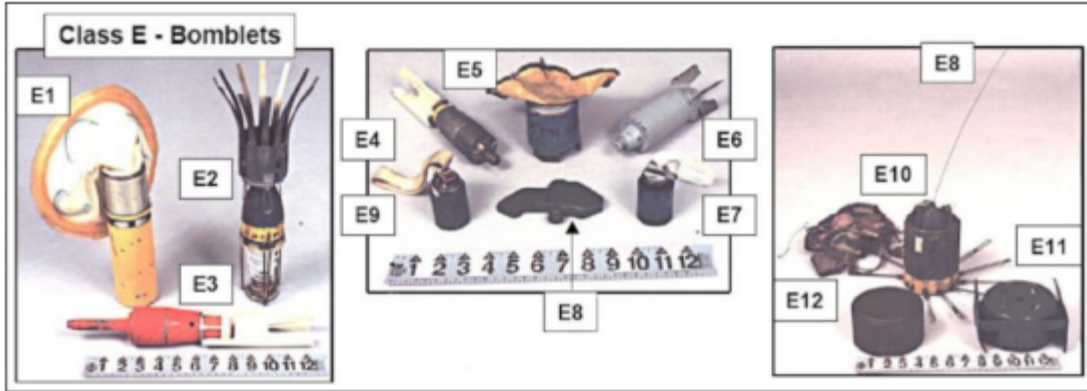


Figure 17. Class E UXOs (Bomblets)

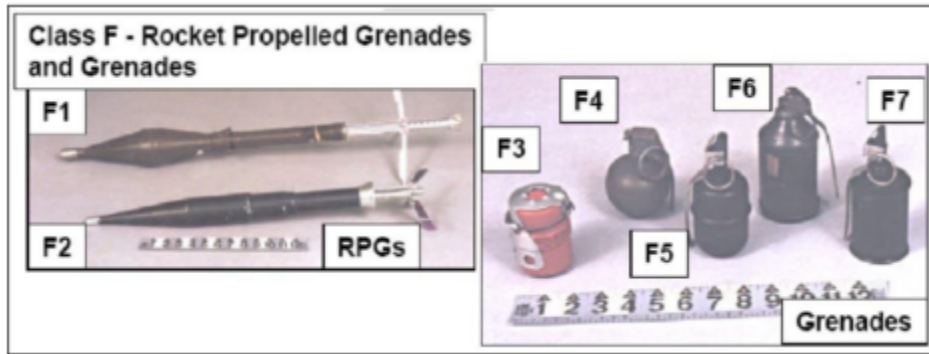


Figure 18. Class F UXOs (Rocket-Propelled Grenades & Hand Grenades)



## Appendix F. MOS Selection Checklist, Desirable- & Undesirable Considerations

MOS Selection Checklist	
1	Are MOSs available that are on the centerline and at either end of the original runway?
2	Crater and spall repairs - how many and what size? (A MOS location that involves the least number and smallest size craters and spalls is usually the most attractive option)
3	Are there longer or wider MOSs than ICC requirements, but do not require additional repairs?
4	Are there MOSs that have expansion potential, yet require limited additional repairs?
5	UXO: a.) Are there any UXO or bomblet fields that exclude a candidate MOS from further consideration (large buried bombs that will require excavation)?; b.) Will in-place detonation make the option worse? c.) Are bomblets so heavily mixed with crater debris that clearance will be too slow? d.) Has time delay for start of crater repair necessitated by UXO clearance been estimated?
6	Have shortest access routes been chosen consistent with the degree of repairs required?
7	Are access/egress routes positioned close to the end of the MOS? (At least two routes are desired, with minimal MOS back-taxiing requirements)
8	Existing MOS: a.) Is there an existing MOS? b.) Is it still operable? c.) Can it be made operable with minimal repair and marking?
9	Can a MOS be made operable by altering operational requirements (types of aircraft expected to use the MOS, gross weights, use of arresting system, unidirectional vs. bidirectional operations, etc.)? Consult with director of operations or supervisor of flying & notify wing commander of possibilities.
10	Arresting System: a.) Is an arresting system required for operations? b.) Is there a MOS candidate that includes an in-place arresting system? Is candidate MOS centered sufficiently with pendant to permit proper arresting system operation? c.) Is there sufficient crater free pavement on both sides of the arresting system? d.) Is a MAAS available?
11	How well trained are ADR teams? Can they complete damage repair in the 4 hours criterion?
12	What is the condition of the troops (fatigue, morale, attrition, etc.)?
13	What is the current condition of the ADR equipment?
14	What is the Chemical-Biological-Radiological-Nuclear (CBRN) state?
15	What are the environmental factors (weather, lighting, etc.)?
16	What is the possibility of reattack?
17	Navigational Aids: a.) Will the MOS location allow the use of existing NAVAIDS? b.) Are NAVAIDS needed? c.) Are existing NAVAIDS operational?

Figure 19. Minimum Operating Strip Selection Checklist

<b>Desireable MOS Selection Aspects</b>	
1	Crater locations on MOS that facilitate repair in pairs rather than single repairs may be desirable to reduce crater repair times. (RQC will normally be more restrictive for closely spaced craters).
2	MOS aligned on existing centerline to reduce marking time and take advantage of surviving NAVAIDS.
3	MOS with one end (either threshold or departure) situated on threshold of the original runway.
4	A MOS that can utilize an existing in-place arresting system.
5	Craters which are located close to material stockpiles.
6	A MOS with access/egress routes at each end.
7	A MOS with a minimal number of crater repair locations.
8	A MOS with dimensions longer and wider than the nominal 5,000' by 50'.

**Figure 20. Desirable Minimum Operating Strip Selection Aspects**

<b>Undesireable MOS Selection Aspects</b>	
1	Craters located so close together that there is no clear working space around them.
2	More craters, spalls, & UXO than a full ADR team can handle in a 4-hour time frame.
3	Craters within the first & last 1,000 feet of the MOS (these are the takeoff/landing touchdown zones; repair RQC in these zones are most restrictive).
4	Boxed-in MOS, one that has large craters situated at the ends that limit expansion potential.
5	Craters in either an aircraft arresting system's cable approach or fixed tape sweep.
6	Only one access route with no potential of developing a second route.

**Figure 21. Undesirable Minimum Operating Strip Selection Aspects**

## Appendix G. Enlisted Civil Engineer Evaluation Protocol

In Table 12 and Table 13 (below), triennial Silver Flag airfield damage assessment exercise data has been provided. This data set includes the performance of five separate teams, evaluating the one-and-one-quarter mile practice runway, located at the Contiguous United States, Contingency Training site, Panama City, Florida. Each team assessed the same configuration of pavement damage and mock explosive hazards under similar environmental and climatological conditions. Each team consisted of one (x1) non-specific enlisted civil engineer specialties: one (x1) enlisted Engineering Assistant ('EA'); and two (x2) enlisted Explosive Ordnance Disposal ('EOD Techs'). The skill levels of the airmen evaluated ranged between three (novice) and seven (expert) levels. Each team was equipped with a six-passenger, light-duty pickup truck, a land-mobile-radio (LMR; with signal booster), and a scaled airfield map. Three of the five teams conducted their Airfield Damage Assessment Team (ADAT) exercise on August 10, 2017, and two teams completed their exercise during their encampment on September 28, 2017. Both of these evaluation periods have been tabulated in Table 12. Similarly, a third evaluation period – consisting of four teams – was conducted on December 12, 2017 (Table 13). Throughout the duration of the exercises, each team was evaluated by a seven-level cadre member of their corresponding specialty.

Table 12 (below) shows eight (x8) total objects; two craters (C), two spall fields (S), three UXOs (X), and one bomblet field (B). Table 7 (below) shows seven (x7) total objects; one spall field (S), two craters (C), and four UXOs (X). Column A ("Item #") identifies which item the team is acknowledging. Column B ("Team") identifies which

team identified which item. Subsequent columns within that row record that team's performance identifying, quantifying, and qualifying the object of interest. Column C ("Type") refers to what the object is identified as; 'C' indicates a crater, 'S' indicates a spall field, 'X' indicates a UXO, and 'B' indicates a bomblet field. Column D ("CL Dist.") indicates the distance (measured in feet) along the centerline – from a predetermined datum – that the team locates the damage to begin. Correspondingly, Column J denotes where the damage or object terminates along the centerline. Column E ("L/R") denotes whether the damage or object is to-the-left or to-the-right of the centerline. Column F ("Distance L/R") indicates the distance (measured in feet) the object or damage begins to-the-left or -right of the centerline. Column G ("D/W") is a quantifier, that specifies whether the damage or object is being measured as a 'diameter' (typically a crater), or as a 'width' (spalls and bomblet fields). Column H ("Size D/W") is the associated measurement (in feet) for the input to the previous column (G). Column I ('Field') is populated if the damage is a 'field' (e.g., spall fields and bomblet fields). Columns J through N are a repeat of previous columns. Their purpose is to quantify the termination of the damage and/or explosive hazards. Column O ("Single/Multi") serves a similar purpose as Column I in that it is populated when there are numerous objects (e.g., pits and blemishes as per a spall field or bomblets and sub-munitions as per a bomblet field). Column P ("Qty") corresponds to the approximate number of blemishes or sub-munitions present within that spall- or bomblet-field. Lastly, Column Q ("Description") is a write-in qualifier for teams to provide additional clarification of their findings. Note: in row associated with the item number, the bold text indicates the solution (correct answer) for each item. The airfield damage items were recorded using the Pavement

Reference Marking System (PRMS) that is native to the EA career field. Non-correspondingly, all explosive hazards were recorded using the Military Grid Reference System (MGRS). At the time of the evaluations, the answer keys were not shared among evaluators. As such, only the pavement damage (PRMS) items – 1, 5, 6, and 7 – have a known solution. Due to the exclusion of a solution set for the explosive hazards, the positive identification (or lack thereof) of the object will be the primary concern (note: the assessment methodology was amended in the December evaluations) a secondary metric will be the relative placement and quantification recorded across each of the nine teams – essentially, how precise are they as a collective, relative to one another.

**Table 12. Enlisted Civil Engineer Exercise Results (Baseline; 1 of 2)**

Data Set #1: Five, 4-Pers Teams, Two Separate Evaluation Periods (Aug 2017 & Oct 2017)																
Item No.	Team	Type	CL Dist - Start	L/R	Dist L/R	D/W	Size D/W	Field	CL Dist - Stop	L/R	Dist L/R	D/W	Size D/W	Single/Multi	Qty	Description
1		S	5450	R	45	W	40	F	5550	R	45	W	45	M	150	
	1	S	5400	R	65	W	30	F	5560	R	30	W	30	M	40	
	2	θ	—	—	—	—	—	—	—	—	—	—	—	—	—	
	3	C	5450	R	100	W	30	F	5550	L	20	W	30	M	50	
	4	S	5450	R	45	W	45	F	5550	R	45	W	45	M	150	
	5	θ	—	—	—	—	—	—	—	—	—	—	—	—	—	
2		X	5000	L	30											<<< No Values Provided - Assumed/Based on Mean Team Performance
	1	X	5050	L	35											
	2	X	5100	L	30											
	3	X	4650	L	32											
	4	X	5100	L	30											
	5	X	5100	L	30											
3		B	4850	R	50	W	30	F	4850	R	40	W	30	M	15	<<< No Val - Assumed
	1	B	4825	R	60	W	30	F	4850	R	30	W	60	M	20	
	2	B	4850	R	45	W	20	F	4900	R	45	W	15	M	15	
	3	B	4820	R	50	W	10	F	4835	R	40	W	10	M	8	
	4	B	4950	R	50	W	30	F	4800	R	50	W	30	M	20	
	5	B	4850	R	60	W	30	F	4800	R	40	W	30	M	10	
4		X	4250	L	30											<<< No Values Provided - Assumed/Based on Mean Team Performance
	1	X	4325	L	30											
	2	X	4300	L	30											
	3	X	4200	L	30											
	4	X	4300	L	30											
	5	X	4320	L	30											
5		C	3875	R	0	D	50									
	1	C	3300	L	0	D	20									
	2	C	3300	L	0	D	60									
	3	--	--	--	--	--	--									
	4	C	3900	--	--	D	45									
	5	C	3900	R	0	D	40									
6		S	3555	L	30	W	5	F	3520	L	30	W	5	M	2	
	1	--	--	--	--	--	--									
	2	--	--	--	--	--	--									
	3	--	--	--	--	--	--									
	4	--	--	--	--	--	--									
	5	S	3550	L	30	W	10	F	3500	R	30	W	10	M	2	
7		C	3275	R	0	D	50									
	1	--	--	--	--	--	--									
	2	--	--	--	--	--	--									
	3	--	--	--	--	--	--									
	4	C	3250	R	10	D	45									
	5	C	3280	L	10	D	50									
8		X	3250	L	10											<<< No Values Provided - Assumed/Based on Mean Team Performance
	1	X	3300	L	0											
	2	X	3300	L	15											
	3	--	--	--	--	--	--									
	4	X	3250	L	2											
	5	X	3280	L	10											

**Table 13. Enlisted Civil Engineer Exercise Results (Baseline; 2 of 2)**

Data Set #2: Four, 4-Pers Teams, One Evaluation Period (Dec 2017)																
Item No.	Team	Type	CL Dist - Start	L/R	Dist L/R	D/W	Size D/W	Field	CL Dist - Stop	L/R	Dist L/R	D/W	Size D/W	Single/Multi	Qty	Description
1		X	5230	R	75											16RFU 44797 22644
	1	X	5200	R	75											
	2	X	5200	R	75											
	3	X	5220	R	75											
	4	X	5200	R	20											
2		S	5450	R	45	W	40	F	5550	R	45	W	45	M	150	
	1	B	5550	R	40	W	15	F	5500	R	45	W	10	M	9	
	2	S	5500	R	50	W	20	F	5550	R	60	W	25	M	9	
	3	S	5575	R	20	W	20	F	5450	R	20	W	20	M	15	
	4	B	5550	R	30	W	10	F	5560	R	30	W	10	M	10	
3		X	4840	L	40											16R FU 44764 22524
	1	X	4850	L	25											
	2	X	4800	L	25											
	3	X	4825	L	25											
	4	X	4825	L	20											
4		X	4584	R	30											16RFU447822447
	1	X	4550	R	40											
	2	X	4575	R	40											
	3	X	4580	R	40											
	4	X	4630	R	20											
5		C	3875	R	0	D	50									
	1	C	3850	L	0	D	50									
	2	--	--	--	--	--	--									
	3	--	--	--	--	--	--									
	4	C	3920	L	0	D	40									
6		X	2664	R	50											16R FU 44800 22166
	1	--	--	--	--	--	--									
	2	--	--	--	--	--	--									
	3	--	--	--	--	--	--									
	4	--	--	--	--	--	--									
7		C	3270	L	0	D	50									
	1	C	3250	L	0	D	75									
	2	--	--	--	--	--	--									
	3	C	3100	L	0	D	40									
	4	C	3260	L	0	D	50									
8		X	3270	L	0											16R FU 44788 22047
	1	X	3300	R	15											
	2	X	3275	R	20											
	3	X	3250	R	35											
	4	X	3280	R	30											

**Table 14. Comparison of Location Precision Among Nine Enlisted Civil Engineer Teams**

Comparison Across Nine Teams			
	Average Difference From True (ft)	Average Difference From True (m)	Order of Magnitude (vs. GPS)
CL precision	72.0	21.9	2.19
L/R precision	10.2	3.1	0.31
W/D precision	7.2	2.2	0.22

**Table 15. Location Accuracy Among Nine Enlisted Civil Engineer Teams**

Comparison of Average Team Performance (vs. Commercial GPS Performance)			
	Average Difference From True (ft)	Average Difference From True (m)	Order of Magnitude (vs. GPS)
CL accuracy	93.21	28.4	2.84
L/R accuracy	16.67	5.1	0.51
W/D accuracy	10.36	3.2	0.32

## Appendix H. Civil Engineer Officer Evaluation Protocol

1. Open the GUI titled ‘MAIN.m’ by double left-clicking the icon in the file folder
  - a. The MATLAB™ application will open with MAIN.m open as the primary script

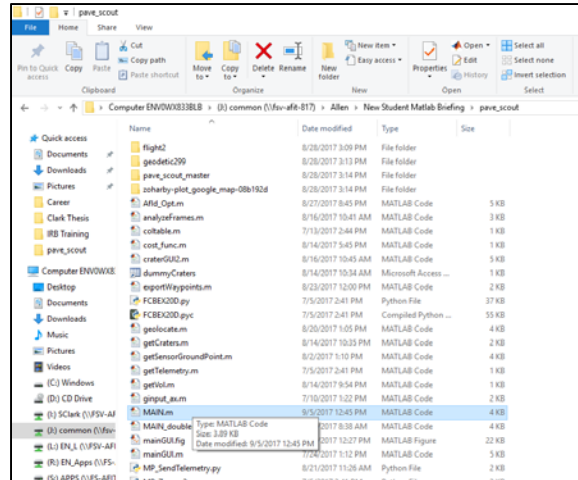
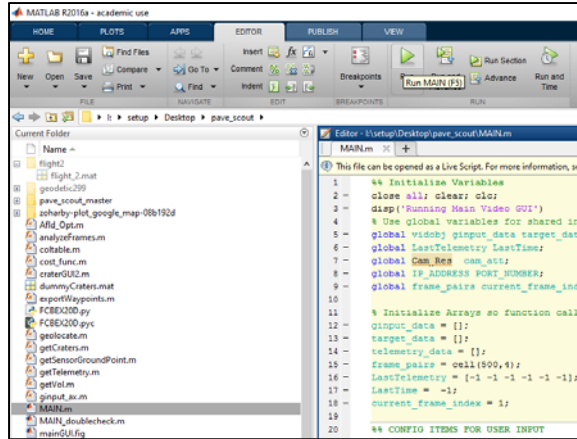


Figure 22. Step 1.a. - Open MAIN.m

- b. Under the “EDITOR” ribbon, single left-click “Run”





**Figure 23. Step 1.b. - Run MAIN.m**

- c. A blank GUI will populate – minimize it and return to the MATLAB™ screen

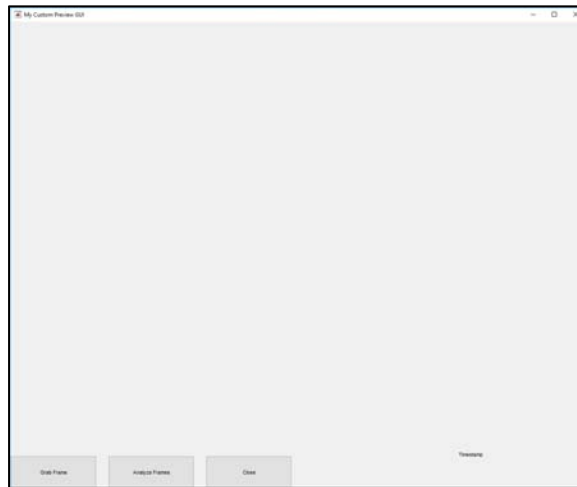


**Figure 24. Step 1.c. - Blank GUI Screen**

- 2. In the “Current Folder” pane, select the “pave\_scout\_master” file by single right-clicking

- a. In the menu that appears, hover your cursor over “Add to Path”, then left-click to select “Selected Folders and Subfolders”

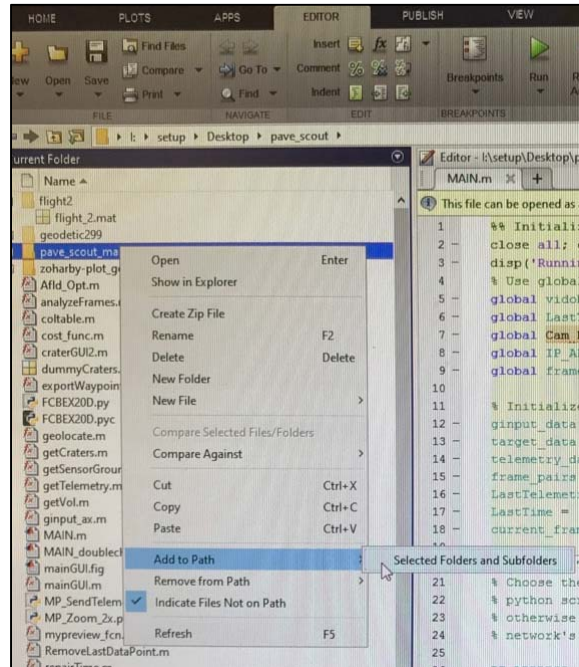


**Figure 25. Step 2. - Adding Folders to Path**

3. Repeat this process for the files “zoharby-plot\_google\_map-08b192d” and “flight2”
4. In the Current Folder pane, left-click the expand icon to the right of “flight2”
  - a. Double left-click “flight\_2.mat” to load telemetry and image data

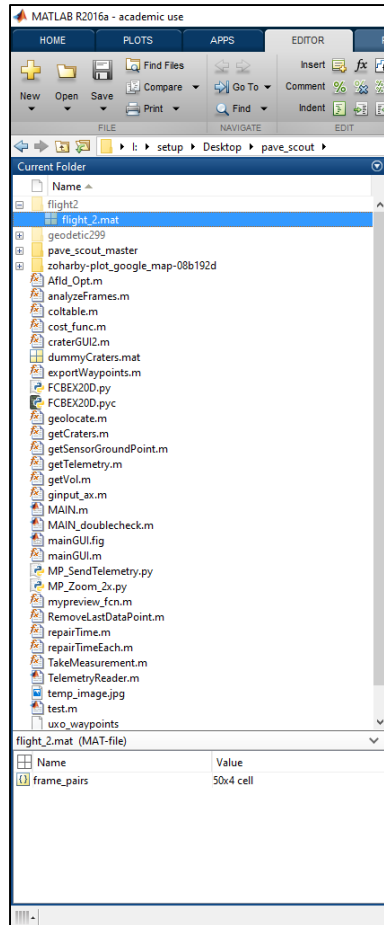


Figure 26. Step 4. - Loading flight\_2.mat

5. In the Current Folder pane, double left-click “analyzeFrames.m”
  - a. Under the “EDITOR” ribbon single left-click “Run”

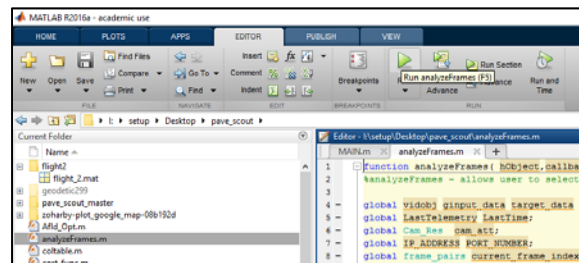
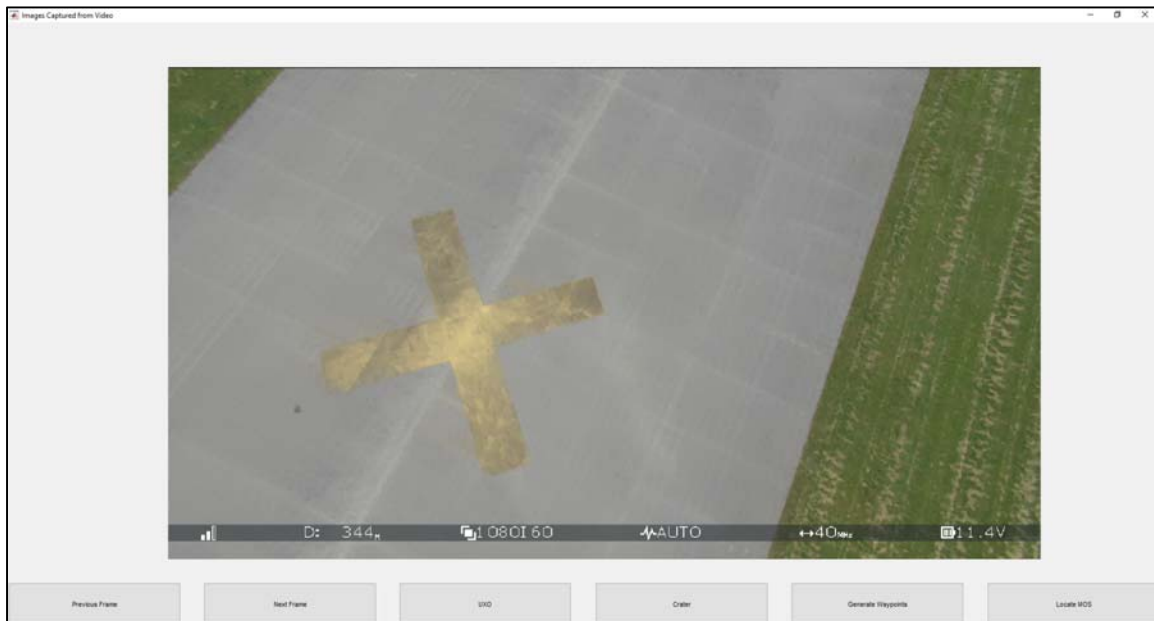


Figure 27. Step 5. - Loading & Running analyzeFrames.m

6. A new GUI will populate with the following options: “Previous Frame”, “Next Frame”, “UXO”, “Crater”, “Generate Waypoints”, and “Locate MOS”
  - a. Single left-click “Next Frame” to display the first image



**Figure 28. Step 6. - Properly Configured Graphical User Interface**

7. Operators advance forward and backward through the images until objects are detected
8. When an operator identifies a UXO, they single left-click “UXO”
  - a. In response, a new window with the same image appears
  - b. The operator then single left-clicks the UXO, specifies their estimate for the UXO class – in a drop down menu that populates
  - c. Lastly, the operator either selects “Confirm Placement”, “Cancel Placement”, or “Go Back” (to the previous screen) with a single left-click

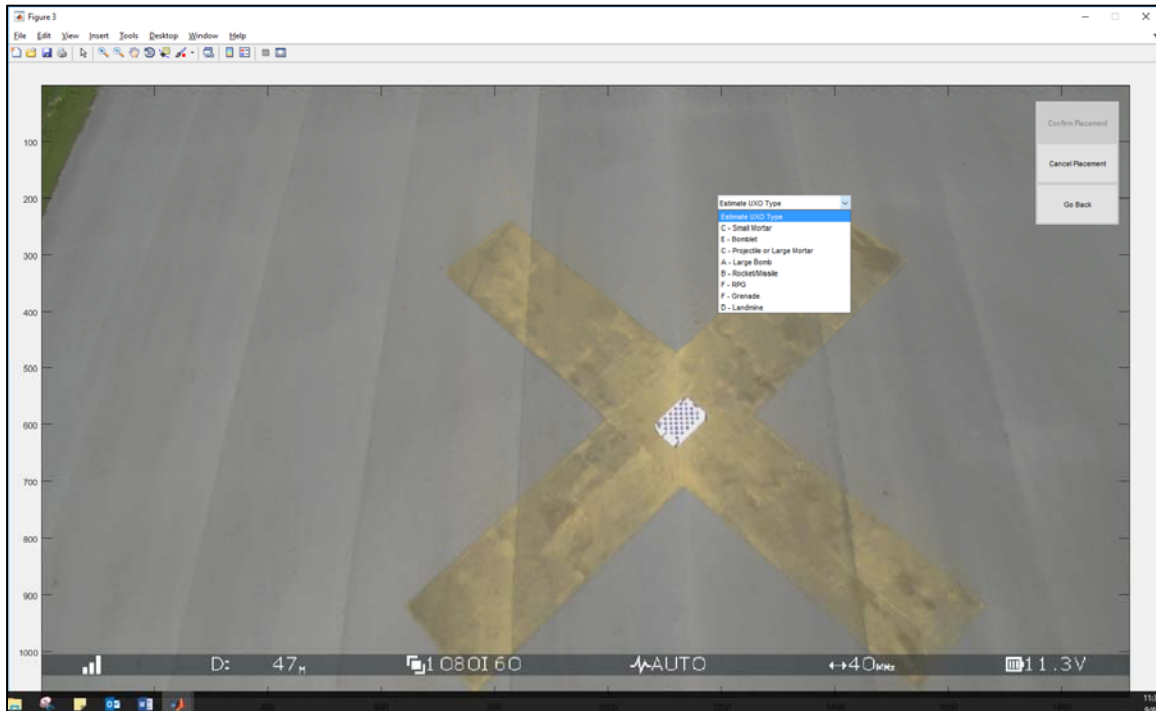


**Figure 29. Step 8. - Identifying and Locating UXOs**

9. The operator then continues his/her inspection
10. When a spall or crater is detected, the operator single left-clicks “Crater”
  - a. In response, a new window with the same image appears
  - b. The operator then single left-clicks a series of points around the edge of the crater
  - c. The GUI will automatically place waypoints and connect them with lines to form a polygon
    - i. A minimum of three points will be required to identify a crater

- d. When complete, the operator single left-clicks either “Confirm Placement”, “Cancel Last Pt” (to remove an erroneous waypoint), or “Go Back” (to navigate back to the previous screen) with a single left-click

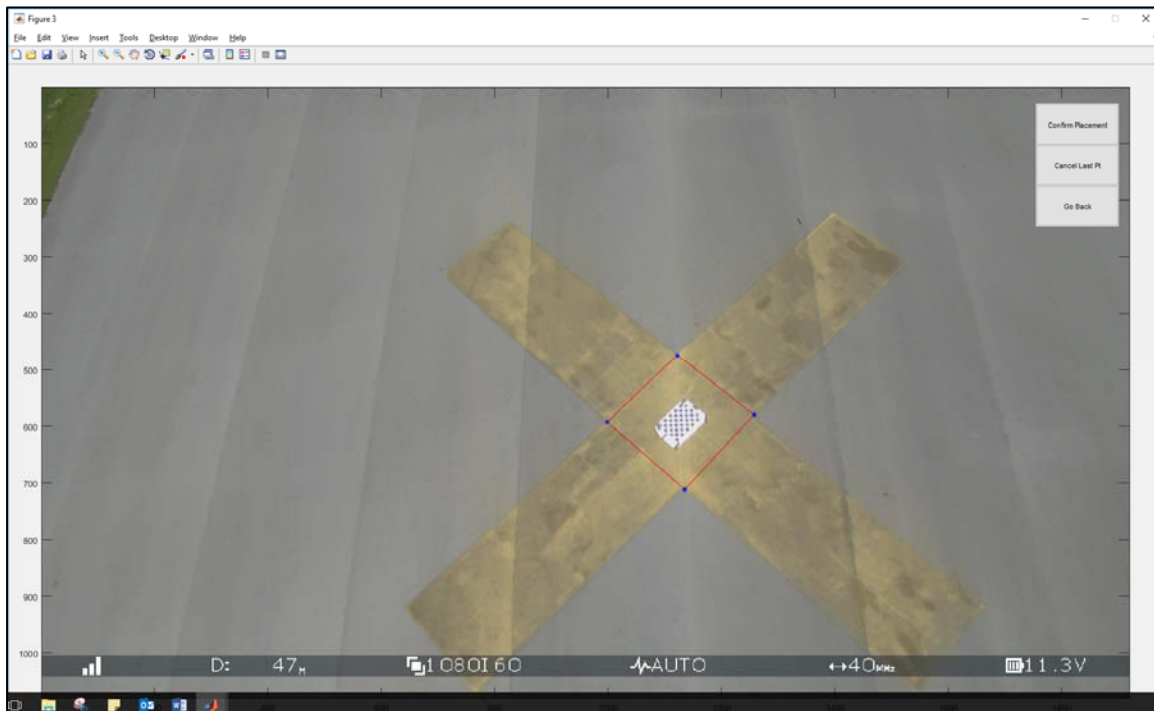


**Figure 30. Step 10. - Identifying & Locating Spalls & Craters**

11. The operator then continues his/her inspection until all images have been analyzed
  - a. At this point, the operator then single left-clicks “Generate Waypoints” to produce a waypoint file to be ingested (using Python™) into MissionPlanner™
  - b. Before the waypoints are generated, the script will ask the operator to specify the altitude with which the hexa-copter will be flown

- i. The operator will specify 20 [meters]

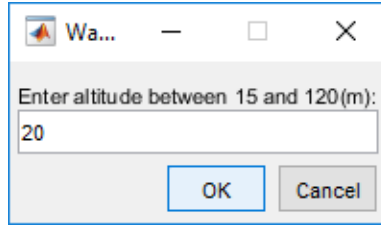


**Figure 31. Step 11.b.i. - Specifying the altitude for multi-rotor inspection**

12. Finally, the operator will single left-click “Locate MOS”
  - a. A figure will appear with the Aircraft landing requirements – depicted in the form of a rectangle – superimposed on a Google Earth™ image of the airfield surface
  - b. Evaluation of the civil engineer officer operator will be complete when the MOS is identified on the airfield surface

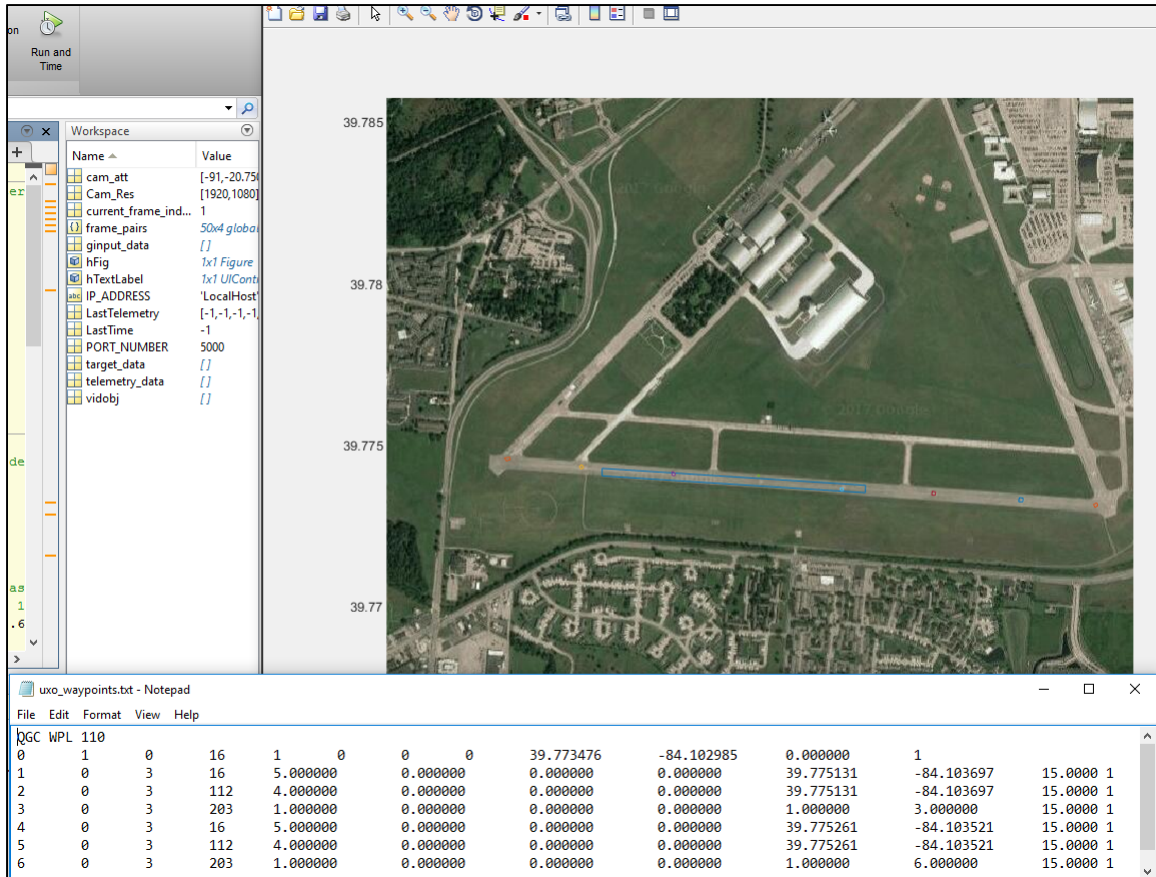


Figure 32. Step 12. - Waypoints and MOS Outputs



## Appendix I. Small Unmanned Aerial Systems Components

### Equipment

**FrSky Taranis Radio Controller.** The FrSky Taranis X9D™ radio (Figure 33. FrSky Taranis X9D Radio Transmitter) is a powerful controller favored by many RC SUAS enthusiasts. This transmitter operates on a 2.4 gigahertz frequency and offers up to 16 channels. Additional features include: audio speech outputs (values, alarms, mode settings, etc.), real-time flight data logging receiver signal strength indicator, and super low latency and vibration alerts. This device weighs eight pounds and is widely available in hobbyist stores as well as in online retailers.



Figure 33. FrSky Taranis X9D Radio Transmitter

**Sony High Definition, Color Block Camera.** The Sony FCB-EV7100 camera (shown in Figure 34 is a 1/2.8 type Exmor CMOS image sensor with full HD (1920x1080) at 60 fps and 10x optical zoom. It features a wide-dynamic range, auto Infrared Cutfilter Removal (ICR), and a compact design (Sony Corporation of America, 2017a).



**Figure 34. Sony High Definition Color Block Camera (FCB-EV7100)**

**CONNEX HD Wireless Video Receiver.** The Amimon CONNEX HD (**Figure 35**) is a 5.8-GHz, wireless video receiver/transmitter that is cable of providing live/near-zero latency, feed from an SUAS imaging platform. This receiver allows up to 1080p resolution at 60 frames per second. The basic system features a range of up to 3,300 feet (line-of-sight), can display data from telemetry modules, and supports encrypted video transmission.



**Figure 35. Amimon CONNEX HD Wireless Video Transmitter/Receiver**

**AV.io video capture card.** The Av.io 4k video capture card (shown in Figure 36) – Epiphan Systems Inc. – is a rugged HD video and audio capture card capable of producing an image resolution of 4096x2160, with 4K UHD video streaming at 30 fps and 1080p at 60fps. In addition, this card pushes PCM audio over HDMI™ at up to 24-bit, 96kHz via two-channel stereo audio outputs, complete with automatic resampling at 48kHz and 16-bit encoding. Lastly, this device captures video and audio with, at most, one to two frames of latency, thus providing a seamless, real-time airfield survey (Epiphan Systems Inc., 2017).



**Figure 36. Epiphan Av.io 4k Video Capture Card**

The purpose of the AV.io 4K card is to collect the live video feed from the Sony Block Camera/ Skywalker and stream it to the GCS in real-time. In Figure 37, the Survey Phase system configuration is shown. Starting with the Sony FCB-EV7100 Block Camera, a live video is fed through an iShot® HDMI™ interface board and ported into a Connex HD video transmitter (Amimon Ltd., 2016). The feed is then channeled across a 5.1-5.8 GHz radio frequency to the Connex receiver located at the GCS. The Connex receiver then ports HDMI™ into the AV.io 4K capture card which is then connected via a universal serial bus 3.0 into the GCS which is running the custom MATLAB™ script (Allen, 2017).

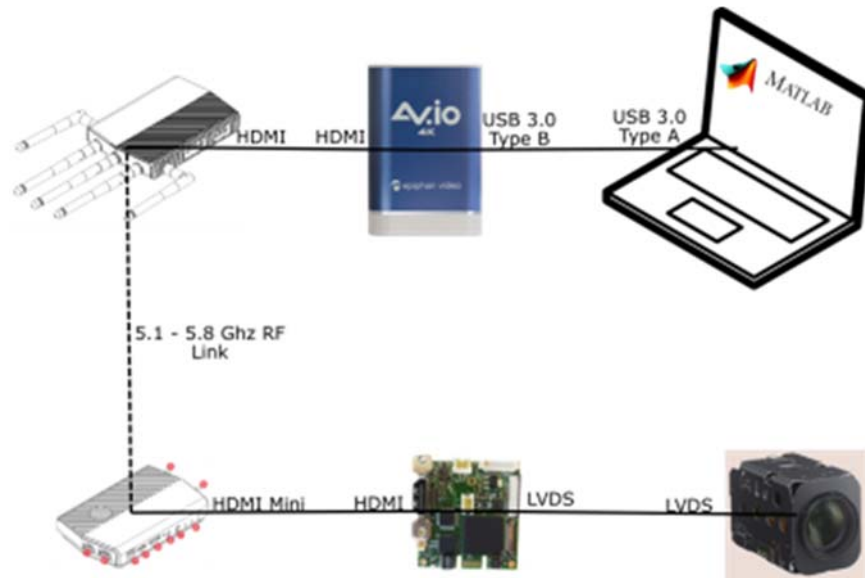


**Figure 37. Skywalker Imaging System Configuration**

**Sony  $\alpha$ 6000 camera.** The Sony  $\alpha$ 6000 (shown in Figure 38) is a mirrorless, compact, E-mount, digital camera that boasts a 24.3-megapixel APS-C CMOS sensor and diffraction-reducing image processor. It is capable of 11 frames-per-second continuous shooting and subject-tracking as well as full HD video recording at 1080p/60p and 24p (Sony Corporation of America, 2017). The base camera has been fitted with an E 20.4 millimeter, F2.8, “pancake” lens, which has a seven-blade circular aperture for rounded defocusing and an aspherical lens that maintains high contrast and minimizes distortion and flatness of the image pane; it has a compact design, faster autofocus response, and reduced minimum focusing distances (Sony Corporation of America, 2017b).



**Figure 38. Sony  $\alpha$ 6000 Digital Camera & 2.8x20mm "Pancake" Lens**

**Storm Pro-3 gimbal.** The Storm Pro-3 (shown in Figure 39) is a universal, three-axis, brushless gimbal that is mounted on the underside of the Tarot T960 frame. It provides 360 degrees of continuous pan axis movement and a self-contained Inertial Measurement Unit (IMU) for stabilization; it can support any camera – including smart phones – weighing 350 – 600 grams (Helipal, 2017a). This gimbal was included such that atmospheric conditions (i.e., wind) would be mitigated during imaging operations. In addition, while not utilized in the final configuration, the Storm Pro-3 is capable of being linked to the Pixhawk 2.0 autopilot. This linkage allows for pinpoint geo-locating accuracy and enhanced image stabilization during flight.



**Figure 39. Storm Pro-3, Universal Three Axis Gimbal**

**Pixhawk Autopilot.** The Pixhawk™ 2.0 (shown in Figure 40) is an autopilot developed by the Pixhawk open hardware community in 2017 (PX4 Autopilot, 2017). It features “14 pulse width modulation/servo outputs”, connectivity options for peripherals, an integrated backup system for in-flight recovery and manual override, multi-tone piezo audio indicator, and microSD card. This autopilot operates on a 32-bit STM32F427 Cortex M4 core with FPU processor, “capable of 168 MHz, 256 kB Ram, 2 MB Flash, and 32-bit failsafe co-processor” (PX4 Autopilot, 2017).



Figure 40. Pixhawk 2.0



**Table 16. SUAS Equipment Cost Summary**

<b>Custom Hex-Rotor Components (www.Helipal.com)</b>	<b>Quantity</b>	<b>Unit Price</b>	<b>Sub-Total</b>
Tarot™ T960 Foldable 6-Axis Hexa-copter Carbon Fiber Frame for FPV TL960A	1	\$ 349.99	\$ 349.99
Tarot™ T810/960 Landing Gear TL96013	1	\$ 74.90	\$ 74.90
Storm Pro-3, Three Axis, Universal Gimbal	1	\$ 599.00	\$ 599.00
1555 15x55 Carbon Fiber Propeller Props CW/CCW for DJI S800 Octocopter Multirotor (pair)	6	\$ 15.12	\$ 45.36
KDE4215XF-465 Brushless Motor for Heavy-Lift Electric Multi-Rotor (SUAS) Series	6	\$ 148.95	\$ 893.70
KDEXF-UAS95HVC 95A+HV Electronic Speed Controller (ESC) for Electric Multi-Rotor (UAS) Series	6	\$ 195.95	\$ 1,175.70
Multistar Hi-Capacity 22,000mAh Lithium-Polymer Battery	2	\$ 145.92	\$ 291.84
Turnigy Bolt V2 850mAh 3S 130C High Voltage Lithium Polymer Battery	1	\$ 9.99	\$ 9.99
Sony a6000 Camera	1	\$ 649.99	\$ 649.99
Sony SEL-20F28 E-Mount 20mm F2.8 Prime Fixed Lens	1	\$ 348.00	\$ 348.00
Pixhawk 2.0 & GNSS Kit	1	\$ 309.39	\$ 309.39
FrSky Taranis X9d+ Transmitter	1	\$ 279.00	\$ 279.00
Lenovo ThinkPad T470 (example ground control station)	1	\$ 979.00	\$ 979.00
Fasteners, Retaining Straps, Adhesives, and Other	1	\$ 100.00	\$ 100.00
<b>Hex-Rotor Total:</b>			<b>\$ 6,105.86</b>

<b>Off-the-Shelf Multi-Rotor (approx \$2,500 assembly fee; www.rc-drones.com)</b>	<b>Quantity</b>	<b>Unit Price</b>	<b>Estimated Total</b>
DJI Spread Wings S800 (excludes: Gimbal, Batteries, Communications Equipment, & Imaging Device)	1	\$ 3,399.00	\$ 6,965.21
DJI Spread Wings S900 (excludes: Gimbal, Batteries, Communications Equipment, & Imaging Device)	1	\$ 3,699.00	\$ 7,265.21
DJI Spread Wings S1000+ (excludes: Gimbal, Batteries, Communications Equipment, & Imaging Device)	1	\$ 3,999.00	\$ 7,565.21
FreeFly CineStar 8 Octocopter (excludes: Gimbal Batteries, Communications Equipment, & Imaging Device)	1	\$ 4,409.00	\$ 7,376.21
Altavian R8700 Galaxy (includes Altavian ground control equipment & sensor)	1	\$15,100.00	\$ 28,230.00

<b>Custom Skywalker X8 Components (www.fpvmodel.com)</b>	<b>Quantity</b>	<b>Unit Price</b>	<b>Sub-Total</b>
Skywalker X-8 'Flying Wing' FPV RC Plane, Black	1	\$ 298.00	\$ 298.00
Turnigy G46 Electronic Brushless Outrunner Motor670kv	1	\$ 55.52	\$ 55.52
13x4 Folding Pusher Propeller	1	\$ 7.99	\$ 7.99
Pixhawk 1.0 & GNSS Kit	1	\$ 216.57	\$ 216.57
Sony FCBEV7100 10x Zoom Full HD CMOS Block Camera	1	\$ 649.95	\$ 649.95
Custom Catapult Launcher	1	\$ 2,000.00	\$ 2,000.00
Epiphan AV.io 4K Capture Card for HD 1080p 60 fps and UHD 4K 30 fps	1	\$ 499.00	\$ 499.00
Amimon CONNEX Wireless HD Video Link Receiver for UAVs	1	\$ 1,930.09	\$ 1,930.09
Turnigy Bolt V2 850mAh 3S 130C High Voltage Lithium Polymer Battery	2	\$ 9.99	\$ 19.98
FrSky Taranis X9d+ Transmitter	1	\$ 279.00	\$ 278.00
Lenovo ThinkPad T470 (example ground control station)	1	\$ 979.00	\$ 979.00
Fasteners, Retaining Straps, Adhesives, and Other	1	\$ 100.00	\$ 100.00
<b>Skywalker Total:</b>			<b>\$ 7,034.10</b>

<b>Off-the-Shelf Multi-Rotor (approx \$700-1000 assembly fee; www.uavsysteminternational.com &amp; www.altavian.com)</b>	<b>Quantity</b>	<b>Unit Price</b>	<b>Estimated Total</b>
Skywalker 1800 (excludes: batteries, imaging device, & launcher)	1	\$ 999.95	\$ 7,455.97
Altavian F7200 AT Nova (includes Altavian ground control equipment & sensor)	1	\$15,180.00	\$ 28,310.00
Altavian F7200 AE Nova (includes Altavian ground control equipment & sensor)	1	\$19,260.00	\$ 32,390.00
MD Group 1400mm FPV Sky Surfer (excludes: batteries, imaging device, & launcher)	1	\$ 1,100.00	\$ 7,556.02

<b>Altavian Off-the-Shelf Ground Stations &amp; Sensor Packages (www.altavian.com)</b>	<b>Quantity</b>	<b>Unit Price</b>	
Altavian Flare Ground Control Station GS20, Software, & 12 Mos Updates	1	\$ 5,950.00	
Altavian Flare GS10 Radio Module	1	\$ 1,370.00	
Altavian Flare Software and Updates	1	\$ 260.00	
Altavian Fusion Modular Sensor Package MP22 CV20SVN	1	\$ 5,550.00	

**Software**

*Mission Planner™.*



The Mission Planner (MP) is a donation-based, open source, hobbyist drone software, developed by Michael Osborne of the ArduPilot™ development team in 2010 (ArduPilot Development Team, 2016). The MP Graphic User Interface (GUI) provides a host of features including flight data, flight planning, configuration and tuning, simulations, telemetry logging, geo-tagging, remote camera triggering, and more. In this thesis approach, MP was used for both the Skywalker X8 and the Tarot 960. MP was leveraged to store tuning presets for each air vehicle, as well as mission parameters (waypoints), which could be rapidly updated and ported to the air vehicle Auto Pilot (Pixhawk 2.0), both on the ground, as well as in-flight. Lastly, MP was used to collect telemetry data and remotely trigger the Tarot 960 Sony  $\alpha$ 6000, as well as provide current air vehicle status and information during flying operations.

#### ***Simple BGC.***

The Simple BGC software, version 2.40b (BaseCam Electronics, 2017) is a GUI designed to tune the Storm Pro-3 gimbal. This GUI enables users to push firmware updates to the gimbal as well as calibrate the accelerometer and gyroscope for IMU accuracy. Lastly, this GUI enables operators to push configuration settings to the gimbal's motherboard to optimize performance. Within the context of the research, the GUI was used to lock down the yaw (pan) axis of the gimbal, such that the camera would rotate in unison with the air vehicle during maneuvering. This differed from a two-axis gimbal in that, should the drone experience rough air or sudden course correction, the yaw-axis would serve as a dampener, thus preserving image stability.

#### ***MATLAB™ R2016a.***

MATLAB is a proprietary numerical computing environment and programming language that was developed by Cleve Moler, chairman of the computer science department at the University of New Mexico, as an alternative to his students having to learn Fortran in 1984 (The MathWorks Inc., 2017). Now, presently owned and licensed by The MathWorks Inc., MATLAB allows programmers to produce matrix manipulations, plot, develop algorithms, and create custom GUIs for interfacing with programs written in other languages such as Python, Fortran, Java, C, C++ and C#.

MATLAB was used in this thesis to develop a custom GUI with which Google Earth™ satellite imagery, MP telemetry logs, and aerial imagery could be used to produce a constellation of geo-located markers (“pins”). The end-product used predetermined aircraft takeoff requirements – graphically displayed as a rectangle in the scale of the satellite image – and particle swarm analysis to optimize the positioning of a MOS with respect to identified craters, spalls, and UXOs. Finally, the ML GUI leveraged a Python™ script to push the finalized waypoints back into MP for the Tarot 960 to navigate for final imaging.

Pix4D™. Pix4D mapper (version 3.3) is “photogrammetry software for professional drone-based mapping, purely from images” produced either through a mobile-, desktop-, or cloud-based system (Pix4D, 2017). Founded in 2011, Pix4D is a clone of École Polytechnique Federale de Lausanne (EPFL) developed in Switzerland. The software produces a dense 3D point cloud via overlapping images. Capabilities include digital surface and terrain modeling, ortho-mosaic (high resolution, geo-located mapping devoid of perspective distortions), volume calculations, contour lines (i.e., topographic surveys), 3D textured modeling, and thermography (radio-metrically accurate mapping with temperature values for each pixel).

The developers’ website lists the following applications of the Pix4D software: mining, 2D and 3D mapping, and forensics. The software is also advertised to support the following industries: surveying (mapping, mining, forensics), construction (earthwork, Building Information Modeling, inspection), agriculture, and real estate.

## Appendix J. Civil Engineer Officer MATLAB™ & 2D Ortho-mosaic Results

**Table 17. Civil Engineer Officer Responses - MATLAB Graphic User Interface**

	1.a. Time to Respond	1.b. Time to Assess(seconds)	1.c. Time to Plot Damage	1.d. Time to Produce MOS/MAOS	2.a. Accuracy of Identifying Damage & FOD	2.a.i. Positive Identification of Damage/FOD; Road Flares	2.a.ii. Positive Identification of Damage/FOD; Pool	2.a.iii. Positive Identification of Damage/FOD; Beach Towel	2.a.iv. Positive Identification of Damage/FOD; Zoo Map	2.a.ix. False Positives - FOD	2.a.x. False Negatives - FOD	2.b. Accuracy of Identifying Explosive Hazards	2.b.i. Positive Identification of Hazards; Mortar 1	2.b.i. Positive Identification of Hazards; Mortar 2	2.b.iii. Positive Identification of Hazards; Mortar 3	2.b.iv. Positive Identification of Hazards; Mortar 4	2.b.v. False Positives - UXO	2.b.vi. False Negatives - UXO	Total Objects Correctly Identified	Total Objects False Positive	Total Objects False Negative
Subject 1	121	0	5	126	0	1	1	1	1	0	1	1	1	0	1	0	1	0	6	0	2
Subject 2	95	0	5	100	0	1	1	1	1	0	1	1	0	0	1	0	2	5	0	3	
Subject 3	125	0	5	130	0	1	1	1	0	1	1	1	1	0	0	2	2	5	2	3	
Subject 4	148	0	5	153	0	1	0	0	0	3	1	1	0	0	0	2	3	2	2	6	
Subject 5	212	0	5	217	0	1	1	1	2	1	1	1	0	0	0	8	3	4	10	4	
Subject 6	278	0	5	283	0	1	0	0	0	3	0	0	0	0	0	4	4	1	4	7	
Subject 7	129	0	5	134	0	0	0	1	0	3	0	0	0	0	0	1	4	1	1	7	
Subject 8	194	0	5	199	0	1	0	0	0	3	0	0	0	0	0	1	4	1	1	7	
Subject 9	199	0	5	204	0	1	1	0	0	2	0	0	0	0	0	0	4	2	0	6	
Subject 10	316	0	5	321	1	1	1	1	1	0	0	1	0	1	2	2	4	6	3	2	
Subject 11	322	0	5	327	0	1	1	0	2	2	0	0	0	0	1	4	2	3	6		
Subject 12	330	0	5	335	1	1	1	1	7	0	1	0	0	0	1	3	5	8	3		
Subject 13	207	0	5	212	0	1	1	0	1	2	0	0	0	0	0	4	2	1	6		
Subject 14	167	0	5	172	0	1	1	0	0	2	0	0	0	0	0	4	2	0	6		
Subject 15	271	0	5	276	1	1	1	1	1	0	0	0	0	0	4	4	4	5	4		
Subject 16	224	0	5	229	1	1	1	1	1	0	0	0	0	0	2	4	4	3	4		
Subject 17	165	0	5	170	1	1	1	0	0	1	0	0	0	0	0	4	3	0	5		
Subject 18	305	0	5	310	1	1	1	0	1	1	0	0	0	0	0	3	4	3	4	5	
Subject 19	370	0	5	375	1	1	1	1	0	0	0	1	0	1	2	2	6	2	2		
Subject 20	132	0	5	137	0	1	1	0	0	2	0	0	0	0	0	4	2	0	6		
Subject 21	258	0	5	263	1	1	1	0	1	1	0	0	0	0	0	4	3	1	5		
Subject 22	125	0	5	130	1	1	1	0	0	1	0	0	0	0	0	4	3	0	5		
Subject 23	159	0	5	164	1	1	1	1	1	0	0	0	0	0	0	4	4	1	4		
Subject 24	327	0	5	332	0	1	1	0	3	2	0	1	0	0	0	3	3	3	5		
Subject 25	243	0	5	248	1	1	1	1	0	0	0	0	0	0	2	4	4	2	4		
AVG	216.88	0.00	5.00	221.88	0.44	0.96	0.84	0.48	0.84	1.28	0.24	0.20	0.00	0.16	1.40	3.40	3.32	2.24	4.68		
MIN	95.00	0.00	5.00	100.00	0.00	0.00	0.00	0.00	0.00	0.00	0.00	0.00	0.00	0.00	0.00	1.00	1.00	0.00	2.00		
MAX	370.00	0.00	5.00	375.00	1.00	1.00	1.00	1.00	7.00	3.00	1.00	1.00	0.00	1.00	8.00	4.00	6.00	10.00	7.00		
RANGE	275.00	0.00	0.00	275.00	1.00	1.00	1.00	1.00	7.00	3.00	1.00	1.00	0.00	1.00	8.00	3.00	5.00	10.00	5.00		

Table 18. Civil Engineer Officer Responses - 2D Ortho-mosaic Interface

	1.a. Time to Respond	1.b. Time to Assess(seconds)	1.c. Time to Plot Damage	1.d. Time to Produce MOS/MAOS	2.a. Accuracy of Identifying Damage & FOD	2.a.i. Positive Identification of Damage/FOD; Road Flares	2.a.ii. Positive Identification of Damage/FOD; Pool	2.a.iii. Positive Identification of Damage/FOD; Beach Towel	2.a.iv. Positive Identification of Damage/FOD; Zoo Map	2.a.ix. False Positives - FOD	2.a.x. False Negatives - FOD	2.b. Accuracy of Identifying Explosive Hazards	2.b.i. Positive Identification of Hazards; Mortar 1	2.b.i. Positive Identification of Hazards; Mortar 2	2.b.iii. Positive Identification of Hazards; Mortar 3	2.b.iv. Positive Identification of Hazards; Mortar 4	2.b.v. False Positives - UXO	2.b.vi. False Negatives - UXO	Total Objects Correctly Identified	Total Objects False Positive	Total Objects False Negative
Subject 1	98	0	5	103	0	1	1	1	1	0	1	1	1	0	0	1	1	1	6	1	2
Subject 2	61	0	5	66	0	1	1	1	1	0	1	1	1	0	0	1	0	1	6	0	2
Subject 3	91	0	5	96	0	1	1	1	1	1	1	1	0	0	0	0	3	4	1	4	
Subject 4	97	0	5	102	0	1	1	1	0	1	1	1	1	0	1	0	1	6	0	2	
Subject 5	321	0	5	326	1	1	1	1	1	1	0	1	1	0	1	3	1	7	4	1	
Subject 6	191	0	5	196	0	1	1	1	0	1	1	1	1	0	1	5	1	6	5	2	
Subject 7	348	0	5	353	0	1	1	0	6	2	1	1	1	0	1	3	1	5	9	3	
Subject 8	146	0	5	151	0	1	1	1	0	1	1	1	1	0	1	1	1	6	1	2	
Subject 9	234	0	5	239	0	1	1	1	1	1	1	1	1	0	1	4	1	6	5	2	
Subject 10	230	0	5	235	1	1	1	1	0	0	1	1	1	0	1	2	1	7	2	1	
Subject 11	231	0	5	236	0	1	1	1	1	1	1	1	1	0	1	3	1	6	4	2	
Subject 12	275	0	5	280	1	1	1	1	9	0	1	1	1	0	1	0	1	7	9	1	
Subject 13	180	0	5	185	0	1	1	1	6	1	1	1	1	0	1	1	1	6	7	2	
Subject 14	190	0	5	195	0	1	1	1	0	1	1	1	0	0	1	0	2	5	0	3	
Subject 15	274	0	5	279	1	1	1	1	2	0	1	1	1	0	1	2	1	7	4	1	
Subject 16	228	0	5	233	0	1	1	1	0	1	1	1	1	0	1	3	1	6	3	2	
Subject 17	354	0	5	359	0	1	1	1	0	1	1	1	1	1	1	6	0	7	6	1	
Subject 18	222	0	5	227	1	1	1	1	1	0	1	1	1	0	1	2	1	7	3	1	
Subject 19	242	0	5	247	1	1	1	1	0	0	1	1	1	0	1	2	1	7	2	1	
Subject 20	125	0	5	130	0	1	1	1	0	1	1	1	1	0	1	1	1	6	1	2	
Subject 21	253	0	5	258	1	1	1	1	0	0	1	1	1	0	1	2	1	7	2	1	
Subject 22	68	0	5	73	0	1	1	1	0	1	0	0	0	0	0	4	3	0	5		
Subject 23	101	0	5	106	0	1	1	1	0	1	1	1	1	0	1	1	1	6	1	2	
Subject 24	600	0	5	605	1	1	1	1	6	0	1	1	1	0	1	0	1	7	6	1	
Subject 25	323	0	5	328	0	1	1	1	8	1	1	1	1	0	0	2	2	5	10	3	
AVG	219.32	0.00	5.00	224.32	0.32	1.00	1.00	0.96	1.68	0.72	0.96	0.88	0.04	0.88	1.76	1.24	6.04	3.44	1.96		
MIN	61.00	0.00	5.00	66.00	0.00	1.00	1.00	0.00	0.00	0.00	0.00	0.00	0.00	0.00	0.00	0.00	3.00	0.00	1.00		
MAX	600.00	0.00	5.00	605.00	1.00	1.00	1.00	1.00	9.00	2.00	1.00	1.00	1.00	1.00	6.00	4.00	7.00	10.00	5.00		
RANGE	539.00	0.00	0.00	539.00	1.00	0.00	0.00	1.00	9.00	2.00	1.00	1.00	1.00	1.00	6.00	4.00	4.00	10.00	4.00		

## Appendix K. Baseline Metrics and Civil Engineer Officer Statistics

**Table 19. Descriptive Statistics for Object False Negatives in the Baseline Metrics**

<i>Teams 1-5: Pure Object False Negative Detection Rate</i>		<i>Teams 6-9: Pure Object False Negative Detection Rate</i>		<i>Combined: Pure Object False Negative Detection Rate</i>	
Mean	0.275	Mean	0.107142857	Mean	0.205882353
Standard Error	0.071499507	Standard Error	0.05952381	Standard Error	0.049398594
Median	0	Median	0	Median	0
Mode	0	Mode	0	Mode	0
Standard Deviation	0.452202587	Standard Deviation	0.314970394	Standard Deviation	0.407351238
Sample Variance	0.204487179	Sample Variance	0.099206349	Sample Variance	0.165935031
Kurtosis	-0.95301373	Kurtosis	5.613784615	Kurtosis	0.219143819
Skewness	1.047504425	Skewness	2.686455177	Skewness	1.487808432
Range	1	Range	1	Range	1
Minimum	0	Minimum	0	Minimum	0
Maximum	1	Maximum	1	Maximum	1
Sum	11	Sum	3	Sum	14
Count	40	Count	28	Count	68
27.50%		10.71%		20.59%	

**Table 20. Descriptive Statistics for Explosive Hazard False Negatives in Baseline Metrics**

<i>Teams 1-5: Explosive Hazard False Negative Detection Rate</i>		<i>Teams 6-9: Explosive Hazard False Negative Detection</i>		<i>Combined: Explosive Hazard False Negative Detection</i>	
Mean	0.05	Mean	0	Mean	0.027778
Standard Error	0.05	Standard Error	0	Standard Error	0.027778
Median	0	Median	0	Median	0
Mode	0	Mode	0	Mode	0
Standard Deviation	0.223606798	Standard Deviation	0	Standard Deviation	0.166667
Sample Variance	0.05	Sample Variance	0	Sample Variance	0.027778
Kurtosis	20	Kurtosis	#DIV/0!	Kurtosis	36
Skewness	4.472135955	Skewness	#DIV/0!	Skewness	6
Range	1	Range	0	Range	1
Minimum	0	Minimum	0	Minimum	0
Maximum	1	Maximum	0	Maximum	1
Sum	1	Sum	0	Sum	1
Count	20	Count	16	Count	36
5.00%		0.00%		2.78%	

**Table 21. Descriptive Statistics for Explosive Hazard False Positives in Baseline**

**Metrics**

<i>Teams 1-5: Explosive Hazard False Positive Detection Rate</i>		<i>Teams 6-9: Explosive Hazard False Positive Rate</i>		<i>Combined: Explosive Hazard False Positive Rate</i>	
Mean	0	Mean	0.071428571	Mean	0.029850746
Standard Error	0	Standard Error	0.049563476	Standard Error	0.020947148
Median	0	Median	0	Median	0
Mode	0	Mode	0	Mode	0
Standard Deviation	0	Standard Deviation	0.262265264	Standard Deviation	0.171459798
Sample Variance	0	Sample Variance	0.068783069	Sample Variance	0.029398462
Kurtosis	#DIV/0!	Kurtosis	11.18343195	Kurtosis	30.87550296
Skewness	#DIV/0!	Skewness	3.519630882	Skewness	5.652816474
Range	0	Range	1	Range	1
Minimum	0	Minimum	0	Minimum	0
Maximum	0	Maximum	1	Maximum	1
Sum	0	Sum	2	Sum	2
Count	39	Count	28	Count	67
0.00%		7.14%		2.99%	

**Table 22. Descriptive Statistics for Incorrect Object Identification in Baseline**

**Metrics**

<i>Teams 1-5: Object Incorrect Identification Rate</i>		<i>Teams 6-9: Object Incorrect Identification Rate</i>		<i>Combined: Object Incorrect Identification Rate</i>	
Mean	0.034482759	Mean	0.08	Mean	0.055555556
Standard Error	0.034482759	Standard Error	0.055377492	Standard Error	0.031464006
Median	0	Median	0	Median	0
Mode	0	Mode	0	Mode	0
Standard Deviation	0.185695338	Standard Deviation	0.276887462	Standard Deviation	0.231212282
Sample Variance	0.034482759	Sample Variance	0.076666667	Sample Variance	0.053459119
Kurtosis	29	Kurtosis	9.640831758	Kurtosis	14.47378227
Skewness	5.385164807	Skewness	3.297525541	Skewness	3.992335155
Range	1	Range	1	Range	1
Minimum	0	Minimum	0	Minimum	0
Maximum	1	Maximum	1	Maximum	1
Sum	1	Sum	2	Sum	3
Count	29	Count	25	Count	54
3.45%		8.00%		5.56%	



**Table 23. Civil Engineer Officer Object False Negative Detection Statistics**

<i>2D 1-25: Pure Object False Negative Detection Rate</i>		<i>MATLAB 1-25: Pure Object False Negative Detection Rate</i>	
Mean	1.96	Mean	4.68
Standard Error	0.2039608	Standard Error	0.31475
Median	2	Median	5
Mode	2	Mode	6
Standard Deviation	1.0198039	Standard Deviation	1.57374
Alpha	0.05	Alpha	0.05
Ho: Avg New Method <=	0.2059	Ho: Avg New Method <=	0.2059
Ha: Avg New Method >	0.2059	Ha: Avg New Method >	0.2059
Range	4	Range	5
Minimum	1	Minimum	2
Maximum	5	Maximum	7
Sum	49	Sum	117
Count (n)	25	Count (n)	25
Degrees of Freedom	24.00	Degrees of Freedom	24.00
t-Statistic	4.610	t-Statistic	9.869
p-Value	1.000	p-Value	1.000
Critical Value	-1.711	Critical Value	-1.711
<b>Goal:</b> find evidence suggesting that the average number of false negative detection for the new method is equal-to or less-than the status quo			
2D Ortho-mosaic: T-Stat (4.610) > Critical Value (-1.711); therefore, Reject Ho			
MATLAB T-Stat (9.869) > Critical Value (-1.711); therefore, Reject Ho			

**Table 24. Civil Engineer Officer Explosive Hazard False Positive Statistics**

<i>2D 1-25: Explosive Hazard False Positive Detection Rate</i>		<i>MATLAB 1-25: Explosive Hazard False Positive Detection Rate</i>	
Mean	3.44	Mean	2.24
Standard Error	0.60575	Standard Error	0.50425
Median	3	Median	2
Mode	1	Mode	0
Standard Deviation	3.02875	Standard Deviation	2.52124
Ho: Avg New Method $\leq$	0.0299	Ho: Avg New Method $\leq$	0.0299
Ha: Avg New Method $>$	0.0299	Ha: Avg New Method $>$	0.0299
Range	10	Range	10
Minimum	0	Minimum	0
Maximum	10	Maximum	10
Sum	86	Sum	56
Count (n)	25	Count (n)	25
Degrees of Freedom	24	Degrees of Freedom	24
t-Statistic	0.679	t-Statistic	-0.558
p-Value	0.748	p-Value	0.291
Critical Value	-1.976	Critical Value	-1.976
<b>Goal:</b> find evidence suggesting that the average number of false negatives for the new method is equal-to or less-than the status quo			
2D Ortho-mosaic: T-Stat (0.679) > Critical Value (-1.976); therefore, Reject Ho MATLAB T-Stat (-0.558) > Critical Value (-1.976); therefore, Reject Ho			

**Table 25. Civil Engineer Officer Incorrect Identification Statistics**

<i>2D 1-25: Object Incorrect Identification Rate</i>		<i>MATLAB 1-25: Object Incorrect Identification Rate</i>	
Mean	1.96	Mean	4.68
Standard Error	0.203961	Standard Error	0.31475
Median	6	Median	3
Mode	6	Mode	2
Standard Deviation	1.019804	Standard Deviation	1.57374
Ho: Avg New Method <=	0.0556	Ho: Avg New Method <=	0.0556
Ha: Avg New Method >	0.0556	Ha: Avg New Method >	0.0556
Range	4	Range	5
Minimum	3	Minimum	1
Maximum	7	Maximum	6
Sum	151	Sum	83
Count (n)	25	Count (n)	25
Degrees of Freedom	24.00	Degrees of Freedom	24.00
t-Statistic	4.610	t-Statistic	9.869
p-Value	1.000	p-Value	1.000
Critical Value	-1.654	Critical Value	-1.654
<b>Goal:</b> find evidence suggesting that the average number of incorrectly identified objects for the new method is equal to or less than the status quo			
2D Ortho-mosaic: T-Stat (4.610) > Critical Value (-1.654); therefore, Reject Ho MATLAB T-Stat (9.869) > Critical Value (-1.654); therefore, Reject Ho			

**Table 26. Summary Statistics (Baseline vs. Civil Engineer Officers)**

<b>Maximum Assessment Time (217 Meter Sample)</b>			
	seconds	minutes	sec/linear-meter
3EXXX Baseline Metric (Conventional Approach)	194	3.2	0.89
32EXX MATLAB GUI (1080p Video Capture)	370	6.2	1.71
32EXX 2D Ortho-Mosaic (24MP Still Imagery)	354	5.9	1.63
<b>Minimum Assessment Time (217 Meter Sample)</b>			
	seconds	minutes	sec/linear-meter
3EXXX Baseline Metric (Conventional Approach)	129	2.2	0.59
32EXX MATLAB GUI (1080p Video Capture)	95	1.6	0.44
32EXX 2D Ortho-Mosaic (24MP Still Imagery)	61	1.0	0.28
<b>Mean Assessment Time (217 Meter Sample)</b>			
	seconds	minutes	sec/linear-meter
3EXXX Baseline Metric (Conventional Approach)	162	2.7	0.75
32EXX MATLAB GUI (1080p Video Capture)	216.88	3.6	1.00
32EXX 2D Ortho-Mosaic (24MP Still Imagery)	203.45	3.4	0.94
<b>False Negative UXO Reports</b>			
	Qty Objects Identified	Total Objects	%UXO False Negative
3EXXX Baseline Metric (Conventional Approach)	35	36	2.8%
32EXX MATLAB GUI (1080p Video Capture)	15	100	85.0%
32EXX 2D Ortho-Mosaic (24MP Still Imagery)	31	100	69.0%
<b>False Negative FOD Reports</b>			
	Qty Objects Identified	Total Objects	%UXO False Negative
3EXXX Baseline Metric (Conventional Approach)	--	--	--
32EXX MATLAB GUI (1080p Video Capture)	68	100	32.0%
32EXX 2D Ortho-Mosaic (24MP Still Imagery)	18	100	82.0%
<b>Overall False Negative Reports</b>			
	Qty Objects Identified	Total Objects	%UXO False Negative
3EXXX Baseline Metric (Conventional Approach)	35	36	2.8%
32EXX MATLAB GUI (1080p Video Capture)	83	200	58.5%
32EXX 2D Ortho-Mosaic (24MP Still Imagery)	49	200	24.5%
<b>T-Statistic</b>			
3EXXX Baseline Metric (Conventional Approach)	17.25		
32EXX MATLAB GUI (1080p Video Capture)	13.14		
32EXX 2D Ortho-Mosaic (24MP Still Imagery)	9.17		
<b>Pearson Correlation</b>			
3EXXX Baseline Metric (Conventional Approach)	-0.833		
32EXX MATLAB GUI (1080p Video Capture)	-0.094		
32EXX 2D Ortho-Mosaic (24MP Still Imagery)	-0.434		

**Table 27. AFIT SUAS 217m Airfield Assessment Times & 3000m Extrapolation**

Skywalker X8		Time (sec)	Personnel	Description
<b>Phase I - Setup</b>	Unpack & Assemble Air Vehicle	718.2	x1 Tech	
	Unpack & Assemble Catapult		x2 Tech	
	Unpack & Assemble Ground Station		x1 GCS Op	
	System Check Air Vehicle		x1 GCS Op, x1 Tech	
	Load Parameters & Mission Plan		x1 GCS Op	
<b>Phase II - Mission</b>	Launch/Achieve Stable Flight	45	x1 Safety Pilot	217m sample (linear approx. 3,000m = 31.1 min)
	Fly Mission Plan (Altitude = 40m, Airspeed = 15m/s)	135	x1 GCS Op, x1 Safety Pilot	
<b>Phase III - Analyze</b>	Recover	30	x1 Safety Pilot	Avg. Subject analysis time (linear approx. 3,000m = 49.9 min) Varies based on internet connection
	Load Frame Pairs	5	x1 GCS Op	
	Analyze	216.9	x1 GCS Op	
	Generate Waypoints Locate MOS	1 3		
<b>Total (seconds):</b>		<u>1119.1</u>	<b>Manpower: x4</b>	
<b>Total (minutes - 217m):</b>		<u>18.7</u>		
<b>Approximate Total (minutes - 3,000m):</b>		<u>93.8</u>		
Tarot Hex-Rotor		Time (sec)	Personnel	Description
<b>Phase I - Setup</b>	Unpack & Assemble Air Vehicle	309	x1 Tech	
	System Check Air Vehicle		x1 GCS Op, x1 Tech	
	Load Parameters & Mission Plan		x1 GCS Op	
<b>Phase II - Mission</b>	Launch/Achieve Stable Flight	42	x1 Safety Pilot	217m sample (linear approx. 3,000m = 35.2 min)
	Fly Mission Plan (Altitude = 80m, Airspeed = 10m/s*)	153	x1 GCS Op, x1 Safety Pilot	
	Recover	30	x1 Safety Pilot	
<b>Phase III - Analyze</b>	Process Images	840	x1 GCS Op	2D Pix4D output (3D = 18-min) Avg. Subject analysis time (linear approx. 3,000m = 46.88 min) Assumes GUI built for Pix4D
	Analyze	203.5	x1 GCS Op	
	Locate MOS	3		
<b>Total (seconds):</b>		<u>1550.5</u>	<b>Manpower: x3</b>	
<b>Total (minutes - 217m):</b>		<u>25.8</u>		
<b>Approximate Total (minutes - 3,000m):</b>		<u>102.0</u>		

## Appendix L. MAIN.m MATLAB™ Script

The following MATLAB script was written by Captain Timothy Allen in 2017.

This script serves as the foundation for the graphic user interface. All subsequent scripts, commands, and inputs run through this script.

```
%% Initialize Variables
close all; clear; clc;
disp('Running Main Video GUI')
% Use global variables for shared info. Could use structure instead
global vidobj ginput_data target_data telemetry_data;
global LastTelemetry LastTime;
global Cam_Res cam_att;
global IP_ADDRESS PORT_NUMBER;
global frame_pairs current_frame_index;

% Initialize Arrays so function calls will work later
ginput_data = [];
target_data = [];
telemetry_data = [];
frame_pairs = cell(500,4);
LastTelemetry = [-1 -1 -1 -1 -1 -1]; % Initialized with dummy numbers
LastTime = -1;
current_frame_index = 1;

%% CONFIG ITEMS FOR USER INPUT
% Choose the IP Address for wherever this main file is called. If the
% python script and matlab script run on the same computer, use LocalHost,
% otherwise both the python script and matlab script need to use the
% network's IP address of the matlab computer.

IP_ADDRESS = 'LocalHost'; % Use for operation on same computer
%IP_ADDRESS = '192.168.1.134'; % IP Address of computer this script runs on
PORT_NUMBER = 5000; % Arbitrary port number (match with .py script)
cam_att = [0 -62 0]; % Body-frame camera angles (Yaw Pitch Roll)

%% Instructions for working with GPS and UTM Coordinates
%[N,E,Zone,lcm]=ell2utm(GPS_origin(1),GPS_origin(2));
%UTM_origin = [N,E,Zone,lcm];
```

```

%{
Take lat long in decimal degrees
Convert to radians
Convert to UTM coordinates (Cartesian Units of North and East)
Add or subtract meters north and east to find new UTM coordinates as needed
Convert new coordinates to ell GPS coordinates
Convert to new coordinates to degrees
Use final answer as needed (Plug into google maps for easy viewing)
%}

%% Set Camera & Hardware settings & values
% Create a video input object. Specify which camera device (2, in my case).
% Specify video format if multiple formats exist (I chose the highest
% resolution)
%vidobj = videoinput('winvideo',1,'YUY2_1920x1080');
%vidobj.ReturnedColorspace = 'rgb';
%vidInfo = propinfo(vidobj);
%Cam_Res = vidInfo.VideoResolution.DefaultValue;

%% Create Video GUI
% Create a figure window. This example turns off the default
% toolbar and menubar in the figure.
hFig = figure('Toolbar','none',...
    'Menubar','none',...
    'NumberTitle','Off',...
    'Name','My Custom Preview GUI');

% Change the size of the GUI and placement in window as desired.
% set(gcf,'units','normalized','outerposition',[0 .04 1 0.96]);
set(gcf,'units','normalized','outerposition',[0 .04 0.65 0.96]);

% Set up the push buttons:
% These buttons call the functions
uicontrol('String','Grab Frame',...
    'Callback',@grabFrame,...
    'Units','normalized',...
    'Position',[0 0 0.15 .07]);
uicontrol('String','Analyze Frames',...
    'Callback',@analyzeFrames,...
    'Units','normalized',...
    'Position',[.17 0 .15 .07]);
uicontrol('String','Close',...
    'Callback','close(gcf)',...
    'Units','normalized',...
    'Position',[0.34 0 .15 .07]);

```

```

% Create the text label for any changing text. Not required
hTextLabel = uicontrol('style','text','String','Timestamp', ...
    'Units','normalized',...
    'Position',[0.6 0 .4 .08]);

% Create the image object in which you want to
% display the video preview data.
vidRes = vidobj.VideoResolution;
imWidth = vidRes(1);
imHeight = vidRes(2);
nBands = vidobj.NumberOfBands;

% Create handle for the video
hImage = subimage(zeros(imHeight,imWidth, nBands));

% Set up the update preview window function.
% NOTE: THIS IS WHAT ALLOWS FOR REAL TIME VIDEO
setappdata(hImage,'UpdatePreviewWindowFcn',@mypreview_fcn);

% Make handle to text label available to update function.
setappdata(hImage,'HandleToTimestampLabel',hTextLabel);

% Begins video playback
preview(vidobj, hImage);

% NOTE: This software requires the following unique toolboxes:
% Image Acquisition Toolbox
% Geodetic Tools (addon); % This must be downloaded
% Video drivers, etc.

```



## Appendix M. AnalyzeFrames.m MATLAB™ Script

The following MATLAB script was written by Captain Timothy Allen in 2017.

This script synthesizes the collected imagery and telemetry logs into a format allowing user commands and resulting in a web-based output.

```
function analyzeFrames( hObject,callbackdata )
%analyzeFrames - allows user to select objects of interest from captured images.

global vidobj ginput_data target_data telemetry_data;
global LastTelemetry LastTime;
global Cam_Res cam_att;
global IP_ADDRESS PORT_NUMBER;
global frame_pairs current_frame_index;
global still_img craterList uxoList current_tele mos;

uxoList = {};
craterList = {};
frame_index = 0;
Cam_Res = [1920, 1080];%uncomment for test

%% Create Video GUI
% Create a figure window. This example turns off the default
% toolbar and menubar in the figure.
hFig = figure('Toolbar','none',...
    'Menubar','none',...
    'NumberTitle','Off',...
    'Name','Images Captured from Video');

% Change the size of the GUI and placement in window as desired.
% set(gcf,'units','normalized','outerposition',[0 .04 1 0.96]);
set(gcf,'units','normalized','outerposition',[0 .04 0.65 0.96]);

% Set up the push buttons:
% These buttons call the functions
uicontrol('String','Previous Frame',...
    'Callback',@prevFrame,...
    'Units','normalized',...
    'Position',[0 0 0.15 .07]);
```

```

uicontrol('String', 'Next Frame',...
    'Callback', @nextFrame,...
    'Units','normalized',...
    'Position',[0.17 0 .15 .07]);
uicontrol('String', 'UXO',...
    'Units','normalized',...
    'Position',[0.34 0 .15 .07],...
    'Callback', @uxoGUI2);
uicontrol('String', 'Crater',...
    'Units','normalized',...
    'Position',[0.51 0 .15 .07],...
    'Callback', @craterGUI2);
uicontrol('String', 'Generate Waypoints',...
    'Callback', @exportWaypoints,...
    'Units','normalized',...
    'Position',[0.68 0 .15 .07]);
uicontrol('String', 'Locate MOS',...
    'Units','normalized',...
    'Position',[0.85 0 .15 .07],...
    'Callback', @Afld_Opt);

function nextFrame(hObject, evt)
    if ~isempty(frame_pairs{frame_index+1,1}) %There is another image
        frame_index = frame_index + 1
        still_img = frame_pairs{frame_index,1};
        imshow(still_img)
        current_tele = frame_pairs{frame_index,2};
    end
end

function prevFrame(hObject, evt)
    if frame_index - 1 > 0 % need to check bounds first
        if ~isempty(frame_pairs{frame_index-1,1})
            frame_index = frame_index - 1;
            still_img = frame_pairs{frame_index,1};
            imshow(still_img)
            current_tele = frame_pairs{frame_index,2};
        end
    end
end
end
end

```

**Air Force Institute of Technology**

---

*System Verification Review*

**Pave Scout® Airfield Damage  
Assessment System**


  
**U.S. AIR FORCE**

Maj Kijun Lee  
Capt Mike Kaniut  
Capt Tim Allen  
Capt Samuel Clark

1Lt R. Josh McGaha  
2Lt Taylor Bodin  
Mr. Gregory Roth

7 Oct 2017

---

  
**U.S. AIR FORCE**

## Overview

---

- CONOPS
- Final System Review
- Software Architecture
- TPMs & Historical Trends
- Requirements Verification & Validation
- Risk Assessment
- Design Shortcomings
- SUAS (SENG 550-650-651) Improvement

---

*Integrity - Service - Excellence*



U.S. AIR FORCE

## CONOPS

### ■ Problem Statement

#### ■ Airfield Damage Assessment is...

Manpower Intensive, Hazardous & Time Consuming (current capes ≈ 8 hrs)

#### ■ CE Flight Plan (2016 - 2036), LOE 2.4 Contingency Basing Resiliency

*Strategic Objective 2.4.1: "By FY20, develop, procure & field enhanced contingency asset protection & base recovery systems that capitalize on current & emerging technologies of robust forward access capability & mission resiliency in contested environments" – Maj Gen Tim Green*

Modernize Airfield Damage Assessment (automate, accelerate, & optimize)

### ■ Operational Concept

*To deliver timely and relevant inspection and assessment of runways, associated taxiways, and parking aprons to Civil Engineer Crews, prepared for runway repair actions*

*Integrity Service - Excellence*



U.S. AIR FORCE

## System Requirements

### ■ Physical requirements

#### ■ Rapid setup, systems check, & deployment (t < 15 min)

### ■ Functional requirements

#### ■ Evaluation of rwy, twy, & apron completed within 90 min

##### ■ Identify & Geo-locate pavement damage

- Spall fields
- Large/Small Craters

##### ■ Identify & Geo-locate UXOs

- Quantity

##### ■ Output algorithm produces actionable information for CE Repair Teams

- Output: crater repair & UXO clearing locations
- Output: Candidate Minimum Operating Strip

#### ■ Useable by non-pilot operators

*Integrity Service - Excellence*



U.S. AIR FORCE

## System Overview

- Initial fixed wing surveyor with live video feed of runway (CONEX HD)
- Video streams down (AV.io 4K) and can be processed with MATLAB code
  - Gather crater dimensions from video
  - Gather initial UXO detection
- Hex-rotor vehicle used for closer inspection of craters and possible UXOs

Integrity Service - Excellence

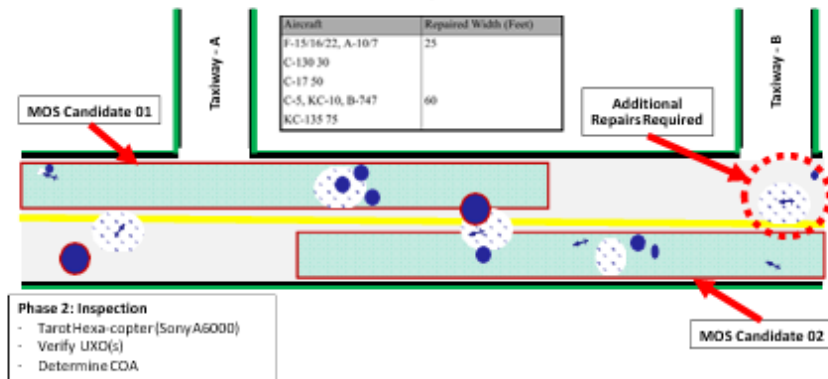


U.S. AIR FORCE

### MOS Template

(Dimensions, Aircraft, Fueling, & Environment Dependent)  
Provided by AFTRP-02, Strategic Air Control Center

### AFPAM 10-219, Volume 4



Integrity Service - Excellence



## Final System Review



*Integrity - Service - Excellence*



## Skywalker Statistics

- Resolution of initial flyover (Skywalker) air-vehicle sensor: **2.54 cm/pixel at 30 m AGL**
- Time to set up and launch system: **12.5 min**
- Time to complete initial flyover with Skywalker (fixed wing) air-vehicle: **10.1 min for two passes**
- Total Flight endurance: **40 Min**
- Time to process data and create report: **12 min** (300 images)
- Geolocation accuracy (RMS):
  - **1.71 m** with calibration
  - **2.88 m** without calibration
- False Positives: **0%** (0 objects)
- False Negatives: **20%** (80% of objects detected, 4/5 objects)

*Integrity - Service - Excellence*



U.S. AIR FORCE

## Hex-Rotor Statistics

- Resolution of initial flyover (Skywalker) air-vehicle sensor: **0.29 cm/pixel at 15 m AGL and 0.39 cm/pixel at 20 m AGL**
- Time to set up and launch system: **11.8 Min**
- Time to complete multi waypoint flight (8): **2.5 min**
- Total Flight endurance: **18-20 Min**
- Geolocation accuracy (RMS):
  - **1.71 m with calibration-need to change**
  - **2.88 m without calibration-need to change**
- False Positives: **0%** (0 objects)
- False Negatives: **20%** (80% of objects detected)

Integrity Service - Excellence



U.S. AIR FORCE

## Results



Integrity Service - Excellence



U.S. AIR FORCE

## Results

- Phase 1.1: Skywalker Pre-Flight: 11.97min
- Phase 1.2: Skywalker Launch @40m Altitude: 1min
- Phase 1.3: Skywalker Survey @40m x217m: 8.5min
  
- Phase 2.1: Tarot Pre-Flight: 5.15min
- Phase 2.2: Tarot Launch @20m Altitude: 0.35min
- Phase 2.3: Tarot Inspection @20m x217m: 2.55min
  
- **Projections\***: Skywalker Only (40m Altitude, 17m/s Airspeed)
  - Sample (217m): 2.25min flight (x2 loops/4 passes), 30 images, 5.28min processing
  - Runway (2,170m): 2.13min flight, 300 images, 52.83min processing
  - Taxiway (350m): 0.34 min flight, 48 images, 8.45min processing
  - Apron (450m): 0.48min flight, 67 images, 11.8min processing
  - Theoretical Airfield Operating Surface: 2.95min flight, 415 images, 73.09min processing
  - **Theoretical Start-to-Finish: 89 minutes (Objective: 90 minutes)**

\*Assumes Linear Approximates

*Integrity Service - Excellence*



U.S. AIR FORCE

## **VIDEO SUBSYSTEM**

*Integrity Service - Excellence*

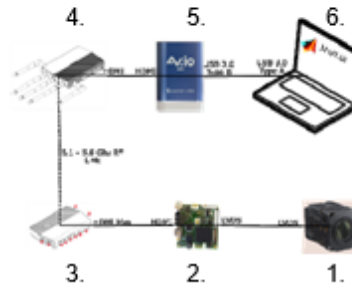




U.S. AIR FORCE

## Configuration Items

1. Sony FCB-EV7100 Block Camera
2. iShot® HDMI Interface Board
3. Connex Video Transmitter
4. Connex Video Receiver
5. Epiphan AV.io 4k capture card
6. GCS w/ MATLAB®



*Integrity Service - Excellence*



U.S. AIR FORCE

## Delivered Images



*Integrity Service - Excellence*



U.S. AIR FORCE

## Delivered Images



*Integrity Service - Excellence*



U.S. AIR FORCE

## Video Performance

UXO #	LAT	LONG	ERROR (m)
1	39.7735	-84.1030	1.80
2	39.7734	-84.1042	MISSED
3	39.7737	-84.1039	MISSED
4	39.7736	-84.1034	MISSED
5	39.7734	-84.1034	2.10
6	39.7735	-84.1030	1.91
7	39.7735	-84.1028	4.68
8	39.7734	-84.1026	MISSED
RMS ERROR:		2.88m	
DEV ERROR		1.19m	
DETECTION:		50%	
DETECTION Corrected:		80%	

*Integrity Service - Excellence*



U.S. AIR FORCE

## MULTI-ROTOR STRUCTURE



3-AXIS - 360° ROTATION  
No cable tangling

TAROT T960 + DJI 15.5 PROPELLER (x6) + KDE 4215XF 465KV BRUSHLESS MOTOR (x6) + KDE XF-UAS 75A ESC (x6)

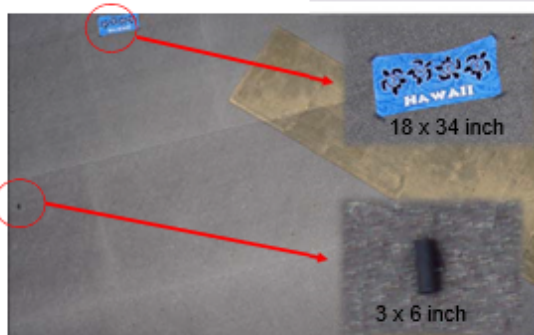
STORM PRO-3 UNIVERSAL GIMBAL (3-AXIS) + SONY A3000 + 20MM PANCAKE LENS

Integrity Service - Excellence



U.S. AIR FORCE

## Still Image quality assessment



17.6 x 11.6m Image @ Alt' 15m (0.29cm/pixel)



23.5 x 15.6m Image @ Alt' 20m (0.39cm/pixel)

### Camera setup

- 1/1000 Exposure, f/5, 20mm focal length, ISO 100, Manual focus infinity

Integrity Service - Excellence



U.S. AIR FORCE

---

## SOFTWARE

---

*Integrity Service - Excellence*



U.S. AIR FORCE

---

## S/W Architecture – Video Imagery

- **Input**
  - Imagery
  - Telemetry
- **Output**
  - Crater Locations
  - Crater Dimensions
  - UXO Locations
  - MOS based on crater data
  - Flight plan for Surveyor
  
- **Operator uses GUI to identify craters/UXOs**

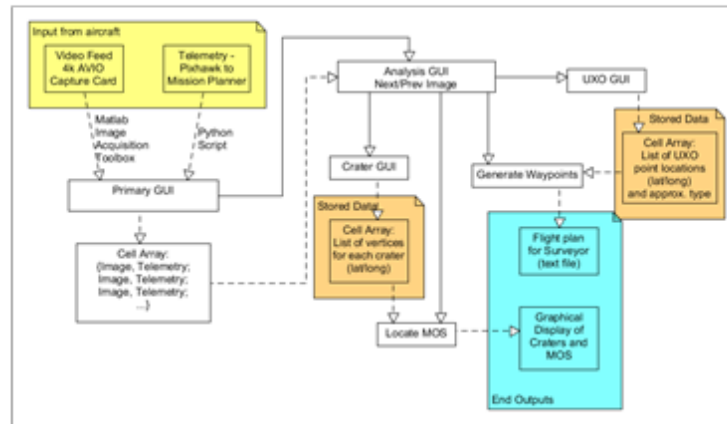
---

*Integrity Service - Excellence*



U.S. AIR FORCE

## S/W Architecture - Diagram



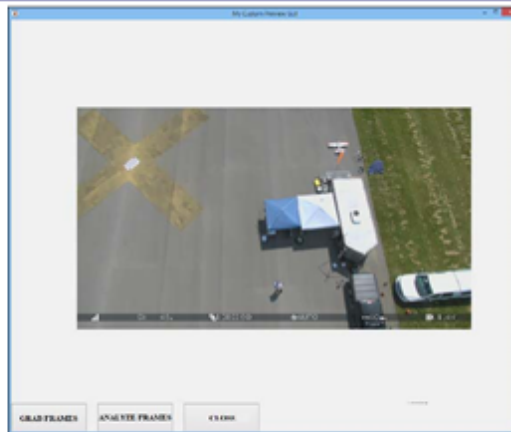
Integrity Service - Excellence



U.S. AIR FORCE

## Input GUI

- **Matlab Imagery Toolbox**
  - Live video from Inspector
- **Python Script**
  - Telemetry feed
  - Msn Planner fcn
- **GUI**
  - Start/Stop frame capture
  - Analyze frames



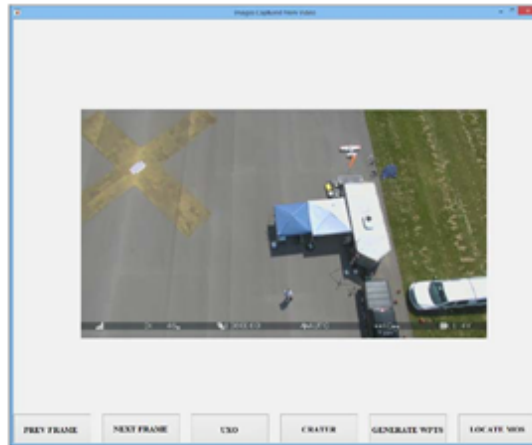
Integrity Service - Excellence



U.S. AIR FORCE

## Analysis GUI

- Review all imagery
- Tag UXOs
- Tag Craters
- Generate waypoint file
- Locate MOS



*Integrity Service - Excellence*



U.S. AIR FORCE

## Locate Craters

- 3+ points
- Geolocate points (auto)
- "Convex hull"



*Integrity Service - Excellence*



U.S. AIR FORCE

## Locate UXOs

- **Geolocate point (auto)**
- **Select UXO type**



*Integrity Service - Excellence*



U.S. AIR FORCE

## Generate Flight Plan – UXOs

- **Text file output**
  - **Fly to waypoint, delay, activate camera**

Dir	File	Format	Time	State
QC	WP	110		
0	1	0	16	1 0 0 0 39.773476 -84.102105 0.000000 1
1	0	3	16	5.000000 0.000000 0.000000 0.000000 39.773686 -84.104185 15.0000 1
2	0	3	117	4.000000 0.000000 0.000000 0.000000 39.773686 -84.104185 15.0000 1
3	0	3	283	1.000000 0.000000 0.000000 0.000000 1.000000 -84.104185 15.0000 1
4	0	3	16	5.000000 0.000000 0.000000 0.000000 39.773686 -84.103937 15.0000 1
5	0	3	112	4.000000 0.000000 0.000000 0.000000 39.773686 -84.103937 15.0000 1
6	0	1	183	1.000000 0.000000 0.000000 0.000000 1.000000 -84.103937 15.0000 1

- **Directly accepted by Mission Planner**

WP	Radius	Later Radius	Default Alt	Relative	Verify Height	Alt Warn	Spline									
1	WAYPOINT	5	0	0	0	39.773686	-84.104185	15	X	Up	Down	Grad %	Angle	Dist	AZ	
2	CONDITION_DELAY	4	0	0	0	39.773686	-84.104185	15	X			0	0	0	0	
3	DO_DIGICAM_CONTROL	1	0	0	0	1	-84.104185	15	X			0	0	0	0	
4	WAYPOINT	5	0	0	0	39.773686	-84.103937	15	X			0	0	0	21.2	90
5	CONDITION_DELAY	4	0	0	0	39.773686	-84.103937	15	X			0	0	0	0	
6	DO_DIGICAM_CONTROL	1	0	0	0	1	-84.103937	15	X			0	0	0	0	

*Integrity Service - Excellence*



U.S. AIR FORCE

## Locate MOS - Craters

- Estimates crater repair times
- Particle swarm optimization
  - Tests many MOS locations
  - Estimates repair time for each
  - Bounded by airfield edges
  - Converges on a minimum – keep scale in mind!
- Displays crater, MOS locations
- Google map view underneath



*Integrity - Service - Excellence*



U.S. AIR FORCE

## RESULTS

*Integrity - Service - Excellence*





U.S. AIR FORCE

## UXOs capture rate

Test ID	# of Images	Images/way point	Captured point / Planned point	Identification /Captured point
1.3	27	3.8	7/7	5/7(72%)
2	20	4	5/7	4/5(80%)



Integrity Service - Excellence



U.S. AIR FORCE

## Hex-Rotor TPMs review



Integrity Service - Excellence



U.S. AIR FORCE

## Hex-Rotor Test Result Review

Test ID	Time Line	Airspeed	Altitude	# of Images	Note	Corrective action	Result
1	Start : 11:10 Setup : 11:32 CheckList : 11:32 Flight : 02:49 Recovery : 01:42	10m/s	15m	Mission Abort	Epoch Chirping	• <del>Angle_Max</del> : 3000 • <del>Shuttle_Accel_P</del> : 0.05 -> 0.03 • POS_XY_P: 0.8 to 1.0	Resolve
					No triggering	• Add 5V 3cell <del>Soc</del> Batt'	
1.2	Start : 12:15 Setup : ??? CheckList : 11:32 Flight : 02:49 Recovery : 01:42	10m/s	20m	27	Epoch Chirping	• POS_XY_P: 1.0->0.8	Resolve
					Gimbal vibration	Physically lock yaw moment	Resolve
					Missing trigger Stamp	Sbtest.delay 39->1	Resolve
					Image Blurriness	Camera AF->MF infinity	Resolve
1.3	Start : 13:45 Setup : 02:53 CheckList : 10:07 Flight : 05:01 Recovery : 00:39	10m/s	20m	27	Gimbal Reset/Alarm	• Pitch derivative gain from 7- >12 • <del>P_gain</del> from 5->4	Resolve
2	Start : 15:05 Setup : 01:42 CheckList : 10:07 Flight : 02:13 Recovery : 02:33	10m/s	20m	20(Skywalker missed UXOs 1&3)	Mission planner	• Offset to default <del>lat/Long</del> to Africa->Mission Planner change	Resolve
					Camera Alignment	• Use a Witness marks	Resolve

Integrity Service - Excellence



U.S. AIR FORCE

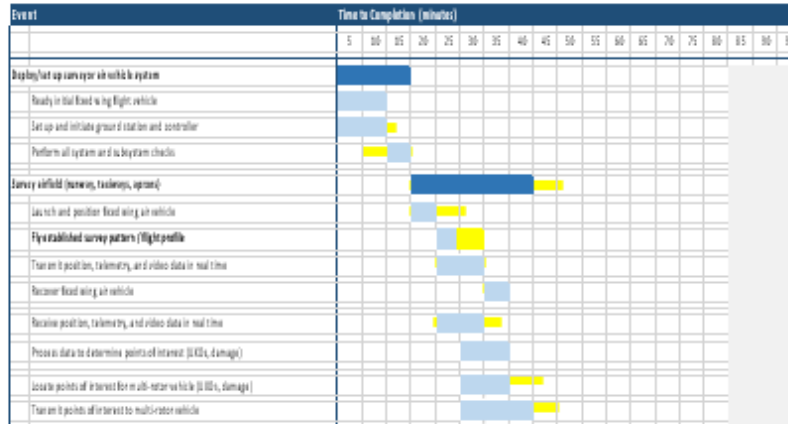
## Processing TPM Assessment

- MOE 1. Time to deliver Civil Engineering damage report
  - MOP 1.3. Time to process collected data and create report: **threshold - 40 minutes, objective - 30 minutes**
    - TPM 1.3.1. Time to process data  
: 23 Aug 2017 – 12 minutes for 300 images
    - TPM 1.3.2. Time to generate report  
: 23 Aug 2017 – 2 minutes
- MOE 2. Location accuracy of objects of interest
  - MOP 2.5. Location of items of interest: **threshold – 3.5 meters DRMS, objective – 2.0 meters DRMS**
    - TPM 2.5.1. Geo-locate items of interest  
: 23 Aug 2017 – 1.71 meters with calibration and 2.88 meters without calibration

Integrity Service - Excellence



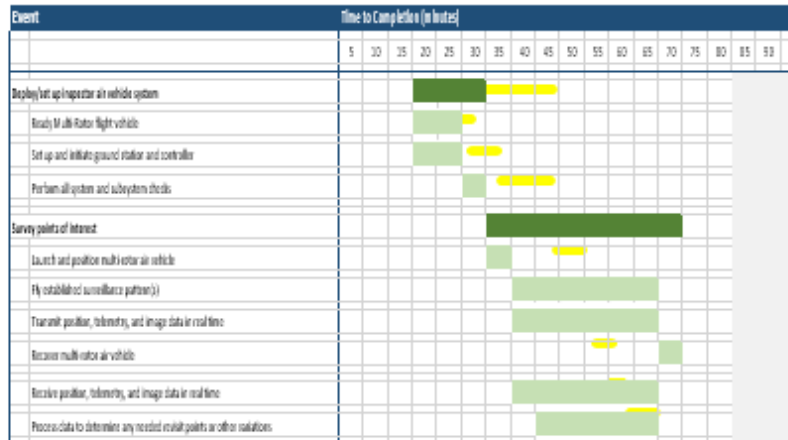
## Skywalker Operational Timeline



Integrity Service - Excellence



## Multi-rotor Operational Timeline



Integrity Service - Excellence



## Post Processing Operational Timeline

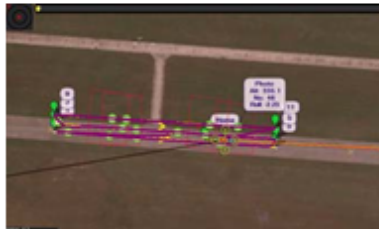
Event	Time to Completion (minutes)																			
	5	10	15	20	25	30	35	40	45	50	55	60	65	70	75	80	85	90	95	
Post process data collected																				
Review photos to determine damage/VICs																				
Generate civil engineering instructions for repair crews																				
Deliver repair instructions for immediate action																				

Integrity Service - Excellence



## Lessons Learned

- False coordinate from fixed wing
  - Hex-rotor's image capture rate depends on the coordinate from fixed wing
- Missed trigger stamp
  - Number of images > trigger stamp (example: 27 stamps vs. 45 images)
  - The more items make difficult to decide the location of items
  - Camera geo-tag module



Integrity Service - Excellence



U.S. AIR FORCE

## RISK ASSESSMENT

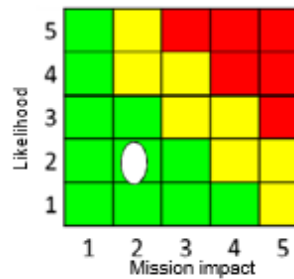
Integrity Service - Excellence



U.S. AIR FORCE

## Performance Risk

- **Risk:** Processing data consumes an unacceptable amount of time. Processing roughly 500 photos with a GSD of 2.5 cm/pixel takes 1.5 hours, exceeding our mission time
- **Mitigation:** Switching to live video streaming, for initial survey, allows for the user to get real time updates. Video saves snapshots every 1 second to allow for post flight processing

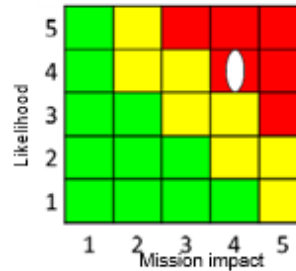


Integrity Service - Excellence



## Performance Risk

- **Risk:** Video SS LOS limit. Software limits placed on transmitter will prevent any communication past 1000 meters.
- **Future Mitigation:** Testing of antenna orientation on aircraft, using a higher power RX/TX pairs, and using relays

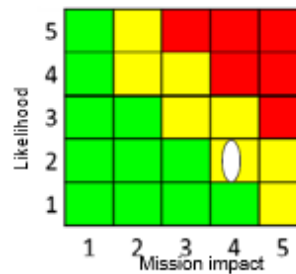


Integrity Service - Excellence



## Performance Risk

- **Risk:** Using the video stream in conjunction with MATLAB code is still unreliable at times. Video capture will not work if MATLAB is nonfunctional.
- **Future Mitigation:** Use a more mature system with better inherent integration. i.e. python. Further testing with MATLAB as well.



Integrity Service - Excellence



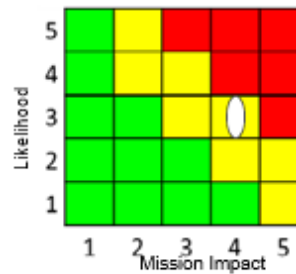
## Performance Risk

- **Risk:** Sub-optimal flight conditions cause fixed wing aircraft to deviate from flight path. This causes the FOV for video to be off target
- **Mitigation:** Telemetry data and live streaming will notify operators and on spot corrections will take place. If unable to make corrections on data points from stable flight conditions will be used.



## Performance Risk

- **Risk:** Less than 100% UXO detection. Sensor quality is insufficient for UXO detection and classification.
- **Future Mitigation:** Purchase higher quality camera for fixed wing aircraft. Fly at lower altitude for better pixel density. Better personnel training for UXO detection.

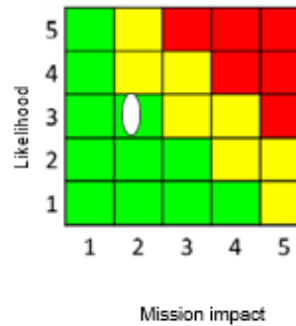


Integrity - Service - Excellence



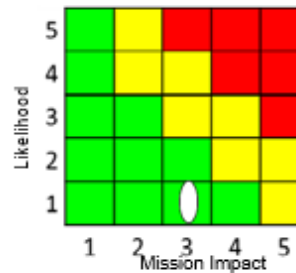
## Performance Risk

- **Risk:** Inoperable flight critical equipment during scheduled test periods. Camera remote triggering is/can be an issue.
- **Mitigation:** When possible bring spare parts and equipment. Isolate information systems. Perform thorough function checks of subsystems before fielding.



## Schedule Risk

- **Risk:** Setup consumes an unacceptable amount of time. Camera calibration can be a lengthy process and make take several tries.
- **Mitigation:** Regular training exercises and dry runs. Routine maintenance and inspection of equipment. Having a separate team calibrate camera during setup/use open CV.



Integrity Service - Excellence





## Design Shortcomings

### ■ Identified Shortcomings

#### ■ Mission Planner

- Camera trigger settings were confusing/non-user friendly
- Presented false negatives for imaging @ waypoints

#### ■ Fixed Wing

- Skywalker X-8 – initialization and tuning (pre-sets)
- Sony Block Cam/Connex HD – dropouts (potentially installation issues)

#### ■ Multi-Rotor

- Tarot Hex
  - Non-foldable
  - Iterations confused power and wiring requirements
- Gimbal
  - Unclear software requirements, requires training

*Integrity Service - Excellence*



## Design Improvements/Lessons Learned

### ■ Proposed Improvements

- Mission Planner – read the manual/ software training

- Fixed Wing – use a more stable air vehicle for inclement weather

- Catapult – Future configurations prefer hand-launch or rolling takeoff

- Sony Block Cam/Connex HD

- Matlab (Custom GUI)

- Mature GUI/ additional features
- ESRI output
- Report generation

#### ■ Multi-Rotor

- Tarot Hex

- Make foldable
- Make lighter/increase endurance

- Gimbal – read SimpleBGC 2.40b manual

- Sony A6000 – read the manual

*Integrity Service - Excellence*

## Bibliography

Abrego, J., & Moore, S. (2017). *Electronic Communication*.

AeroVironment, I. (2018). Raven UAS. Retrieved from

[https://www.avinc.com/uas/small\\_uas/raven/](https://www.avinc.com/uas/small_uas/raven/)

Air Force Civil Engineer Center. (2015a). AIRFIELD DAMAGE REPAIR OPERATIONS. *Air Force Pamphlet, 10-219(4)*, 182.

Air Force Civil Engineer Center. (2015b). CIVIL ENGINEERING CONTINGENCY RESPONSE AND RECOVERY PROCEDURES. *Air Force Pamphlet, 10-219(3)*, 141.

Alavi, A. H., Hasni, H., Lajnef, N., & Chatti, K. (2016). Continuous health monitoring of pavement systems using smart sensing technology. *Construction and Building Materials, 114*, 719–736. <http://doi.org/10.1016/j.conbuildmat.2016.03.128>

Alavi, A. H., Hasni, H., Lajnef, N., Chatti, K., & Faridazar, F. (2015). Damage detection using self-powered wireless sensor data: An evolutionary approach. *Measurement, 82*, 254–283. <http://doi.org/10.1016/j.measurement.2015.12.020>

Allen, T. (2017). MATLAB GUI.

Altavian. (2018). *Altavian Catalog*.

Amimon Ltd. (2016). FPV UAV Connex HD Video Racing Drone Link Wireless Transmitter.

ArduPilot Development Team. (2016). Mission Planner. Retrieved from <http://planner.ardupilot.com/>

BaseCam Electronics. (2017). Simple BGC 2.40b.

Casella, E., Rovere, A., Pedroncini, A., Stark, C. P., Casella, M., Ferrari, M., & Firpo, M. (2016). Drones as tools for monitoring beach topography changes in the Ligurian Sea (NW Mediterranean). *Geo-Marine Letters*, 36(2), 151–163. <http://doi.org/10.1007/s00367-016-0435-9>

Colomina, I., & Molina, P. (2014). Unmanned aerial systems for photogrammetry and remote sensing: A review. *ISPRS Journal of Photogrammetry and Remote Sensing*, 92, 79–97. <http://doi.org/10.1016/j.isprsjprs.2014.02.013>

D'Oleire-Oltmanns, S., Marzloff, I., Peter, K. D., & Ries, J. B. (2012). Unmanned aerial vehicle (UAV) for monitoring soil erosion in Morocco. *Remote Sensing*, 4(11), 3390–3416. <http://doi.org/10.3390/rs4113390>

Department of Defense. (2002). Airfield Damage Repair. *Unified Facilities Criteria*, 3-270-07, 36.

- Department of Defense, & NAVSTAR. (2008). Global Positioning System Standard Positioning Service. *Www.Gps.Gov*, (September), 1 – 160. Retrieved from <http://www.gps.gov/technical/ps/2008-SPS-performance-standard.pdf>
- Duncan, D. (2007). *Rapid Runway Repair (RRR): an optimization for minimum operating strip selection*. Air Force Institute of Technology.
- Earth Imaging Journal. (2015). Sensing Challenge: Airfield Damage Assessment. Retrieved from <http://ejournal.com/print/articles/sensing-challenge-airfield-damage-assessment>
- Echerri, J. (2015). New sensors expected to speed up ADR process. *AFCEC*, 1–2. Retrieved from <http://www.afcec.af.mil/DesktopModules/ArticleCS/Print.aspx?PortalId=17&ModuleId=2425&Article=871470>
- Ellenberg, A., Kotsos, A., Moon, F., & Bartoli, I. (2011). New methodology for the application of vibration-based damage detection techniques. *Structural Control and Health Monitoring*, (May 2011), n/a–n/a. <http://doi.org/10.1002/stc>
- Epiphan Systems Inc. (2017). Epiphan AV.io 4K™ Technical Specifications.
- Eschmann, C., Kuo, C. M., Kuo, C. H., & Boller, C. (2013). High-Resolution Multisensor Infrastructure Inspection With Unmanned Aircraft Systems. *International Archives of the Photogrammetry, Remote Sensing and Spatial*

*Information Sciences*, XL(September). <http://doi.org/10.5194/isprsarchives-XL-1-W2-125-2013>

Federal Highway Administration. (2000). *State Highway Public Owned Roads - Rural and Urban Miles, Lane Miles, and Daily Travel*. Retrieved from <https://www.fhwa.dot.gov/ohim/hs00/hm81r.htm>

Filler, L., & Diltz, R. (2016). *Electronic Correspondance*. Panama City.

First Concrete Runway - Ford Field - Dearborn, MI. (2016). Retrieved from <http://explorer.acpa.org/explorer/places/united-states/michigan/dearborn/airport/first-concrete-runway-ford-field-dearborn-mi/>

Fpvmodel. (2017). Skywalker X8 - Flying FPV Wing.

Gallagher, D. (2017). *OH/IN UAS Center Interview*. Retrieved from <http://www.dot.state.oh.us/Divisions/uas/Pages/default.aspx>

Getzin, S., Nuske, R. S., & Wiegand, K. (2014). Using unmanned aerial vehicles (UAV) to quantify spatial gap patterns in forests. *Remote Sensing*, 6(8), 6988–7004. <http://doi.org/10.3390/rs6086988>

Getzin, S., Wiegand, K., & Schöning, I. (2012). Assessing biodiversity in forests using very high-resolution images and unmanned aerial vehicles. *Methods in Ecology and Evolution*, 3(2), 397–404. <http://doi.org/10.1111/j.2041-210X.2011.00158.x>

Grandsaert, P. J. (2015). *Integrating Pavement Crack Detection and Analysis Using Autonomous Unmanned Aerial Vehicle Imagery*. Retrieved from <http://oai.dtic.mil/oai/oai?verb=getRecord&metadataPrefix=html&identifier=ADA615401>

Helipal. (2017a). Storm Pro-3 - 3-Axis, Brushless Gimbal.

Helipal. (2017b). Tarot T960 Aerial Filming Frame.

Henrickson, J. V, Rogers, C., Lu, H., & Valasek, J. (2016). Infrastructure Assessment with Small Unmanned Aircraft Systems. *2016 International Conference on Unmanned Aircraft Systems (ICUAS)*, 933–942. <http://doi.org/10.1109/ICUAS.2016.7502652>

Hu, J. P., Wu, W. Bin, & Tan, Q. L. (2012). Application of Unmanned Aerial Vehicle Remote Sensing for Geological Disaster Reconnaissance along Transportation Lines: A Case Study. *Applied Mechanics and Materials*, 226-228, 2376–2379. <http://doi.org/10.4028/www.scientific.net/AMM.226-228.2376>

Idaho National Laboratory. (2009). Damage Assessment of the Rapid King for UAVs. Retrieved from <http://www.satnews.com/story.php?number=1868392077>

Iqbal, U., Irtiza, S., Shah, A., Jamil, M., Gillani, S. O., & Ayaz, Y. (2015). Selection of Unmanned Aerial System (Uas) for Disaster Relief Operations : a Comparison. *Sci.Int.(Lahore)*, 27(4), 3199–3203.

- Johnson, R., Smith, K., & Wescott, K. (2015). Unmanned Aircraft System (UAS) Applications to Land and Natural Resource Management. *Environmental Practice*, 17(03), 170–177. <http://doi.org/10.1017/S1466046615000216>
- KDE Direct. (2015). Latest News.
- Lindner, G., Schraml, K., Mansberger, R., & Hübl, J. (2016). UAV monitoring and documentation of a large landslide. *Applied Geomatics*, 8(1), 1–11. <http://doi.org/10.1007/s12518-015-0165-0>
- Losey, S. (2016). Now hiring : USAF needs to rebuild the ranks to keep up with demands. *Air Force Times*, pp. 1–14. Retrieved from <https://www.airforcetimes.com/articles/now-hiring-usaf-needs-to-rebuild-the-ranks-to-keep-up-with-demands>
- Meeks, M. (2016). *EVALUATING STORM SEWER PIPE CONDITION USING AUTONOMOUS DRONE TECHNOLOGY*.
- Messinger, M., Asner, G. P., & Silman, M. (2016). Rapid assessments of amazon forest structure and biomass using small unmanned aerial systems. *Remote Sensing*, 8(8), 1–16. <http://doi.org/10.3390/rs8080615>
- Morrison, G. (2013). LED LCD vs. plasma vs. LCD. Retrieved January 24, 2018, from <https://www.cnet.com/news/led-lcd-vs-plasma-vs-lcd/>

- Na, W., & Baek, J. (2016). Impedance-Based Non-Destructive Testing Method Combined with Unmanned Aerial Vehicle for Structural Health Monitoring of Civil Infrastructures. *Applied Sciences*, 7(1), 15. <http://doi.org/10.3390/app7010015>
- Pix4D. (2017). Pix4Dmapper v3.3.
- PX4 Autopilot. (2017). Pixhawk 2 Autopilot. Retrieved from <https://pixhawk.org/>
- Sankarasrinivasan, S., Balasubramanian, E., Karthik, K., Chandrasekar, U., & Gupta, R. (2015). Health Monitoring of Civil Structures with Integrated UAV and Image Processing System. In *Procedia Computer Science* (Vol. 54). <http://doi.org/10.1016/j.procs.2015.06.058>
- Schleppi, B. (2018). Road Profiling. Retrieved from <http://www.dot.state.oh.us/Divisions/Planning/TechServ/infrastructure/Pages/RoadProfiling.aspx>
- Shepherd, A., & Storm, R. (2017a). *290 Acre Kiln Runway Quality Report*.
- Shepherd, A., & Storm, R. (2017b). *30 Acre KSGH Runway Intersection Quality Report*.
- Shepherd, A., & Storm, R. (2017c). *7 Acre Overpass Quality Report*.
- Shepherd, A., & Storm, R. (2017d). *Sinclair Community College – Pathfinder Report*.



Siebert, S., & Teizer, J. (2014). Mobile 3D mapping for surveying earthwork projects using an Unmanned Aerial Vehicle (UAV) system. *Automation in Construction*, 41, 1–14. <http://doi.org/10.1016/j.autcon.2014.01.004>

Sinclair Community College. (2017). *Enabling Industry: Development of Civil UAS Applications*.

Sony Corporation of America. (2017a). FCB-EV7100 Camera Block.

Sony Corporation of America. (2017b). Sony a6000 E-mount camera with APS-C Sensor.

Stratech Group. (2013). iFerret RADAS. Retrieved from [http://www.thestrategroup.com/iv\\_iferret\\_radas.asp](http://www.thestrategroup.com/iv_iferret_radas.asp)

The MathWorks Inc. (2017). MATLAB.

UAV Systems International: Skywalker Ready-to-fly Drone. (2018). Retrieved from <https://www.uavsystemsinternational.com/product/Skywalker-ready-to-fly-drone/>

www.RC-Drones.com. (2018). Retrieved from [http://www.rc-drones.com/DJI-Spreading-Wings-S800-EVO-Custom-Built-HexaCopter-wWookong-M\\_p\\_404.html](http://www.rc-drones.com/DJI-Spreading-Wings-S800-EVO-Custom-Built-HexaCopter-wWookong-M_p_404.html)

Xu, Z., Yang, J., Peng, C., Wu, Y., Jiang, X., Li, R., ... Tian, B. (2014). Development of an UAS for post-earthquake disaster surveying and its application in Ms7.0 Lushan Earthquake, Sichuan, China. *Computers & Geosciences*, 68, 22–30. <http://doi.org/10.1016/j.cageo.2014.04.001>

Yuan, C., Zhang, Y., & Liu, Z. (2015). A survey on technologies for automatic forest fire monitoring, detection, and fighting using unmanned aerial vehicles and remote sensing techniques. *Canadian Journal of Forest Research*.

<http://doi.org/10.1139/cjfr-2014-0347>

Zhang, C., & Kovacs, J. M. (2012). The application of small unmanned aerial systems for precision agriculture: A review. *Precision Agriculture*, 13(6), 693–712.

<http://doi.org/10.1007/s11119-012-9274-5>

Zhang, S., Bogus, S. M., & Lippitt, C. D. (2015). Pavement Surface Permanent Deformation Detection and Assessment Based on Digital Aerial Triangulation. *Computing in Civil Engineering 2015*, (November).

<http://doi.org/10.1061/9780784479247.010>

Zhang, S., Lippitt, C. D., Bogus, S. M., & Neville, P. R. H. (2016). Characterizing pavement surface distress conditions with hyper-spatial resolution natural color aerial photography. *Remote Sensing*, 8(5), 1–24. <http://doi.org/10.3390/rs8050392>

## Vita

Captain Samuel M. Clark graduated from Astoria High School in Astoria, Oregon in 2008. He was enrolled in the Air Force Reserve Officer Training Corps, Detachment 695, at the University of Portland in Portland, Oregon where he graduated with a Bachelor of Science degree in Civil Engineering and a commission as a second lieutenant in the United States Air Force in 2013. His first assignment was at Dover Air Force Base in Dover, Delaware. He served in numerous roles, including project management, squadron executive officer, Dignified Transfer Officer-in-Charge – supporting the Air Force Mortuary Affairs Operations – and culminated as the Readiness and Emergency Management Flight Commander. In September 2014, he entered Liberty University's online Master of Business Administration program.

In August 2016, he entered the Graduate School of Engineering and Management, Air Force Institute of Technology at Wright-Patterson Air Force Base, Dayton, Ohio. In March 2017, he was conferred the advanced academic degree in Master of Business Administration by Liberty University, in Lynchburg, Virginia. Upon graduation from the Air Force Institute of Technology, he will be assigned to the 319th Civil Engineer Squadron, Grand Forks Air Force Base, in Grand Forks, North Dakota as the Engineering Deputy Flight Chief.

# REPORT DOCUMENTATION PAGE

Form Approved  
OMB No. 0704-0188

Public reporting burden for this collection of information is estimated to average 1 hour per response, including the time for reviewing instructions, searching existing data sources, gathering and maintaining the data needed, and completing and reviewing this collection of information. Send comments regarding this burden estimate or any other aspect of this collection of information, including suggestions for reducing this burden to Department of Defense, Washington Headquarters Services, Directorate for Information Operations and Reports (0704-0188), 1215 Jefferson Davis Highway, Suite 1204, Arlington, VA 22202-4302. Respondents should be aware that notwithstanding any other provision of law, no person shall be subject to any penalty for failing to comply with a collection of information if it does not display a currently valid OMB control number. **PLEASE DO NOT RETURN YOUR FORM TO THE ABOVE ADDRESS.**

<b>1. REPORT DATE (DD-MM-YYYY)</b> 22-03-2018		<b>2. REPORT TYPE</b> Master's Thesis		<b>3. DATES COVERED (From - To)</b> September 2016 - March 2018	
<b>4. TITLE AND SUBTITLE</b>  United States Air Force Applications of Unmanned Aerial Systems: Modernizing Airfield Damage Assessment				<b>5a. CONTRACT NUMBER</b>	
				<b>5b. GRANT NUMBER</b>	
				<b>5c. PROGRAM ELEMENT NUMBER</b>	
<b>6. AUTHOR(S)</b> Clark, Samuel, M., Capt, USAF				<b>5d. PROJECT NUMBER</b>	
				<b>5e. TASK NUMBER</b>	
				<b>5f. WORK UNIT NUMBER</b>	
<b>7. PERFORMING ORGANIZATION NAME(S) AND ADDRESS(ES)</b>  Air Force Institute of Technology Graduate School of Engineering and Management (AFIT/EN) 2950 Hobson Way, Building 640 WPAFB OH 45433-8865				<b>8. PERFORMING ORGANIZATION REPORT NUMBER</b>  AFIT-ENV-18-M-188	
<b>9. SPONSORING / MONITORING AGENCY NAME(S) AND ADDRESS(ES)</b> Air Force Civil Engineer Center Dr. Robert Diltz, Readiness Directorate (CXAE) Address: none-provided Panama City, Florida, 32403 Robert.diltz@us.af.mil				<b>10. SPONSOR/MONITOR'S ACRONYM(S)</b> AFCEC/CXAE	
				<b>11. SPONSOR/MONITOR'S REPORT NUMBER(S)</b>	
<b>12. DISTRIBUTION / AVAILABILITY STATEMENT</b>  <b>DISTRIBUTION STATEMENT A.</b> APPROVED FOR PUBLIC RELEASE; DISTRIBUTION UNLIMITED.					
<b>13. SUPPLEMENTARY NOTES</b> This material is declared a work of the U.S. Government and is not subject to copyright protection in the United States.					
<b>14. ABSTRACT</b> Modernizing airfield damage assessment has long been a priority mission at the Air Force Civil Engineer Center (AFCEC). Previously, AFCEC has made advances to expedite unexploded ordnance (UXO) neutralization and pavement repair. Missing from these initiatives is the initial assessment component. This thesis expands the idea of using Small Unmanned Aerial Systems (SUAS), applies it to the Air Force mission, and provides SUAS vehicle configuration and sensor recommendations. In this study, 25 civil engineer officers reviewed airfield imagery gathered using two small air vehicles. For the first review, participants attempted to identify UXOs and foreign object debris (FOD) in a computer interface that leverages images collected by a fixed-wing air vehicle. The second review uses a two-dimensional map created using a hex-rotor. The results of both systems were then compared to the status quo. Resulting statistics indicate that, irrespective of image resolution, additional analysis time does not result in greater object detection or correct identification. Overall, this thesis concludes that SUAS use for afield damage assessment shows promise. Moreover, they can provide the Air Force improved precision for locating UXOs and FOD, as well as estimate dimensions of damage. Dedicating resources to developing this technology will also assist with improving object detection and manpower efficiency. Further research is required for optimal image characterization requisite for reducing and/or eliminating the occurrence of false negative events.					
<b>15. SUBJECT TERMS</b> Unmanned Aerial Systems, Airfield Damage Assessment					
<b>16. SECURITY CLASSIFICATION OF:</b>			<b>17. LIMITATION OF ABSTRACT</b>  UU	<b>18. NUMBER OF PAGES</b>  165	<b>19a. NAME OF RESPONSIBLE PERSON</b> Dr. David R. Jacques
<b>a. REPORT</b> U	<b>b. ABSTRACT</b> U	<b>c. THIS PAGE</b> U			<b>19b. TELEPHONE NUMBER (include area code)</b> (937) 255-3355 x3329 david.jacques@afit.edu

Standard Form 298 (Rev. 8-98)  
Prescribed by ANSI Std. Z39.18